GERMANIUM BASED NANOTUBES: FACT OR FICTION?

by

SOMILKUMAR JAGDISHCHANDRA RATHI

Presented to the Faculty of the Graduate School of

The University of Texas at Arlington in Partial Fulfillment

of the Requirements

for the Degree of

MASTER OF SCIENCE IN PHYSICS

THE UNIVERSITY OF TEXAS AT ARLINGTON

August 2008

ACKNOWLEDGEMENTS

I am highly indebted to my advisor Professor Asok Ray, and to him, I give maximum thanks. Dr. Ray imparted a significant amount of knowledge on me and also, I learned a great deal of physics from him, all of which made my transition from electrical engineering to physics a smooth one. He was extremely generous and kind, and thanks to him, I am leaving UTA to pursue further research with extreme confidence.

Besides my advisor, I have had a great opportunity to work with wonderful and good people whiles pursuing my master's research. I give heartfelt thanks to Dr. Raymond Atta-Fynn, a Research Assistant Professor in Dr. Ray's group. Apart from the stimulating discussions that I had with Dr. Atta-Fynn, he taught me a great deal, especially how to write complex and efficient computer codes. I want to thank Dr. Fhokrul Islam, a Postdoctoral Fellow working with Dr. Ray for useful discussions and help.

Special thanks go to the following: Professor Truman Black and Professor Nail Fazleev, for serving on my thesis committee. I am also grateful to my peers in Dr. Ray's group: Pratik Dholabhai, Kazi Alam, Souptik Mukherjee, and Molly Averitte. I am also grateful to the UTA, especially the Physics department, and the Welch Foundation for the financial support during the period of my graduate studies and research.

July 10, 2008

ABSTRACT

GERMANIUM BASED NANOTUBES: FACT OR FICTION?

Somilkumar Jagdishchandra Rathi, M.S

The University of Texas at Arlington, 2008

Supervising Professor: Asok K Ray

Unlike carbon nanotubes, nanostructures of Ge, a group IV semiconductor, have not been fully explored. In particular, there is limited data available on Germanium-based nanotubes. The aim of this thesis is to explore the structural and electronic properties of Germanium based nanotubes and their potential future electronic applications. We have thus performed a systematic *ab initio* study of the electronic and geometric structures of three different types of single-walled SiGe and GeC nanotubes in armchair (*n, n*) and zigzag (*n,* 0) ($3 \leq n \leq 11$) configurations using hybrid density functional theory and the finite cluster approximation. Also we provide the detailed analysis of pure Si (armchair, zigzag and chiral) and Ge nanotubes in the armchair and zigzag format with similar dimensions. The Gaussian '03 suite of programs was used for all computations which involved full geometry and spin optimizations. A detailed stability investigation of the topologically similar nanotubes with dependence of the electronic band gaps on the tube diameters, energy density of states, and dipole moments have been carried out. Using the Mulliken charge analysis, charge density distribution along the tube lengths is also calculated. In depth structural analysis and distribution of molecular orbitals are also reported. The spatial positions of the atoms, ionicity, and

curvature are the primary governing factors in the determinations of the stabilities and the electronic behavior of the nanotubes. The interesting findings from this detailed study of Ge based hybrid nanotubes can be useful to fabricate and manipulate the future nano-electronic devices.

TABLE OF CONTENTS

LIST OF ILLUSTRATIONS

LIST OF TABLES

CHAPTER 1

INTRODUCTION

1.1 Overview of Carbon nanotubes

Discovery and synthesis of the "buckyball" C_{60} in the early 1990's led scientists towards a new miracle material called *carbon nanotubes* (CNTs) which are thin tubes of carbon atoms [1,2]. With the tremendous success of CNTs, over the years quasi-one-dimensional nanostructures such as nanotubes and nanowires have stirred extensive interests in condensed matter physics and in fact, the entire research world, partly because of their fascinating electronic and mechanical properties and partly because of novel technological applications [3-11]. Single walled nanotubes particularly have been studied more extensively both experimentally and theoretically. One interesting fact observed both experimentally and theoretically in the case of carbon nanotubes is that single walled carbon nanotubes are believed to exhibit metallic or semiconducting behavior depending on the tube diameter and chirality. Length and curvature also are found to influence the structure and energetics of a nanotube [1-18]. Conductivity enhancement in CNTs bundles doped with alkali metals and metal-semiconductor and semiconductor-semiconductor transitions induced by intercalating alkali atoms has also been studied extensively [19,20]. Study of structure-dependent Coulomb blockade of carbon nanotubes showed that Coulomb staircase is evident at lower temperatures, could be suppressed by temperature elevation [21]. On the application side of CNTs numerous studies have been performed. For example, transistor based on carbon nanotubes offer a unique functionality. It can operate as a ballistic field-effect transistor, with excellent characteristics even when scaled to 10 nm dimensions [22]. An effective forward-biased p-n junction, without dopants, can also be created from carbon nanotubes by appropriately biasing the nanotube device [23]. Also sensors based on CNTs have demonstrated high sensitivity

towards the detection of electromagnetic and acoustic signals as well as different chemicals [24-25]. A wealth of information is also available on the transport properties of CNTs. Koller *et al.* [26] investigated linear and nonlinear transport in interacting single wall carbon nanotubes that are weakly attached to ferromagnetic leads. They also derived the equations of motion which account for an arbitrarily vectored magnetization of the contacts. Schonenberger [27] while carrying out the studies on transport properties of CNTS showed that because of the low carrier density and therefore reduced screening, the Fermi energy can be tuned by electrostatic gates. Also Schonenberger [27] showed that single walled nanotubes (SWNTs) offer many advantages over multiwalled nanotubes (MWNTs) for spin transport studies, including increased scattering lengths, well-defined electronic band structure, enhanced Coulombic interactions (leading to novel physical phenomena), and the possibility to modify the nanotube resistance with a capacitively coupled gate. The electrical properties of individual bundles, or "ropes," of single-walled carbon nanotubes have been measured by Bockrath *et al.* [28] below 10 kelvin, and the low-bias conductance was suppressed for voltages less than a few millivolts. In addition, they found out that dramatic peaks were observed in the conductance as a function of a gate voltage that modulated the number of electrons in the rope. They interpreted these results in terms of single-electron charging and resonant tunneling through the quantized energy levels of the nanotubes composing the rope. Martel *et al.* [29] fabricated field-effect transistors based on individual single- and multi-wall carbon nanotubes and analyzed their performance. They showed that transport through the nanotubes is dominated by holes and, at room temperature. Also they reported that by varying the gate voltage the conductance of a single-wall device can be successfully modulated the by more than 5 orders of magnitude. A model carbon nanotube (CNT)-$(CH)_n$-CNT structure is studied by Bruque *et al.* [30] to understand the electron transport through an interface between two conjugated systems. They reported that conductance of the CNT-$(CH)_n$-CNT structures strongly depends on the bonding angle of the $(CH)_n$-CNT bond and the minimum-energy relaxed geometry is relatively coplanar.

Also the relationship of the conductance on the length of the $(CH)_n$ depends on the geometry of the $(CH)_n$-CNT interface. Exhaustive research has also indicated that nanotube and nanoform conformations are not possessed by only carbon but also by many other elements and compounds [31-43].

1.2 Nanotubes of Pure Silicon

Moving on to Silicon, we know that Si resides is in the column IV of the periodic table below carbon and progressively increasing research is currently being performed in the area of silicon nanotubes and nanostructures. Research in recent years has underscored the importance and development of silicon at nanoscale. Nano-silicon is believed to be a potential candidate for diverse applications such as creating better disease detectors and biochemical sensors, as well as tiny electronics such as ultra-high density memory chips for ultra fast computing. It is widely believed that Si nanotubes (SiNTs) and nanoforms will be the next most compatible and miscible materials with the current micro and nanoelectronics devices [44-49].It is well known fact that carbon prefers sp^2 hybridization with π bonding, which helps to form graphitic, tubular and aromatic structures. On the other hand, silicon tends to prefer tetrahedral sp^3 bonding. Hence, forming tubular structures of Si (thereby forcing Si to have sp^2 bonding) was initially considered to be hypothetical at best. As a result, considerable theoretical and experimental efforts have been carried out over the past and recent years to investigate the existence and fabrication of SiNTs. One of the earliest theoretical works on SiNTs was done by Fagan *et al*. [50] using *ab inito* density functional theory (DFT). They showed that the band structure, electronic density of states, and cohesive energies of single-walled SiNTs are similar to that of CNTs having the same type. They also found relevant discrepancy concerning the energy difference between the cohesive energies per atom for tubes compared to the corresponding bulk structure. In a follow up study, Fagan *et al*. investigated the stability and thermal behavior of SiNTs and CNTs from first principles calculations and Monte Carlo simulations with the Tersoff empirical potential [51].The band gap was found to decrease with

increasing tube diameter but significant discrepancies were observed in the thermal stabilities and cohesive energies of SiNTs and CNTs compared with corresponding bulks. Seifert *et al.* [52] performed atomistic stimulations on silicides and SiH nanotubes using nonorthgonal tight-binding DFT scheme and their results supported the possible existence of SiNTs. Another theoretical work by Zhang *et al* [53] using the semi empirical molecular orbital PM3 method, at the HF/3-21G and HF/3-21G (d) levels of theory and concluded that dangling bond terminated SiNTs exist as severely puckered structure (with a corrugated surface) with Si-Si distances ranging from 1.85 Å to 2.25 Å. Barnard and Russo [54] used an *ab inito* pseudopotential DFT-GGA method with the Perdew-Wang exchange correlation functional (PW91) to study the structure and energetics of single-walled armchair and zigzag SiNTs. They showed that the individual cohesive energies and strain energies are both dependent on the nanotube diameter and chirality. Also, Zhang *et al.* [55] using hybrid DFT have clearly shown that SiNTs exist stably in armchair configuration. In a more recent work, a study of possible structures of SiNT via Tight-Binding Molecular Dynamics was done by Zhang and co-workers [56]. Predictions of gearlike structures containing alternating tetrahedral and trigonal-planar Si configurations were made.

Comparison of single-walled SiNT (both gearlike and hexagonal) with corresponding CNTs has been done by Yang *et al.* [57]. A recent study on double walled silicon nanotubes (DWSiNTs) with faceted wall surfaces (with Hydrogen passivation effects included) using first-principle calculations have been reported by Zhao *et al*. [58]. They showed that hexagonal and tetrahedral like structures of these DWSiNTs are almost energetically equal. Classical potential studies of the stability of infinite and finite clean and hydrogenated open-ended SiNTs was performed by Ponomarenko *et al*. [59] to study their energetics. Thermal behavior of Si nanocages and nanotubes using classical molecular dynamics simulations based on Tersoff potential has been studied by Kang *et al*. [60]. Their results were in good agreement with previous density functional theory results. Mechanical characteristics of SiNTs have also been

studied by various groups. For example molecular dynamics simulation of temperature effect, strain rate and vacancies on tensile and fatigue behavior of Si based nanotubes using Tersoff-Brenner man body potential functions has been performed by Jeng *et al.* [61]. Bai *et al.* [62] have provided evidence for the possible existence of one dimensional single-walled Si nanostructure having square, pentagonal and hexagonal building blocks, all of which have different local geometries from diamond Si but still maintains four-fold co-ordinations. Their calculations showed that the nanotubes have zero band gaps, suggest that their structure were possibly metallic rather than semi-conductor. The response of hypothetical SiNTs under axial compression has been investigated by Kang *et al.* [63] using atomistic simulations. Electronic and Magnetic properties of Si based nanotubes after doping with transition metals has also been examined by different groups [64-66]. There are some novel experimental evidences in literature which show the presence of nanotubular forms of silicon.

More recently, the presence of Y-, T- branched and coiled tubular structures with the help of Transmission electron microscopy and electron energy loss near-edge technique has been confirmed [67]. Crescenzi *et al*. [68] has reported single nanotubes constituted by oxidized silicon atoms with diameter ranging from 2 to 35 nm and atomic arrangement compatible with a puckered structure and different chiralities. They have also reported that SiNTs can be semiconducting as well as metallic character. Yamada *et al.* [69] has confirmed the presence of multiwall nanotubes composed of rolled-up quasi two dimensional honeycombs nets of silicon atoms with the help of electron microscopy and electron diffraction technique. Si nanotubes have been successfully prepared in the labs also. Self assembled SiNTs with one-dimensional structure have been synthesized from silicon monoxide powder under critically hydrothermal conditions by Tang *et al*. [70]. Sha *et al*. [71] successfully fabricated SiNTs by chemical vapor deposition process using nanochannel Al_2O_3 substrate. Using molecular beam epitaxy, synthesis of SiNTs on porous alumina has been done by Jeong *et al*. [72].

1.3 Nanotubes Based on Pure Ge and Related Compounds

Given that germanium is in the column IV of the periodic table as carbon and silicon and is isoelectronic with them, it has been suggested that Ge and associated compounds at nanoscale might also be promising candidates for future nanoelectronics based technologies [73, 74]. As compared to previously mentioned CNTs and SiNTs, not much has been reported on one dimensional Ge based nanotubes. One of the initial density-functional tight binding study was performed by Seifert *et al.* [75], where the tubes were constructed by rolling sheets of polygermyne. The results obtained indicated a possibility of germanium nanotubes with interesting photoluminescence properties and the GeH nanotubes were found to be semi-conducting, with the gap size growing from about 1.1eV from the smallest nanotube towards the value of 1.35eV of germyne sheets. Using ab initio total energy calculations Singh and group members [76] demonstrated that the nanotubes of germanium with atomic structure based on an alternate prism and antiprism stacking of hexagonal rings, can be stabilized by metal encapsulation.

Germanium carbide (GeC) in bulk form is an indirect wide band gap semiconductor in both polytypes 3C and 2H (zinc-blende and wurtzite), has high bulk modulus, and the percentage of covalency is comparable to SiC. Another important characteristic of bulk GeC is the significantly ionic nature due to rather compact orbitals [77, 78]. It is reasonable to assume that the unique properties of bulk GeC, along with properties due to quantum size effects, would reflect in GeC structures in the nanoscale regime. Charge transport properties of plasma deposited a-Ge_XC_Y:H amorphous semiconductors can be correlated with nanostructures consisting of nanometer-size germanium clusters organized in large domains of approximate sizes of 100 nm [79]. Domrachev *et al.* [80] have successfully prepared Ge-filled CNTs with an average diameter of 15–100 nm, and Ge-filled carbon microtubes (CMTs) with an average diameter of 100-8000 nm, using MOCVD techniques. They used powder X-ray diffraction (XRD), transmission electron microscopy (TEM), atomic force microscopy (AFM), scanning

Auger microscopy (SAM), Raman spectroscopy, and field emission measurements in order to characterize composite structures of arrays of CNTs/Ge nanowires (GeNWs) and CMTs/GeNWs. A more complicated atomic arrangement of Si and Ge in tubular forms, which are known as SiGe nanotubes (a hybrid structure) and one dimensional structure in form of SiGe nanowires have also been focus of scientific community lately. Very recently, by means of *ab initio* calculations, Migas and Borisenko [81] showed that SiGe and Si-Ge core-shell nanowires with the <001> orientation and having a diameter of 1.5 nm display a competitive indirect-direct character of the gap. To illustrate the unique features of SiGe nanotubes, Schmidt and Eberl created these tubes using two different methods [82].Using general method they were able to prepare nanotubes, which yielded an aspect ratio of 60 and also by involving specialized method they successfully prepared nanotubes of length 20μm with diameter of 530nm. Theoretical analysis and molecular dynamics simulations done by Zang *et al.* demonstrated, that a free standing Si nanofilm may bend into a nanotube with Ge as inner layer, opposite to the normal bending configuration defined by misfit strain [83]. Also they noticed that such rolled-up nanotubes can accommodate a high level of strain, even beyond the magnitude of lattice mismatch.

This thesis is organized as follows: Chapter 2 contains theory, Chapter 3 contains the discussions on bare Si and Ge nanotubes, followed by GeC and SiGe nanotubes in Chapters 4 and 5. Chapter 6 presents the conclusions and suggestions for future work.

CHAPTER 2

THEORY

2.1 Introduction

Density functional theory (DFT) methods are the most widely used approximate first principles approach to computational material science today. DFT is in principle an exact formulation for the ground state of many-electron systems and it expresses ground state properties– such as equilibrium positions, total energies, and magnetic moments as functionals of the electron density $\rho(\vec{r})$. Conceptually simpler and formally rigorous density functional theory provides an elegant way of mapping a *N* variable system to a single variable, the system's density, and hence reducing the computational cost significantly over the traditional *ab initio* theories such as Hartree-Fock theory, while retaining the much of the computational accuracy.

The initial attempt to formulate the density functionals was based on the Thomas-Fermi model due to Thomas [84] and Fermi [85]. Within the model, the total energy is expressed as a functional of the electron density. However, the model suffered from inaccuracies stemming from the crude formulation of the kinetic energy functional and the mean field approximation to the electron-electron interaction. Later on, Dirac included electron exchange contributions to the Thomas-Fermi functional but then, it still suffered from electron correlation effects [86]. Two elegant theorems by Hohenberg and Kohn [87], which made the Thomas-Fermi model and similarly the Hartree theory exact, brought DFT theory to the forefront of electronic structure theory [88-94]. Here is a short description of density functional theory starting with Born-Oppenheimer nonrelativistic approximation.

2.2 Theory

For an isolated system with N electrons in the Born-Oppenheimer nonrelativistic approximation, is given by

$$H\Psi = E\Psi \tag{2.1}$$

Where H is the Hamiltonian in atomic units,

$$H = \sum_{i=1}^{N} (-\frac{1}{2}\nabla_i^2) + \sum_{i=1}^{N} v(r_i) + \sum_{i<j}^{N} \frac{1}{r_{ij}} \tag{2.2}$$

in which

$$v(r) = -\sum_{\alpha} \frac{Z_\alpha}{|r_i - R_\alpha|} \tag{2.3}$$

is the "external" potential due to nuclei of charges Z_α acting on the i^{th} electron. E is the electronic energy and $\Psi = \Psi(x_i, x_2, ..., x_n)$ is the many-electron wave function, where x_i denote the particle coordinates and spins. It has been an important goal of physics to solve this many particle problem for a few decades. Generally speaking, there are two approaches. One is to consider the many-electron wave function $\Psi(x_i, x_2, ..., x_n)$. In the Hartree approximation [95], in which the many-electron wave function is constructed from the product of single particle functions,

$$\Psi(x_i, x_2, ..., x_n) = \Psi_1(x_1)\Psi_2(x_2)...\Psi_n(x_n) \tag{2.4}$$

Each of the functions $\Psi_1(x_1)$ satisfies a one-electron Schrödinger equation with a potential term arising from the average field of the other electrons,

$$\left[-\frac{h^2}{2m}\nabla^2 + V_{ext} + \Phi_i\right]\Psi_i(x) = \varepsilon_i \Psi_i(x) \tag{2.5}$$

where the Coulomb potential Φ_i is given by Poisson's equation

$$\nabla^2 \Phi_i = 4\pi e^2 \sum_{j=1, i \neq j}^{N} | \Psi_j |^2 \qquad (2.6)$$

and V_{ext} is the potential due to the nuclei. Considering Pauli Exclusion Principle, the simple product wave function can be replaced by a single determinantal function, which leads to the so-called Hartree-Fock approximation [96-97]. The inclusion of Fermi statistics which introduces an additional, nonlocal exchange term in the Schrödinger equation improves the total energy calculation, but the single particle picture, with the wave function described in terms of orbital with particular spins and occupation numbers is unchanged. It has noted that a single configuration (Slater determinant) wave function must inevitably lead to a poor energy since the lowest-lying configuration is generally only one of very many with comparable energies, and a better approximation would result from taking a linear combination [98]. This approach known as "configuration interaction" (CI) includes the correlation effects beyond Hartree-Fock approximation by improving the many-particle wave functions. In principle, CI provides an exact solution of the many-electron problems. In practice, however, the explosive increase in the number of configurations with increasing electron number limits its application to only small systems with relatively few electrons. Furthermore, the complexity of the resulting solutions means that a simple interpretation of the results is often difficult.

An alternative approach which is originated from the Thomas-Fermi model [84-85] is based on the density of electrons in the system, n(r),

$$n(r) = N \int dr_2 ... \int dr_n \Psi^*(r_1, r_2, ..., r_n) \Psi(r_1, r_2, ..., r_n). \qquad (2.7)$$

The Thomas-Fermi model assumes that the motions of the electrons are uncorrelated and that the corresponding kinetic energy can be described by a local approximation based on the results for uniform electron gas, $[n(r)]^{5/3}$. Shortly after, Dirac [86] proposed that exchange effects can be included by incorporating a term derived from the exchange energy density in a homogenous system. The exchange potential in a system of variable density could be

approximated by a term with a local dependence ~ $[n(r)]^{1/3}$ on electron density. In fact, this dependence on the density is a consequence of the concept of the "exchange" or "Fermi" hole, i.e., the region near an electron is avoided by electrons of the same spin, and not on the exchange potential in a homogenous system. The Thomas-Fermi model provided a prototype for modern density functional theory based upon two Hohenberg-Kohn theorems [87].

Note that the Hamiltonian in (2.2) contains the number of electrons N and the external potential $v(r)$. Hence, N and $v(r)$ will determine all properties for the ground state. In place of N and $v(r)$, the first two Hohenberg-Kohn theorem legitimizes the use of electron density $n(r)$ as the basic variable. It states: *The external potential $v(r)$ is determined, within a trivial additive constant, by the electron density $n(r)$.*

The proof is rather straightforward. Consider the electron density $n(r)$ for the nondegenerate ground state of some N-electron system. It determines the number of electrons by

$$\int n(r)dr = N \tag{2.8}$$

If $n(r)$ also determines $v(r)$, it follows that $n(r)$ determines the ground-state wave function Ψ and hence all other electronic properties of the system. Suppose that there were two external potentials v and v_1 differing by more than a constant, each giving the same $n(r)$ for its ground state, we would then have two Hamiltonians H and H_1 whose ground-state densities were the same although the normalized wave functions Ψ and Ψ_1 would be different,

$$H\Psi = E\Psi \tag{2.9}$$

$$H_1\Psi_1 = E_1\Psi_1 \tag{2.10}$$

E and E_1 are the ground-state energies for H and H_1 respectively. Therefore, the expectation value of H in Ψ_1 would be greater than E, namely,

$$E < \langle \Psi_1 | H | \Psi_1 \rangle = \langle \Psi_1 | H + H_1 - H_1 | \Psi_1 \rangle$$

$$= \langle \Psi_1 | H_1 | \Psi_1 \rangle + \langle \Psi_1 | H - H_1 | \Psi_1 \rangle \quad (2.11)$$

$$= E_1 + \int n(r)[v(r) - v_1(r)]dr$$

Similarly, the expectation value of H_1 in Ψ would be greater than E_1,

$$E_1 < \langle \Psi | H_1 | \Psi \rangle = \langle \Psi | H_1 + H - H | \Psi \rangle$$

$$= \langle \Psi | H | \Psi \rangle + \langle \Psi | H - H_1 | \Psi \rangle \quad (2.12)$$

$$= E + \int n(r)[v(r) - v_1(r)]dr$$

Adding (2.11) and (2.12), we obtain

$$E + E_1 < E_1 + E \quad (2.13)$$

This is a contradiction, and so there cannot be two different external potentials that give the same ground-state densities.

Thus, $n(r)$ determines both N and v and hence all properties of the ground state. Therefore, the ground state total energy can be written as a functional of the electron density,

$$E[n] = T[n] + V_{ne}[n] + V_{ee}[n] = \int n(r)v(r)dr + F_{HK}[n] \quad (2.14)$$

where $T[n]$ is the kinetic energy, $V_{ne}[n]$ is the nuclei-electron interaction energy and $V_{ee}[n]$ is the electron-electron Coulomb interaction energy and $F_{HK}[n]$ is a universal functional of $n(r)$ in a sense that $F_{HK}[n]$ is defined independently of the external potential $v(r)$,

$$F_{HK}[n] = T[n] + V_{ee}[n] \quad (2.15)$$

The second Hohenberg-Kohn theorem states: *For a trial density* $n_1(r)$, *such that* $n_1(r) \geq 0$ *and* $\int n_1(r)dr = N$,

$$E_0 \leq E[n_1] \quad (2.16)$$

where $E[n_1]$ *is the energy functional of (2.14).*

This theorem gives the energy variational principle. It means that the ground-state electron density is the density that minimizes $E[n]$. The proof is as follows. Since the first theorem assures that $n_1(r)$ which determines its own v_1, Hamiltonian H_1, and wave function Ψ_1, can be taken as a trial function for the Hamiltonian H of interest with external potential v. Thus,

$$\left\langle \Psi_1 \mid H \mid \Psi_1 \right\rangle = \int n_1(r)v(r)dr + F_{HK}[n_1] = E[n_1] \geq E[n] \tag{2.17}$$

The variational principle (2.16) requires that the ground-state density satisfy the following stationary principle,

$$\delta\left\{E[n] - \mu\left[\int n(r)dr - N\right]\right\} = 0 \tag{2.18}$$

which gives the Euler-Lagrange equation

$$\mu = \frac{\delta \mathrm{E}[n]}{\delta n(r)} = v(r) + \frac{\delta F_{HK}[n]}{\delta n(r)} \tag{2.19}$$

The quantity μ is the chemical potential.

If we knew the exact $F_{HK}[n]$ (2.18) would be an exact equation for the ground-state density. Once we have an explicit form either approximate or accurate for $F_{HK}[n]$, we can apply this method to any system. Equation (2.19) is the basic working equation of density-functional theory. However, accurate computational implementations of the density-functional theory are far from easy to achieve, because of the unfortunate fact that is hard to obtain the explicit form of the functional $F_{HK}[n]$. Although the Hohenberg-Kohn theorems do not give insights of actual methods of calculation, and it is usually $v(r)$ rather than $n(r)$ that is known, that is known, they provide confidence that it is sensible to seek solutions of many-body problems based on the density rather than the wave functions.

Early attempts to approximate the universal functional $F_{HK}[n]$ used the Thomas-Fermi approximation for the kinetic component $T[n]$. It was soon realized that only very crude answers can be obtained with this local functional for the kinetic energy, no matter how sophisticated the approximation for the $V_{ee}[n]$ component is. Kohn and Sham therefore proposed a highly nonlocal functional giving the major part of the kinetic energy and the scheme makes the density functional theory practical. They invoked a noninteracting reference system, with the Hamiltonian,

$$H_s = \sum_i^N (-\frac{1}{2}\nabla_i^2) + \sum_i^N v_{eff}(r_i) \tag{2.20}$$

For which the ground-state electron density is exactly $n(r)$. There will be an exact determinantal ground-state wave function for this system.

$$\Psi_s = \frac{1}{\sqrt{N!}} \det[\Psi_1 \Psi_2 ... \Psi_n] \tag{2.21}$$

where the Ψ_i are the N lowest eigenstates of the one-electron Hamiltonian h_s:

$$h_s \Psi_i = \left[-\frac{1}{2}\nabla^2 + v_{eff}(r)\right]\Psi_i = \varepsilon_i \Psi_i \tag{2.22}$$

and

$$n(r) = \sum_i^N \sum_s |\Psi_i(r,s)|^2 \tag{2.23}$$

The kinetic energy is then given by $T_s[n]$,

$$T_s[n] = \sum_{i=1}^N \left\langle \Psi_i \left| -\frac{1}{2}\nabla^2 \right| \Psi_i \right\rangle \tag{2.24}$$

This is the kinetic energy of the independent electrons (i.e. electrons without mutual Coulomb repulsion) in their ground state, under the action of an external potential such that their ground state density is $n(r)$. Then the universal functional can now be rewritten as

$$F_{HK}[n] = T[n] + V_{ee}[n]$$

$$= T_s[n] + J[n] + \left(T[n] - T_s[n] + V_{ee}[n] - J[n]\right)$$

$$= T_s[n] + J[n] + E_{xc}[n] \tag{2.25}$$

where $J[n]$ is the classical Coulomb interaction energy,

$$J[n] = \frac{1}{2}\int \frac{n(r)n(r')}{|r-r'|} dr dr' \tag{2.26}$$

while the defined quantity

$$E_{xc}[n] \equiv T[n] - T_s[n] + V_{ee}[n] - J[n] \tag{2.27}$$

is called the exchange-correlation energy. Here, we note that $T_s[n]$ is not the true kinetic energy of the interacting system whose ground state density is $n(r)$, but in the final optimized description it is much closer to the kinetic energy $T[n]$ than the Thomas-Fermi kinetic energy. The exchange correlation energy $E_{xc}[n]$ includes two parts of contributions: one is from the non-classical effects of the electron-electron interactions and the other is from the kinetic energy. The Euler equation now becomes

$$\mu = v_{eff}(r) + \frac{\delta T_s[n]}{\delta n(r)} \tag{2.28}$$

where the Kohn-Sham effective potential is defined by

$$v_{eff}(r) = v(r) + \frac{\delta J[n]}{\delta n(r)} + \frac{\delta E_{xc}[n]}{\delta n(r)} \tag{2.29}$$

$$= v(r) + \int \frac{n(r')}{|r-r'|} dr' + v_{xc}(r)$$

which the exchange-correlation potential

$$v_{xc}(r) = \frac{\delta E_{xc}[n]}{\delta n(r)} \tag{2.30}$$

The Kohn-Sham computational scheme for DFT is shown in the flowchart in figure 2.1. As we can see from equation (2.29) that the effective potential v_{eff} is also a functional of the electron density, such that equations (2.22) to (2.30) have to be solved self-consistently. We can start with a guessed density $n_0(r)$ which is usually constructed from the atomic wave functions. Then calculate the effective potential v_{eff} through equation (2.29) and use it in equation (2.22) to solve the single-electron Schrödinger equation. A new electron density $n(r)$ will be formed from equation (2.23). Once the convergent requirement is achieved, we can compute the total energy from equations. (2.14, 2.24 to 2.27).

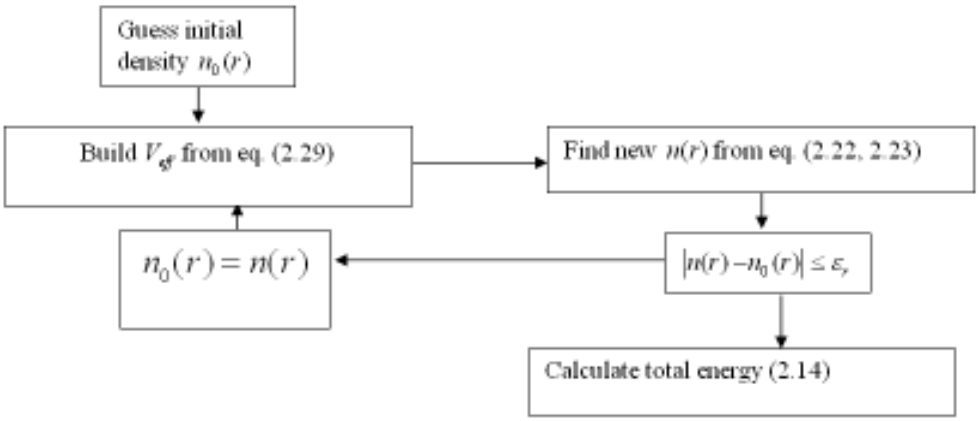

Figure 2.1 Flowchart for DFT calculations

The single Euler equation (2.22) has the same form as the Hartree equation but includes a more general local effective potential that incorporates the exchange and correlation interactions between electrons. Therefore, the computational efforts to solve the Kohn-Sham equations will be the same as to solve the Hartree equations and significantly less than to solve the Hartree-Fock equations, which, by definition lack of correlation effects. In principle, the Kohn-Sham equations will yield exact ground state properties if exact exchange correlation potential is given. However, the Kohn-Sham scheme does not provide methods to obtain the

explicit exchange and correlation functionals and therefore, approximations have to be considered.

There are basically three distinct approximations in DFT to the exchange correlation functionals, namely, the local density approximation (LDA), the generalized gradient approximation (GGA) and the hybrid approximation.

2.2.1. Local Density Approximation

This local density approximation was proposed by Kohn and Sham. They showed that it could be applied to the limiting case of a slowly varying density [89].

$$E_{xc}^{LDA}[n] = \int n(r)\varepsilon_{xc}(n)dr \tag{2.31}$$

where $\varepsilon_{xc}(n)$ is the exchange and correlation energy per particle of a uniform electron gas of density $n(r)$. The functional derivative of $E_{xc}^{LDA}[n]$ gives the local approximation to the Kohn-Sham exchange-correlation potential

$$v_{xc}^{LDA}(r) = \frac{\delta E_{xc}^{LDA}}{\delta n(r)} = \varepsilon_{xc}(n(r)) = n(r)\frac{\delta \varepsilon_{xc}(n)}{\delta n} \tag{2.32}$$

The Kohn-Sham equation becomes

$$\left[-\frac{1}{2}\nabla^2 + v(r) + \int \frac{n(r')}{|r-r'|}dr' + v_{xc}^{LDA}(r)\right]\Psi_1 = \varepsilon_i \Psi_i \tag{2.33}$$

$$\varepsilon_{xc}(n) = \varepsilon_x(n) + \varepsilon_c(n) \tag{2.34}$$

where $\varepsilon_x(n)$ is the exchange energy per particle of a homogenous electron gas,

$$\varepsilon_{xc}(n) = -\frac{3}{4}\left(\frac{3}{\pi}\right)^{1/3} n(r)^{1/3} = -\frac{0.4582}{r_s} \tag{2.35}$$

and $\varepsilon_c(n)$ is the correlation energy per particle of a homogenous electron gas,

$$\varepsilon_c(n) = \frac{1}{2}\left(\frac{g_0}{r_s} + \frac{g_1}{r_s^{3/2}} + \frac{g_2}{r_s^{2}} + \ldots\right) \qquad \text{for } r_s >> 1 \tag{2.36}$$

Here r_s is the Wigner-Seitz radius,

$$\frac{4}{3}\pi r_s^3 = \frac{1}{n} \tag{2.37}$$

The Kohn-Sham-LDA is further extended to the spin dependent case by replacing the scalar external potential $v(r)$ by a spin dependent potential $v_{\alpha\beta}(r)$ and replacing the charge density $n(r)$ by the density matrix $n_{\alpha\beta}(r)$ [99-101]. The electron densities with spin projection up $n_\alpha(r)$ and down $n_\beta(r)$ are treated separately. Similarly, one can deal with $n(r) = n_\alpha(r) + n_\beta(r)$, along with the polarization $\zeta(r) = \left[n_\alpha(r) - n_\beta(r)\right] / n(r)$. ζ takes values between -1 (fully polarized downwards) and +1 (fully polarized upwards). The spin-up and spin-down densities are generated from the spin-up and spin-down Kohn-Sham wave functions. This so-called local spin density (LSD) approximation improved LDA for atomic and molecular systems with unpaired spins.

LDA and its spin generalization LSD allow one to use the knowledge of the uniform electron gas to predict properties of the in homogenous electron gases occurring in atoms, molecules and solids. The success and importance of LDA and LSD computational schemes in the solid state computations can hardly be exaggerated. Specifically, LSD usually has moderate accuracy for most systems of interest, making errors of order 5-10%. It's most remarkable feature is it's reliability, making the same kinds of errors on every system it's applied to. The success of LDA and LSD is attributed to the fact that the exchange-correlation hole $n_{xc}^{LDA}(r_1, r_2)$ is spherically symmetric and it obeys the sum rule which corresponds to the fact that, if an electron has been found at r_1, then there is one less electron left to find elsewhere (i.e , by integral over all r_2),

$$\int n_{xc}^{LDA}(r_1, r_2) dr_2 = -1 \tag{2.38}$$

where the exchange-correlation hole $n_{xc}^{LDA}(r_1, r_2)$ is defined by

$$V_{ee} = \iint \frac{1}{r_{12}} n_2(r_1, r_2) dr_1 dr_2 = J[n] + \frac{1}{2} \iint \frac{1}{r_{12}} n(r_1) n_{xc}^{LDA}(r_1, r_2) dr_1 dr_2 \quad (2.39)$$

with $J[n]$ being the classical Coulomb interaction. This is true because for every r_1, $n_{xc}^{LDA}(r_1, r_2)$ is the exact exchange-correlation hole of a homogenous electron gas with density $n(r_1)$. Hence, the LDA and LSD describe the total charge of $n_{xc}^{LDA}(r_1, r_2)$ correctly.

2.2.2. Generalized Gradient Approximation

Since the LDA formula for E_{xc} is formally justified for systems with slow varying densities, it seemed natural to seek gradient corrections to E_{xc}^{LDA} by the gradient expansion approximation (GGA), which expands the functional in a Taylor series in gradients of the density [102].

$$E_{xc}^{GEA}[n_\alpha, n_\beta] = E_{xc}^{LSD}[n_\alpha, n_\beta] + \sum_{\alpha\beta} \int C_{\alpha\beta}(n_\alpha(r), n_\beta(r)) \frac{\nabla n_\alpha(r)}{n_\alpha^{2/3}} \cdot \frac{\nabla n_\beta(r)}{n_\beta^{2/3}} d^3 r \quad (2.40)$$

However, GGA does not give better energy than LDA for systems such as atom and molecule. The reasons can be summarized as (1) GGA exchange-correlation hole improves the LDA hole only at short separations, but is poorly damped and oscillatory at large separations, and (2) GGA violates the sum rule of the exchange-correlation hole. Accordingly, Perdew and others introduced the so-called generalized gradient approximation [103-107] such that the exchange correlation energy can be written as a functional of both the density and its gradient:

$$E_{xc}^{GGA}[n_\alpha, n_\beta] = \int d^3 r f(n_\alpha(r), n_\beta(r), \nabla n_\alpha(r), \nabla n_\beta(r)) \quad (2.41)$$

The first modern GGA proposed the idea of truncating the gradient expansion for the exchange-correlation hole. Considering the problems encountered by GGA, Perdew *et al*. [107,108] proposed several versions of GGA functional by introducing the real-space cutoff procedure on the hole, which restores the sum rule or the normalization and negativity conditions on the GGA

hole and generates a short-ranged hole whose angular and system average was much closer to the true hole. The Perdew-Wang 1991 (PW91) GGA functional [108] incorporates no free parameters and is entirely determined from uniform electron gas properties and extract constraints. The Perdew-Burke-Ernzerhof [107] functional is a simplified and refined version of the PW91 functional. Becke [99] derived an exchange functional known as B88 incorporating the known behavior of the exchange hole at large distances outside a finite system. Lee, Yang and Parr [104] obtained the correlation energy as an explicit functional of the density and its gradient and Laplacian, now generally known as the "LYP" functional.

The well-known GGA functionals systematically improve the LDA and, in some calculations, approach the accuracy of traditional quantum chemical (e.g. Configuration Interaction) methods, at much less computational cost. However, according to the quasilocal nature of GGA, the dispersion or long-ranged van der Waals interaction arising from long-ranged correlated electronic density fluctuations in the weak bonding systems such as noble gas dimmers could not be accurately described by either LDA or GGA. On the other hand, similar to LDA, GGA has the difficulty to describe the hole centered for from the electron causing the hole.

2.2.3. Hybrid Density Functional Method

Considering the local or semi local nature of LDA and GGA, Becke proposed the so-called Hybrid Density Functional method which incorporates the exact treatment of exchange by Hartree-Fock theory with DFT approximations for dynamical correlation. This idea was motivated by re-examination of the adiabatic connection,

$$H_\lambda = T + \lambda V_{ee} + \sum_i v_\lambda(r_i) \qquad (2.42)$$

where λ is an inter-electronic coupling-strength parameter that "switches on" the $1/r_{12}$ Coulomb repulsion between electrons. $\lambda = 0$ Corresponds to the non-interacting Kohn-

Sham reference system, while $\lambda = 1$ corresponds to the fully interacting real system, with $n(r)$ being fixed as the exact ground state density of H_λ. The $E_{xc}[n]$ can be written as

$$E_{xc}[n] = \int_0^1 d\lambda U_{xc}^{\lambda}[n] \tag{2.43}$$

where,

$$U_{xc}^{\lambda}[n] = \left\langle \Psi_n^{\lambda} \mid V_{ee} \mid \Psi_n^{\lambda} \right\rangle - J[n] \tag{2.44}$$

The obvious first approximation for the λ dependence of the integrated in equation (2.43) is a linear interpolation, resulting in the Becke's half-and-half functional:

$$E_{xc}^{h\&h}[n] = \frac{1}{2}\left(U_{xc}^{0} + U_{xc}^{1}\right) \tag{2.45}$$

where U_{xc}^{o} is the exact exchange energy of the KS determinant and U_{xc}^{1} is the potential energy contribution to the exchange-correlation energy of the fully interacting system. This half and half functional has the merit of having a finite slope as $\lambda \to 0$, and becomes exact if $E_{xc,\lambda=1}^{DFT}$ is exact and the system has high density. However, its does not provide a good quality of the total energy and the uniform gas limit is not obtained. Due to this Becke proposed the semi-empirical generalization of 3-parameter hybrid exchange-correlation functional

$$E_{xc}^{B3} = E_{xc}^{LSDA} + a_o(E_x^{exact} - E_x^{LSDA}) + a_x \Delta E_x^{GGA} + a_c \Delta E_c^{GGA} \tag{2.46}$$

where a_o, a_x and a_c are semiempirical coefficients to be determined by an appropriate fit to experimental data. E_x^{exact} is the exchange energy of the Slater determinant of the Kohn-Sham orbitals. ΔE_x^{GGA} is the gradient correction for the exchange and ΔE_c^{GGA} is the gradient correction for the correlation.

2.3 Computational Details

One of the primary considerations involved in these calculations is the determination of the methodology scheme which can efficiently reproduce the geometric and electronic details

with a high degree of accuracy and low computational overhead. Therefore all of our first principles calculations have been performed using hybrid density functional theoretical formalism incorporating HF exchange with DFT exchange-correlation functional. Specifically we have we used the hybrid functional B3LYP [101, 104] and the Los Alamos National Laboratory double-ζ basis set (LANL2DZ) [109] as implemented in the Gaussian 03 suite of programs [110]. For the Si and Ge atoms, the Hay–Wadt pseudo-potential [109] and the associated basis set are used for the core (for Si 1s, 2s, 2p and for Ge 1s, 2s, 2p, 3s, 3p, 3d) and the valence electrons, respectively. For the C atom, the all electron Dunning–Huzinaga double-ζ basis set is employed [109] (See tables 2.1 to 2.5 for the basis set parameters used for Si, Ge, and C atoms).

Since all calculations were performed using the Gaussian 03 suite of programs, we briefly describe below, using flow charts, how Gaussian 03 works:

1. Start with a guess density ρ_0 (usually the superposition of neutral atomic densities is used).

2. Establish grid for charge density and exchanger correlation potential

3. Compute Kohn-Sham matrix (equivalent to the F matrix in Hartree-Fock method) elements and overlap integrals matrix.

4. Solve the equations for expansion coefficients to obtain KS orbitals.

5. Calculate the new density ρ

7. If self-consistency in the charge density is reached, then go to step 8. Otherwise set $\rho_0 = \rho$ and go to step 1.

8. Calculate derivatives of energy vs. atom coordinates, and update atom coordinates. This may require denser integration grids and re computing of Coulomb and exchange-correlation potential.

9. If gradients are still large, or positions of nuclei moved appreciably, go to step 1.

10. Calculate properties and print results.

A typical flowchart for calculations in Gaussian 03 suite of programs is shown in figure 2.2.

To check the validity of the present theoretical scheme, calculations on Si, Ge and C atoms, Si_2, Ge_2, SiH, GeH, CH, and GeC dimers were performed and matched with experimental observations. For Si atom, the ionization potential and electronic affinity are 8.462 eV and 0.896 eV to be compared with the experimental values of 8.151 eV and 1.385 eV, respectively [111]. For Si dimers our bond length is 2.20 Å compared to the experimental value of 2.25 Å and for SiH our values are 1.547 Å in comparison with experimental value of 1.52 Å [111]. For Ge atom, the ionization potential and electron affinity are 8.01eV and 0.841eV to be compared with the experimental values of 7.9 eV and 1.233eV, respectively and for C atom, our values are 11.604eV and 0.789eV, and the experimental values are 11.262eV and 1.2eV, respectively [111]. A very large basis set is necessary for the theoretical electron affinity to approach the value of the experimental electron affinity and this was not considered to be necessary and computationally feasible for the large clusters representing the nanotubes studied in this work. For C-C dimer, our bond length is 1.34 Å and binding energy is 2.68eV compared to the experimental values of 1.31 Å and 3.145eV, respectively [111]. For Ge-Ge dimer, our values for bond length and binding energy are 2.52 Å and 1.17eV to be compared with the experimental values of 2.40 Å and 1.36eV, respectively [111]. For GeC dimer our values for the theoretical binding energy and bond lengths are 1.45eV and 1.98 Å to be compared with the experimental value for the binding energy of 2.38eV [111].

Table 2.1 Basis Functions for Silicon Atom

Exponents (α_i)	Coefficients (c_i)
s orbitals	
1.2220000	-0.570733903
0.2595000	1.2823826070
0.0931100	1.0000000000
p orbitals	
2.5800000	-0.0777249974
0.2984000	1.0197869670
0.0931100	1.0000000000

Table 2.2 Basis Functions for Germanium Atom

Exponents (α_i)	Coefficients (c_i)
s orbitals	
0.8935000	-2.175659078
0.4424000	2.449346675
0.1162000	1.000000000
p orbitals	
0.1877000	-0.1006778966
0.2623000	1.0306255650
0.7980000	1.0000000000

Table 2.3 Hay- Wadt Pseudopotentials for Silicon Atom

n_k	ζ_k	d_k
d potential		
1	505.3138	-10.0000
2	103.2221	-84.9236
2	23.4569	-30.3299
2	6.7506	-12.1049
2	2.1603	-1.8945
s-d potential		
0	689.4911	3.0000
1	114.1729	60.5207
2	35.7424	201.3086
2	9.4530	65.9400
2	2.2544	19.0301
p-d potential		
0	88.9379	5.000
1	76.7774	6.6414
2	56.1481	247.5972
2	21.1874	129.3715
2	6.8277	47.4617
2	2.1001	11.7377

Table 2.4 Hay- Wadt Pseudopotentials for Germanium Atom

n_k	ζ_k	d_k
f potential		
1	318.2167583	-28.00000000
2	61.5370967	-180.98916760
2	13.2986899	-55.00439090
2	3.8985215	-19.79065260
2	1.2137666	-1.85335720
s-f potential		
0	205.1886932	3.00000000
1	68.9790278	65.22625580
2	27.9194879	225.23545220
2	8.5481650	94.01254720
2	2.3173734	29.94150050
p-f potential		
0	33.2488002	5.00000000
1	15.7777247	23.47781570
2	14.9260722	45.09804140
2	5.8416394	56.33269570
2	1.8349575	16.60586400
d-f potential		
0	42.0206343	3.00000000
1	19.2096363	23.73715180
2	9.4133917	56.47922490
2	3.3282907	25.89018350
2	0.8522331	3.02298360

Table 2.5 Dunning/Huzinaga Basis Set for Carbon Atom

Exponents (α_i)	Coefficients (c_i)
s orbitals	
4232.6100	0.002029
634.8820	0.015535
146.0970	0.075411
42.4974	0.257121
14.1892	0.596555
1.9666	0.242517
5.1477	1.000000
0.4962	0.542048
0.4533	0.517121
p orbitals	
18.1557	0.018534
3.9864	0.115442
1.1429	0.386206
0.3594	0.640089
0.1146	1.000000

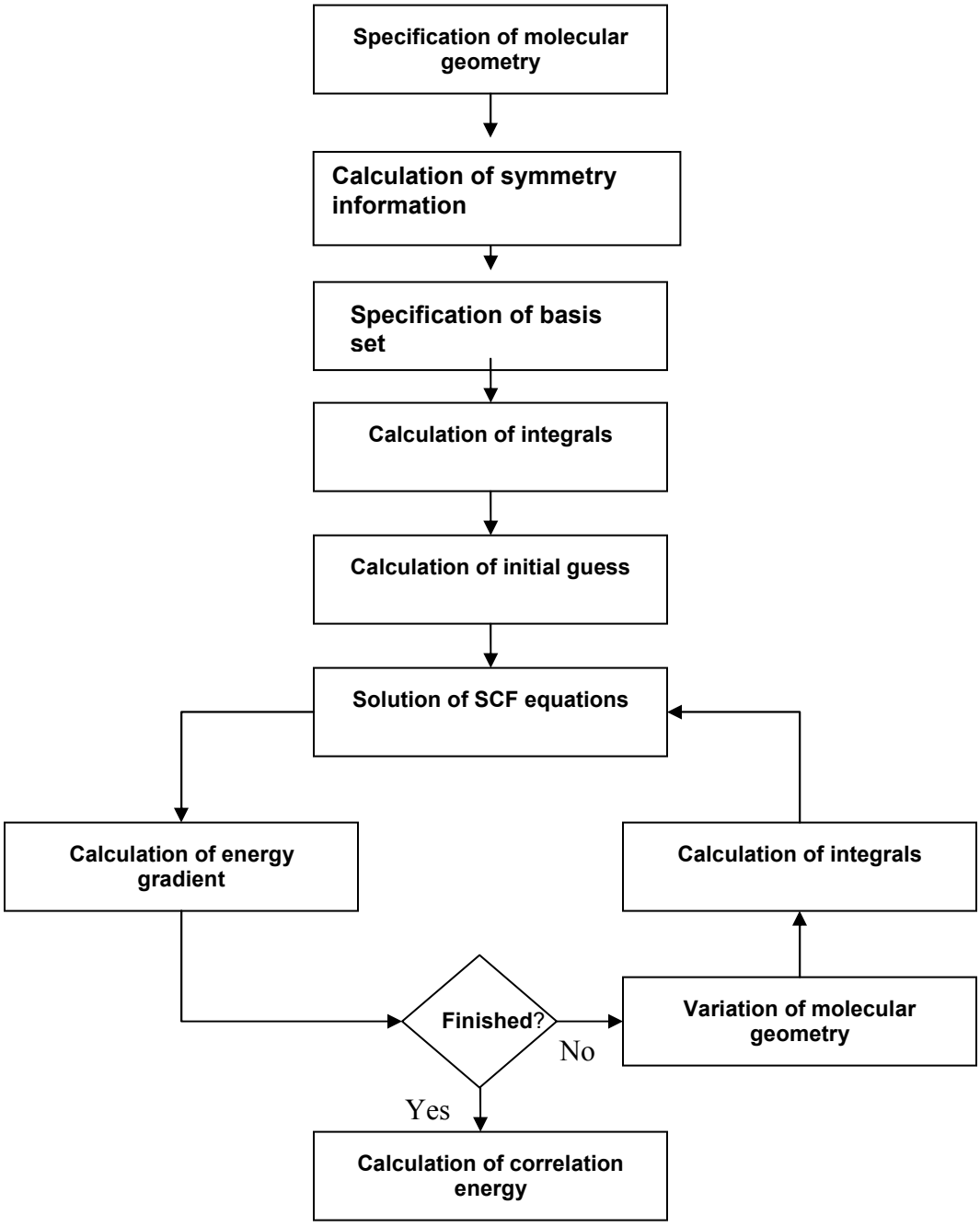

Figure 2.2 Flowchart for Gaussian 03 calculations.

The theoretical bond lengths obtained for GeH and CH are 1.63 Å and 1.14 Å as compared to the experimental values of 1.59 Å and 1.10 Å, respectively [111]. Thus, overall, our choices of hybrid density functional theory and the pseudopotential with the associated basis set can be considered to be quite satisfactory. All nanotubes have been hydrogen terminated at the two ends to saturate the dangling bonds and to simulate the effects of infinite tubes. All structures reported here are *geometry as well as spin optimized* using the *Gaussian '03* suite of programs [110] at the supercomputing center of the University of Texas at Arlington. The force convergence criterion was set to be 0.0001eV/Å.

CHAPTER 3

PURE SILICON AND GERMANIUM NANOTUBES

3.1 Construction of Nanotubes

The method of constructing SiNTs and GeNTs is entirely based on single walled CNT approach. It can be conceptualized by wrapping a graphite like sheet of Si or Ge to form a tubular cylindrical structure. Depending upon the number of layers used while wrapping we can get either single walled or multi walled nanotube. In the present report, the scope of our research is only limited to single walled cases. These nanotubes can be simply defined in terms of length and chirality. Diameter and length of the tube can be uniquely described in terms of the magnitude of the components of chiral vector $C_h = na_1 + ma_2$ with integers *n* and *m* (which denotes the number of unit vectors along two directions in the honeycomb crystal lattice of graphene sheet) and a and b are the unit vectors of a hexagonal, grapheme like sheet (figure 3.1). Now depending on these integers *n* and *m* there can be three different kinds of nanotubes. If *m*=0, the nanotubes are called zigzag. If *n*=*m*, the nanotubes are called armchair. Otherwise, they are called chiral. All of our nanotubes are hydrogen terminated at the two ends to saturate the dangling bonds.

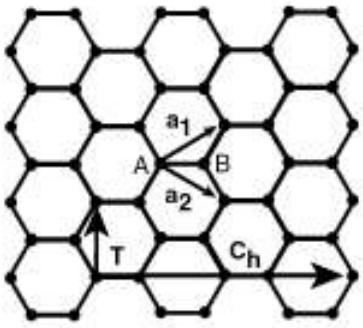

Figure 3.1 2D-graphene sheet with lattice vectors.

3.2 Results and discussions for pure Si nanotubes

In this section we present a detailed analysis of armchair (n, n), zigzag (n, 0) with n = 3 to 9 and chiral nanotubes with (n, m) with n = 2 to 6 and m = 1 to n-1 for pure SiNTs. As mentioned earlier all the nanotubes are spin as well as geometry optimized. Figures 3.2 to 3.4 show the different tube morphologies. In terms of diameter the smallest chiral nanotube studied is (2, 1) tube with stoichiometry $Si_{50}H_6$, and the largest structure is $Si_{342}H_{22}$ (6, 5), for zigzag nanotube smallest is $Si_{66}H_6$ (3, 0) and largest is $Si_{198}H_{18}$ (9, 0). In case of armchair nanotubes, the smallest structure is $Si_{60}H_{12}$ (3, 3) and largest is $Si_{180}H_{36}$ (9, 9). We have further divided chiral nanotubes into sub-groups depending on the chiral vector n, for example if n is 3 then m will have values 1 and 2 (from our definition of chiral nanotubes), so a sub-group of (3,1), (3,2) chiral tubes is formed. Similarly for n = 4 we have (4, 1), (4, 2), (4, 3) three chiral nanotubes under one sub-group and so on. While constructing the nanotubes initial bond lengths were assumed to be uniform throughout the tube. We know the fact that both carbon and silicon fall under the same group in the periodic table still their chemical behavior is quite different from each other. The reason to this difference is the type of hybridization they form. Carbon prefers sp^2 while silicon prefers sp^3 hybridization state. We have calculated the binding energy per atom using the formula:

$$E_C = \frac{1}{(a+b)}[aE(Si) + bE(H) - E(Si_a H_b)] \qquad (3.1)$$

where a and b are number of Si and H atoms respectively ,E(Si) and E(H) are ground state energies of Si and H atoms respectively and $E(Si_aH_b)$ is the total energy of the optimized clusters representing the nanotubes.

Tables 3.1 to 3.3 show the binding energies per atom for all different nanotubes. Average value of binding energy of armchair nanotubes is found to be 3.09 eV/ atom with the largest SiNT studied (9, 9) has value of 3.13 eV/atom which is about 68 % of the bulk binding energy of 4.63 eV/ atom.

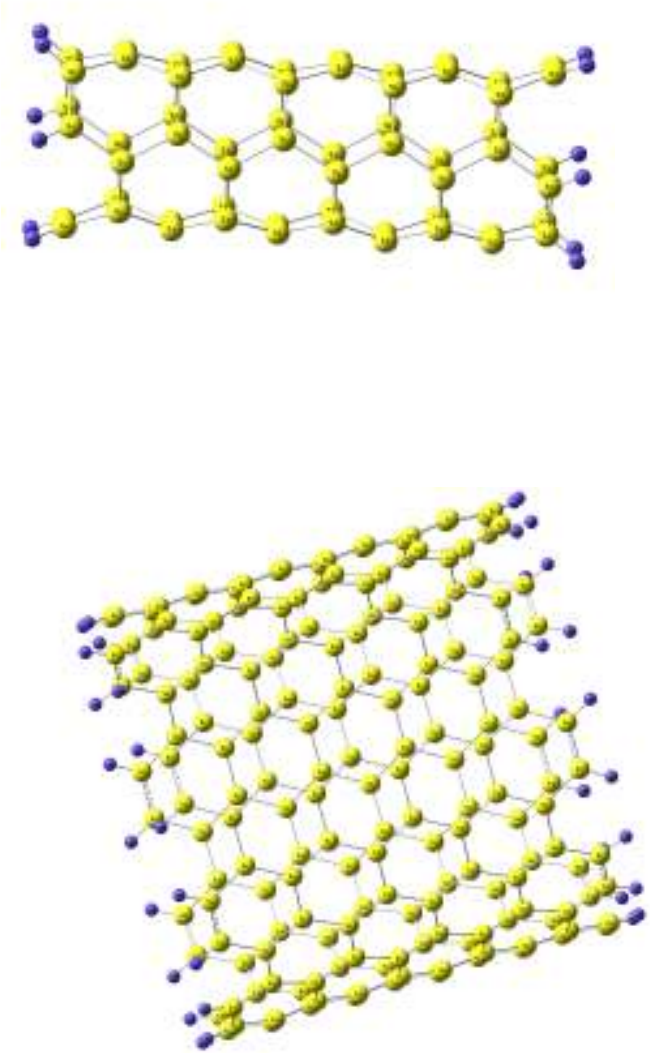

Figure 3.2 (Top) Smallest (3, 3) and (bottom) largest (9, 9) armchair Si nanotubes.

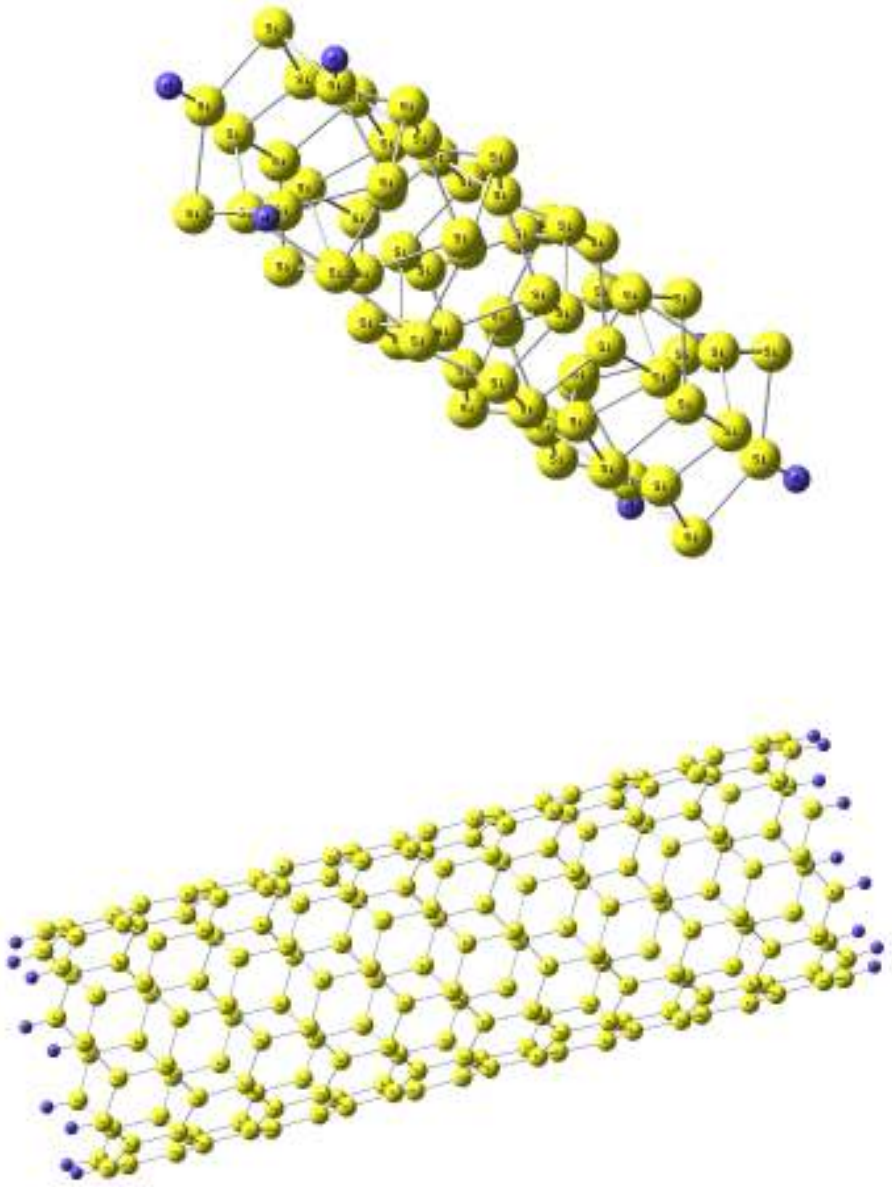

Figure 3.3 (Top) Smallest (3, 0) and (bottom) largest (9, 0) zigzag Si nanotubes.

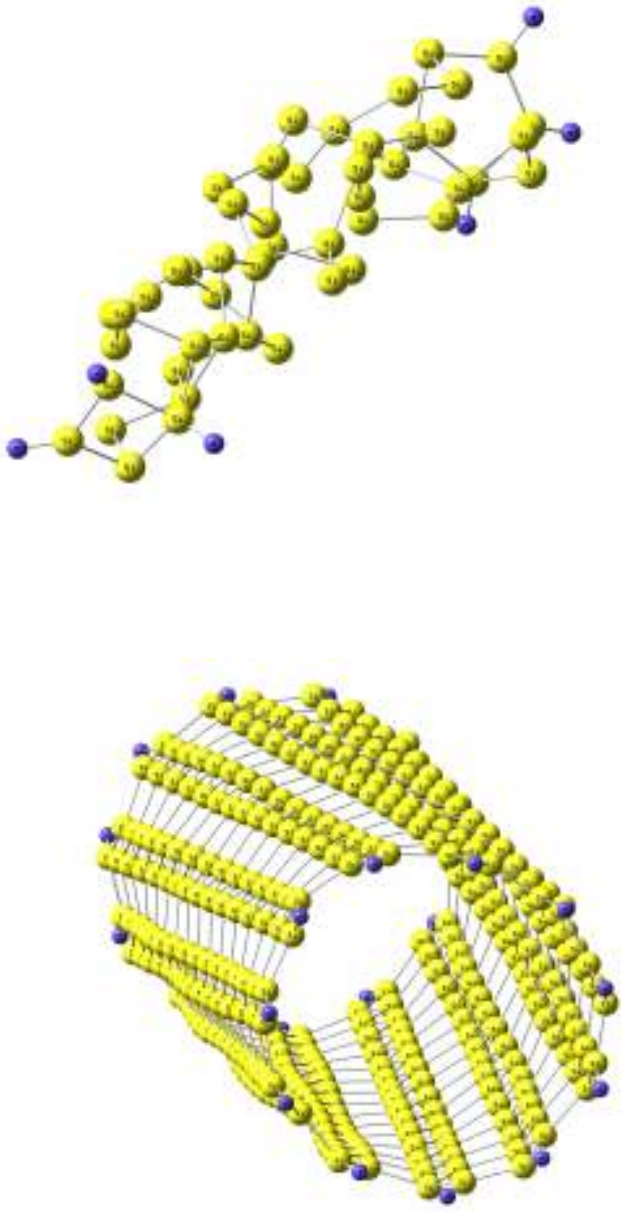

Figure 3.4 (Top) Smallest (2, 1) and (bottom) largest (6, 5) chiral Si nanotubes.

Table 3.1 Electronic States, Binding Energies Per Atom (E_b) in eV, HOMO-LUMO Gaps in eV, Diameters in Å, and Dipole Moments in Debye for Armchair Si Nanotubes.

Nanotube	Model	State	E_B(eV)	Gap(eV)	Diameter (Å)	Dip.Mnt (Debye)
(3,3)	$Si_{60}H_{12}$	$^1A_1$	2.981	0.933	6.737	0.000
(4,4)	$Si_{80}H_{16}$	$^1A_1$	3.058	0.937	8.984	0.105
(5,5)	$Si_{100}H_{20}$	$^1A_1$	3.095	1.028	11.229	0.008
(6,6)	$Si_{120}H_{24}$	^{1}A1	3.109	1.061	13.476	0.000
(7,7)	$Si_{140}H_{28}$	$^1A_1$	3.125	1.054	15.722	0.003
(8,8)	$Si_{160}H_{32}$	$^1A_1$	3.133	1.019	17.968	0.002
(9,9)	$Si_{180}H_{36}$	$^1A_1$	3.138	0.993	20.214	0.027

Table 3.2 Electronic States, Binding Energies Per Atom (E_b) in eV, HOMO-LUMO Gaps in eV, Diameters in Å, and Dipole Moments in Debye for Zigzag Si Nanotubes.

Nanotube	Model	State	E_B (eV)	Gap (eV)	Diameter (Å)	Dip.Mnt(Debye)
(3,0)	$Si_{66}H_6$	^3A_G	2.883	0.633	3.890	0.000
(4,0)	$Si_{88}H_8$	^3A_G	2.994	0.650	5.187	0.248
(5,0)	$Si_{110}H_{10}$	^{3}B	3.061	0.622	6.484	0.147
(6,0)	$Si_{132}H_{12}$	^{1}A	3.102	0.560	7.780	0.000
(7,0)	$Si_{154}H_{14}$	^3A_U	3.139	0.455	9.077	0.000
(8,0)	$Si_{176}H_{16}$	$^3A_2$	3.155	0.219	10.374	0.000
(9,0)	$Si_{198}H_{18}$	^{3}B	3.172	0.367	11.670	0.057

Table 3.3 Electronic States, Binding Energies Per Atom (E_b) in eV, HOMO-LUMO Gaps in eV, Diameters in Å, and Dipole Moments in Debye for Chiral Si Nanotubes.

Nanotube	Model	State	E_B (eV)	Gap (eV)	Diameter (Å)	Dip.Mnt (Debye)
(2,1)	$Si_{50}H_6$	$^1A_1$	2.813	0.949	3.431	1.878
(3,1)	$Si_{44}H_8$	$^1A_1$	2.940	0.956	4.675	0.822
(3,2)	$Si_{66}H_{10}$	$^1A_1$	2.966	0.454	5.652	0.471
(4,1)	$Si_{46}H_{10}$	$^1A_1$	2.941	1.041	5.942	0.275
(4,2)	$Si_{44}H_{12}$	$^1A_1$	2.952	0.847	6.862	0.000
(4,3)	$Si_{134}H_{14}$	$^1A_1$	3.103	1.068	7.887	0.969
(5,1)	$Si_{180}H_{36}$	$^1A_1$	3.07	0.462	7.219	20.930
(5,2)	$Si_{90}H_{14}$	$^1A_1$	3.064	0.615	8.098	0.022
(5,3)	$Si_{180}H_{16}$	$^1A_1$	3.144	0.141	9.077	0.023
(5,4)	$Si_{226}H_{18}$	$^1A_1$	3.169	1.039	10.127	0.300
(6,1)	$Si_{158}H_{14}$	$^1A_1$	3.133	0.580	8.503	9.739
(6,2)	$Si_{192}H_{16}$	$^1A_1$	3.151	0.129	9.351	0.000
(6,3)	$Si_{66}H_{18}$	$^1A_1$	3.031	1.159	10.292	0.024
(6,4)	$Si_{132}H_{20}$	$^1A_1$	3.129	0.512	11.304	0.192
(6,5)	$Si_{342}H_{22}$	$^1A_1$	3.217	0.890	12.369	0.687

In zigzag nanotubes the smallest structure (3, 0) gave a binding energy of 2.88 eV/atom and biggest structure (9, 0) yielded 3.17 eV/ atom. In case of chiral tubes as there are different sub-groups, we have considered the biggest structure among each group for binding energy analysis i.e. (2, 1), (3, 2), (4, 3), (5, 4), and (6, 5) nanotubes. Figures 3.5 to 3.10 show the per atom variations of binding energies of silicon with total number of atoms and nanotube diameter. Clearly from the figures 3.5 to 3.10 we can predict that the value of binding energies are attaining a saturation level as we increase the number of atoms or increase the diameter of the tube. The non-linearity in the energy relationship indicates that binding energy is not only purely dependent on diameter but also has contribution from the curvature of the tube. We believe that the binding energy per atom of extremely large nanotube will be close to that of graphene like sheet of Si.

As from tables 3.4 to 3.6 it is quite evident that there is a little variation in bond lengths of Si-Si atom in armchair, zigzag and chiral nanotubes. Figures 3.11 to 3.13 show the tube diameter variation with number of atoms. Considering the case of (7, 7) armchair nanotube the Si-Si bond lengths vary from 2.188 Å to 2.666 Å throughout the tube. For (4, 0) zigzag nanotube average bond lengths vary from 2.230 Å to 2.332 Å, and in chiral (4, 3) they vary from 2.177 Å to 2.314 Å. A detailed analysis shows that bond lengths show more alternations on the edges than the middle part of tube. The average optimized bond length remains almost constant in case of armchair nanotubes except the smallest structure (3, 3) (bond lengths expanded). There is a decreasing pattern in case on zigzag nanotubes and bond lengths get shortened also. Same pattern is observed in the case of chiral nanotubes. The diameters of 7.62 Å and 10.11 Å for (6, 0) and (8, 0) respectively, are not much different from 7.44 Å and 9.22 Å as reported by Fagan *et al*. [51] and 7.48 A and 9.96 Å by Barnard and Russo [54] in their papers. Looking at overall trend, the SiNTS bond lengths gets contracted after the geometry is optimized. Over all if we compare the structural trends of different SiNTs with CNTS, we find that the bond length alternations are more pronounced and hence, there is a weak π-π bonding and a tendency of

bond delocalization exists in SiNTs and which accounts for the corrugated tubular shapes of armchair, zigzag and chiral nanotubes.

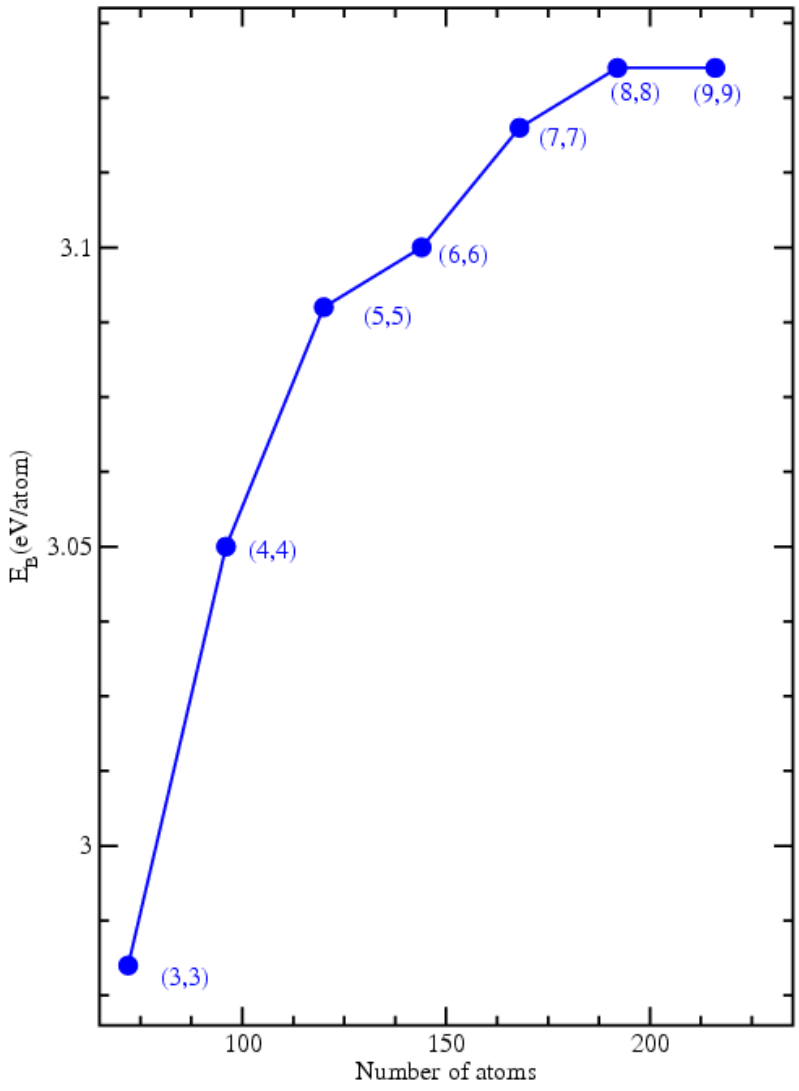

Figure 3.5 Binding energy as a function of the total number of atoms in the Si armchair nanotubes.

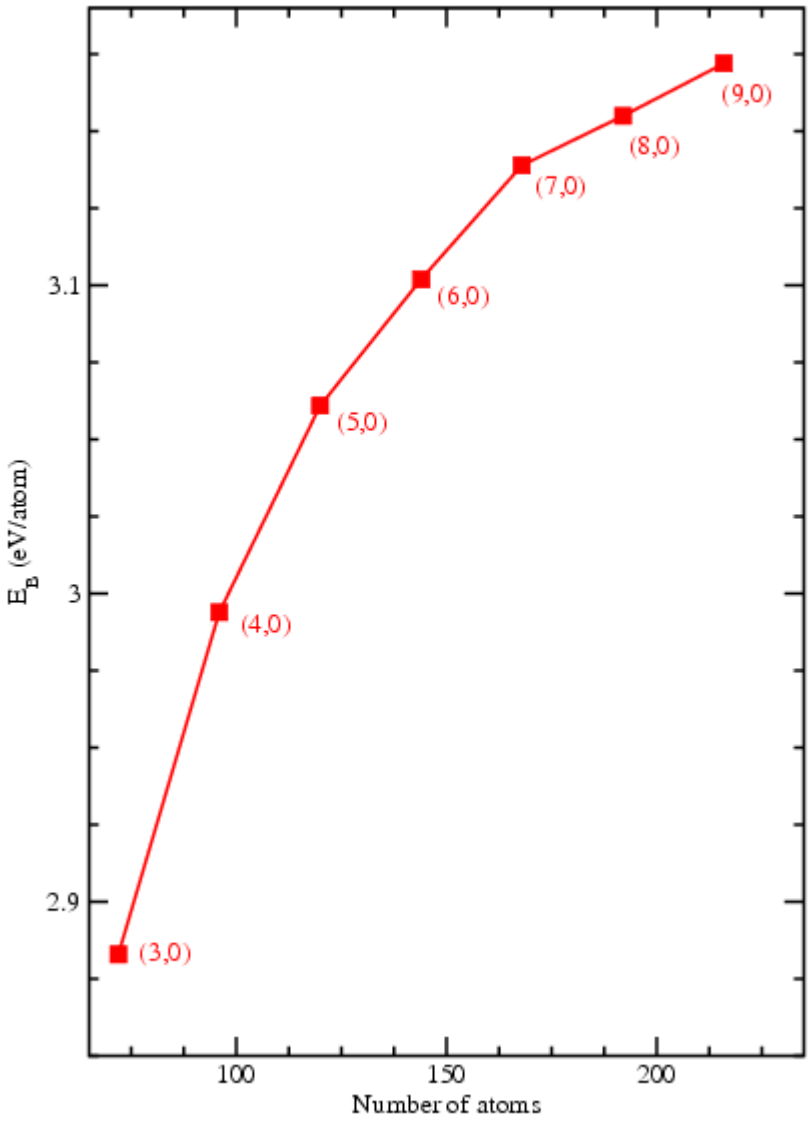

Figure 3.6 Binding energy as a function of the total number of atoms in the Si zigzag nanotubes.

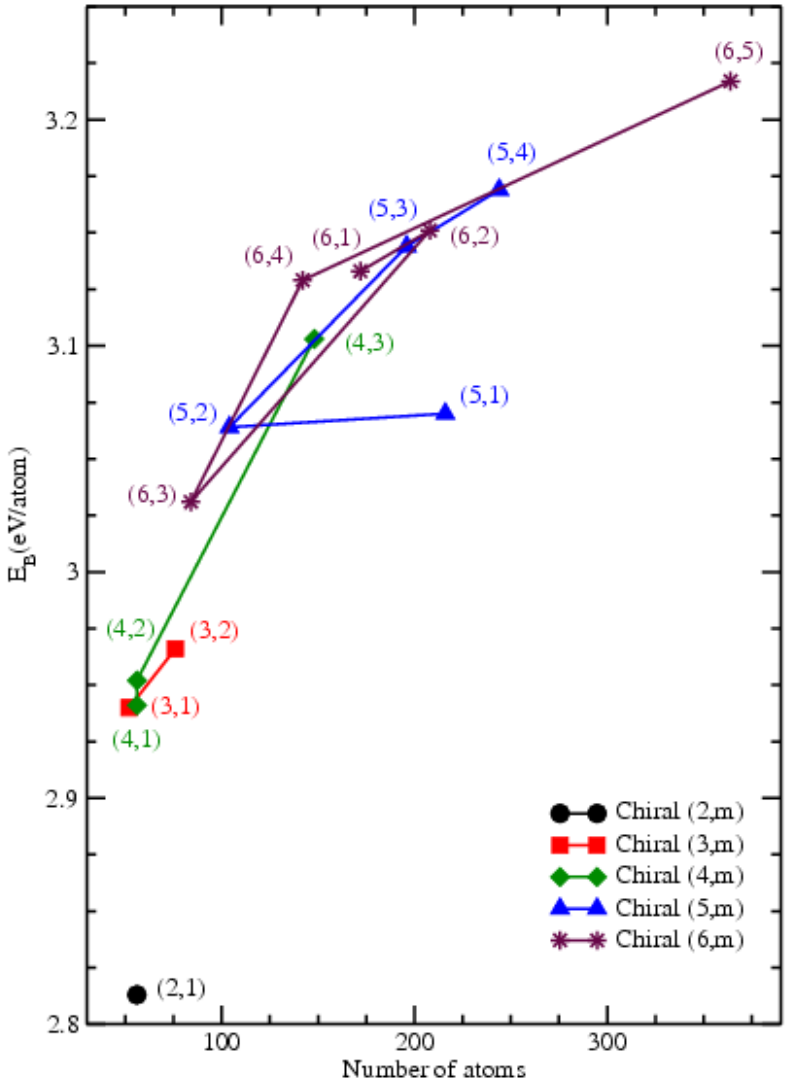

Figure 3.7 Binding energy as a function of the total number of atoms in the Si chiral nanotubes.

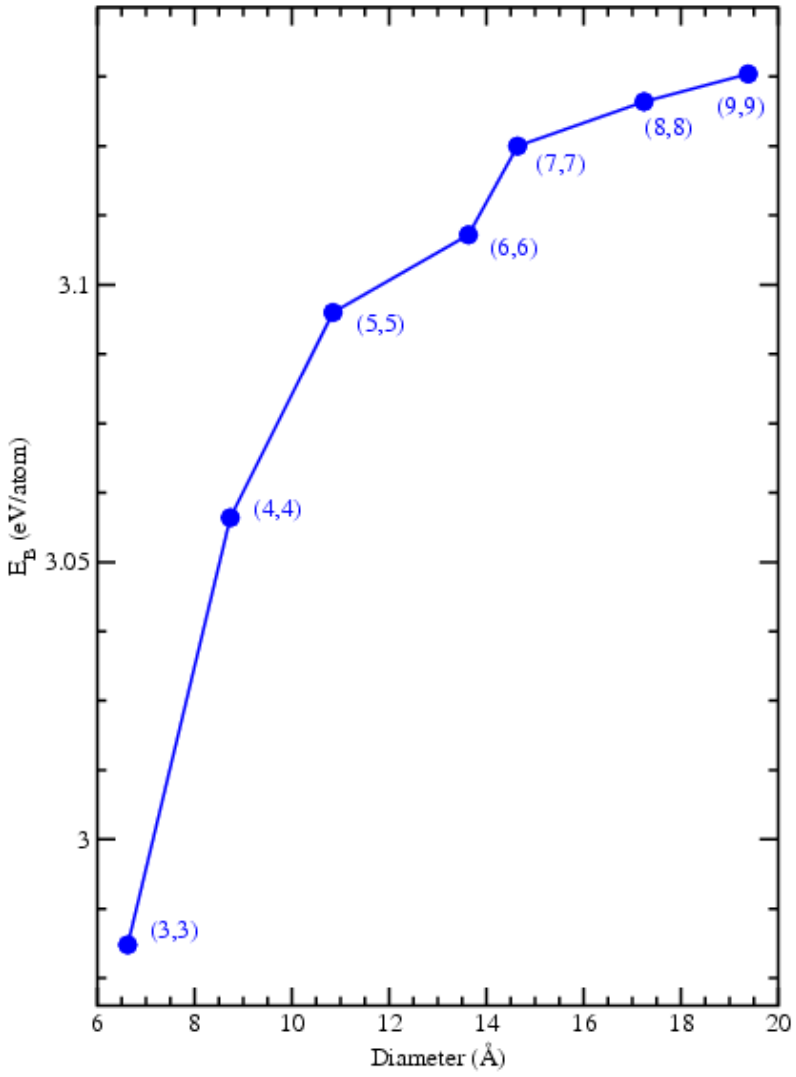

Figure 3.8 Binding energy as a function of the tube diameter in the Si armchair nanotubes.

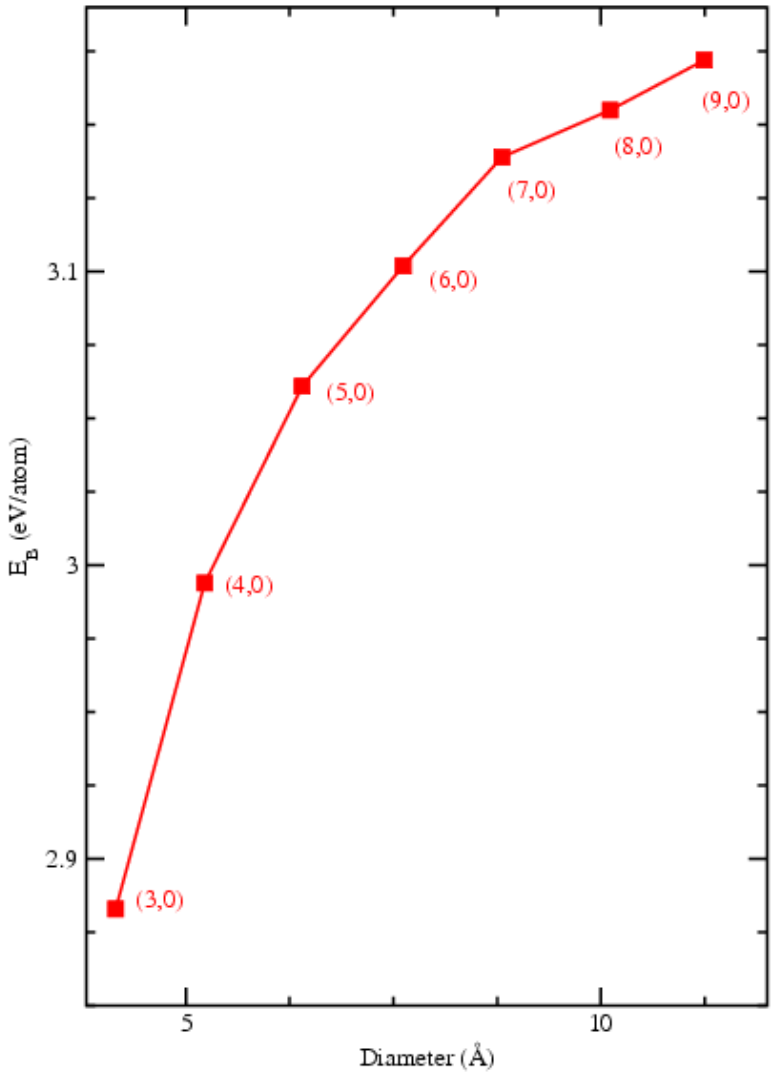

Figure 3.9 Binding energy as a function of the tube diameter in the Si zigzag nanotubes.

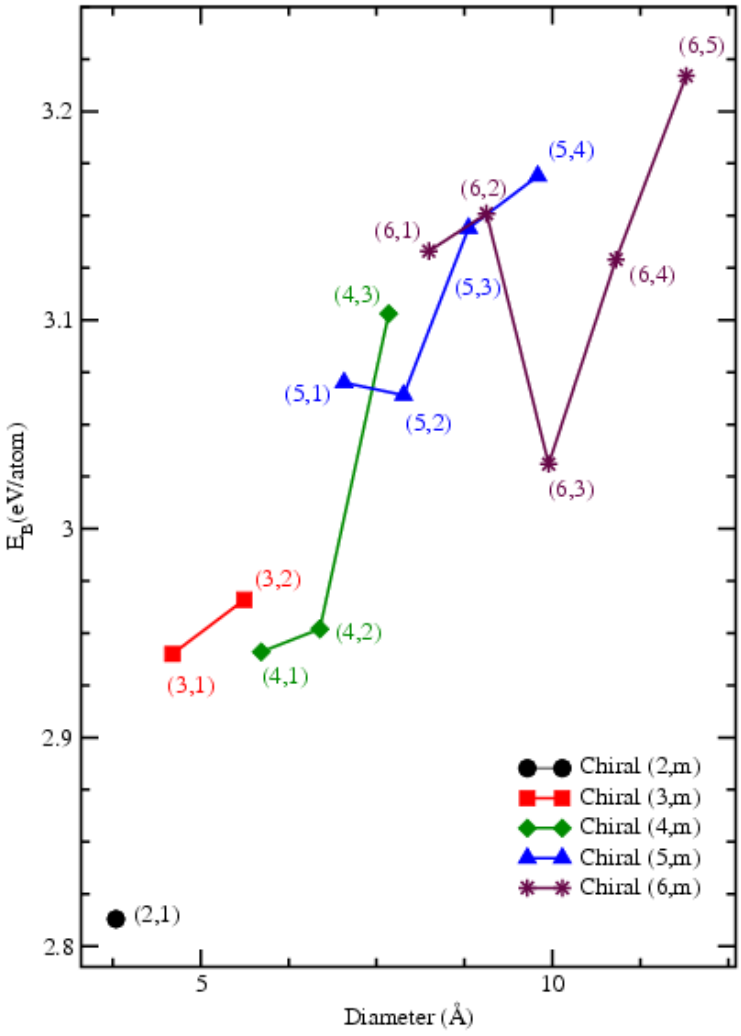

Figure 3.10 Binding energy as a function of the tube diameter in the Si chiral nanotubes.

Table 3.4 Average, Minimum, Maximum Bond Lengths (in Å) of Armchair Si Nanotubes.

Nanotube	Ave.B.L	Min.B.L	Max.B.L
(3,3)	2.257	2.164	2.292
(4,4)	2.248	2.188	2.281
(5,5)	2.245	2.190	2.269
(6,6)	2.244	2.184	2.256
(7,7)	2.242	2.188	2.266
(8,8)	2.241	2.189	2.264
(9,9)	2.241	2.188	2.264

Table 3.5 Average, Minimum, Maximum Bond Lengths (in Å) of Zigzag Si Nanotubes.

Nanotube	Ave.B.L	Min.B.L	Max.B.L
(3,0)	2.349	2.285	2.386
(4,0)	2.309	2.230	2.332
(5,0)	2.281	2.248	2.309
(6,0)	2.272	2.233	2.293
(7,0)	2.268	2.238	2.281
(8,0)	2.262	2.253	2.270
(9,0)	2.247	2.227	2.256

Table 3.6 Average, Minimum, Maximum Bond Lengths (in Å) of Chiral Si Nanotubes.

Nanotube	Ave.B.L	Min.B.L	Max.B.L
(2,1)	2.402	2.234	2.496
(3,1)	2.348	2.260	2.479
(3,2)	2.296	2.173	2.361
(4,1)	2.284	2.195	2.353
(4,2)	2.267	2.190	2.334
(4,3)	2.265	2.177	2.314
(5,1)	2.280	2.189	2.466
(5,2)	2.260	2.188	2.314
(5,3)	2.250	2.182	2.284
(5,4)	2.249	2.180	2.281
(6,1)	2.269	2.206	2.417
(6,2)	2.248	2.191	2.274
(6,3)	2.245	2.181	2.276
(6,4)	2.246	2.183	2.288
(6,5)	2.253	2.189	2.286

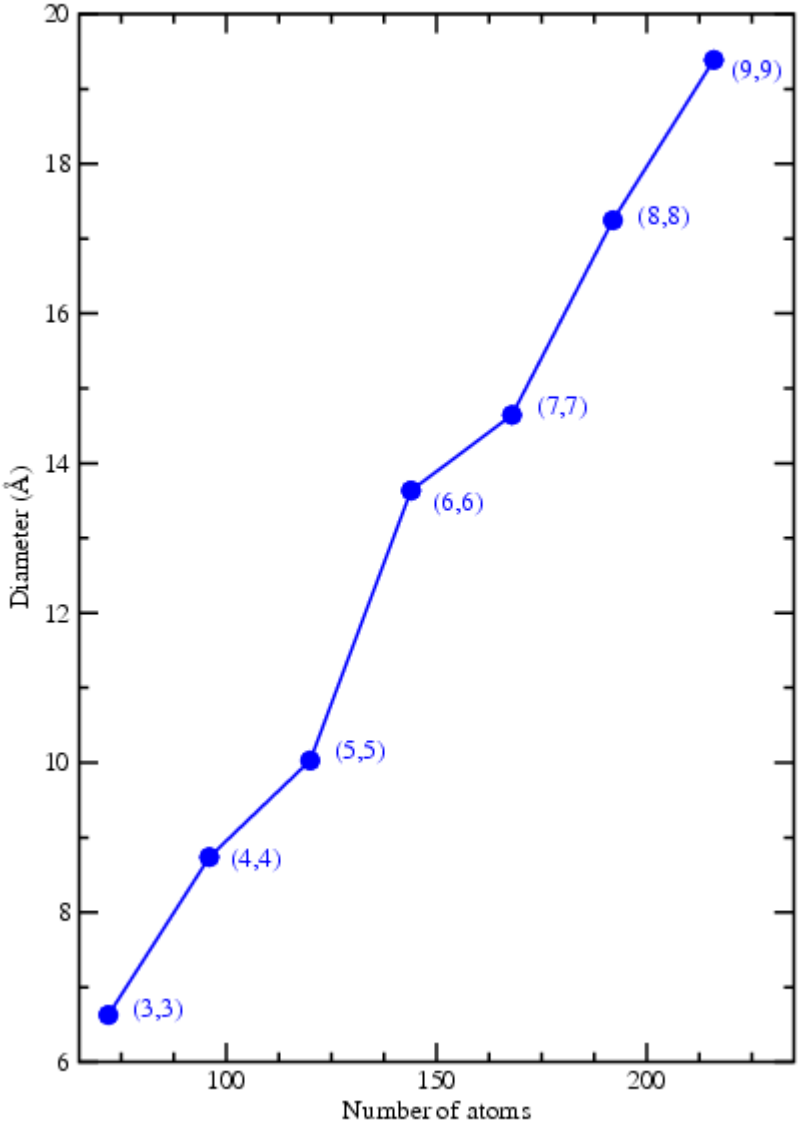

Figure 3.11 Tube diameter as a function of the total number of atoms in Si armchair nanotubes.

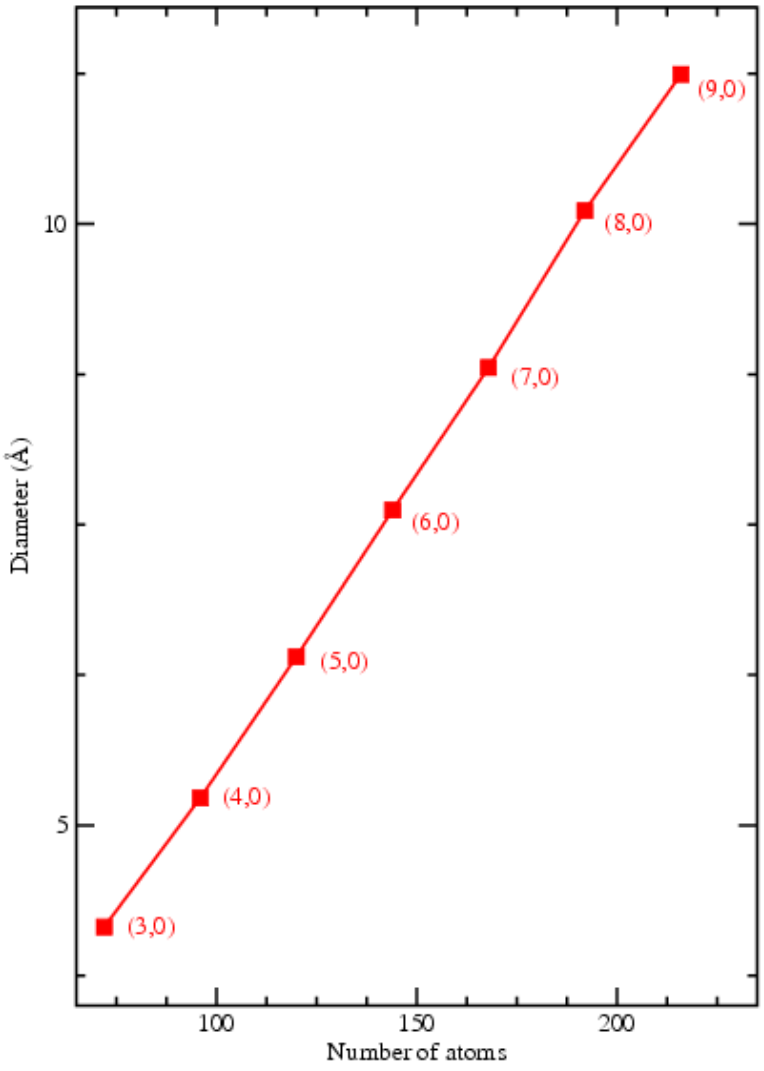

Figure 3.12 Tube diameter as a function of the total number of atoms in Si zigzag nanotubes.

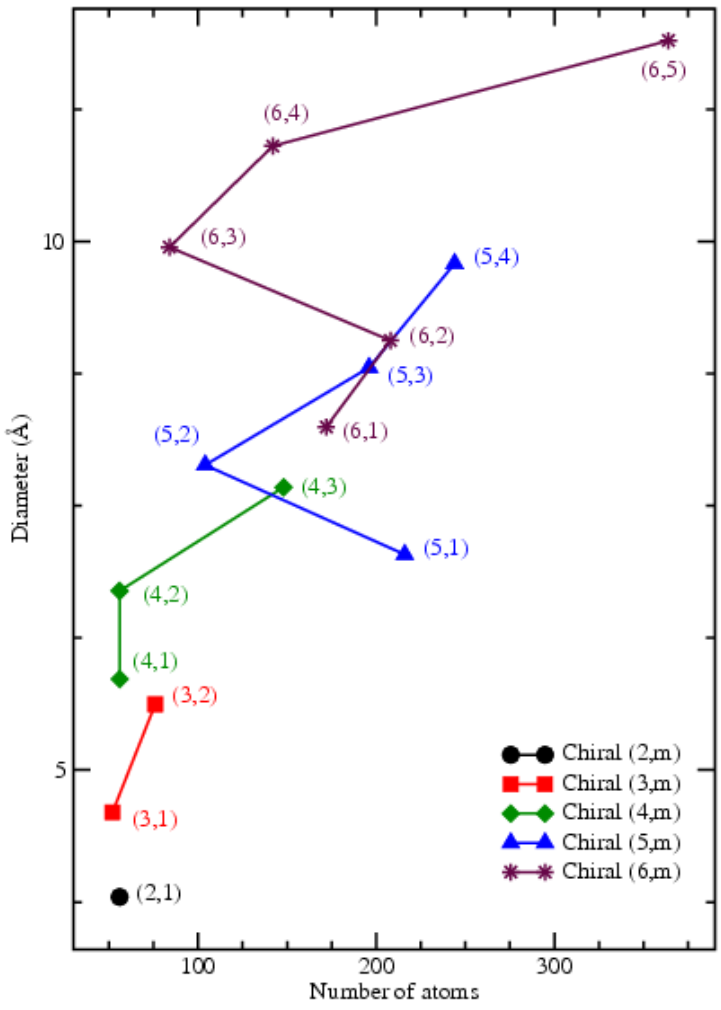

Figure 3.13 Tube diameter as a function of the total number of atoms in Si chiral nanotubes.

We have also studied the Mulliken charge distribution for the SiNTs and found that all the armchair nanotubes have covalent bonding which is evident from the figures 3.14. On the other hand zigzag nanotubes are predominantly ionic type (figure 3.15), since charge transfer occurs between Si atoms almost everywhere in the tube except in the middle of the tube where we found a ring of atoms with covalent type bonding. For chiral nanotubes there is no fixed trend. The arbitrarily taken chiral (4, 3) structure has predominant ionic type bonding (figure 3.16) near the edges and covalent type bonding in the center region. Among all the nanotubes we have studied, three of them (2, 1), (5, 1), and (6, 1) have very high dipole moment values, which indicates their high over all highly asymmetric charge distribution. All other nanotubes have very low dipole moments which is manifestation of their symmetric charge distribution. The structures with high dipole moments may be expected to be synthesized in nanotube-bundles.

In order to predict the conducting properties of nanotube, it is highly important to study the possible metallic or semi-conducting behavior of these nanotubes. To do so, we have calculated the highest-occupied-molecular-orbital to lowest-unoccupied-molecular-orbital (HOMO-LUMO) gaps for all the nanotubes under considerations. Band gaps for different SiNTs are listed in tables 3.1 to 3.3. The gaps for armchair SiNTs are in the range of 0.93 eV to 1.02 eV. Figures 3.17 to 3.22 show the band gap variation with number of atoms and tube diameter. In case of armchair nanotubes there is a monotonous increase in band gaps values as we move from (3, 3) to (6, 6), after that gaps values tend to decrease as we approach (9, 9) nanotubes (figure 3.17 and 3.20). As seen from the figures 3.18 and 3.21, for zigzag SiNTs there is monotonous decrease in gap from the 0.63 eV (3, 0) nanotube till 0.219 eV (8,0) nanotube, then again it goes up for the (9,0) nanotube. For chiral nanotubes oscillatory pattern has been observed with the increase in diameter. We can clearly see in the figures 3.19 and 3.22 that chiral nanotubes (3, 2), (5, 1), (5, 3) are small gap materials but does not indicate any metallic behavior where as (6, 2) chiral tube has a possible metallic characteristics. At this point, we cannot predict the long term variance of band gaps with diameter.

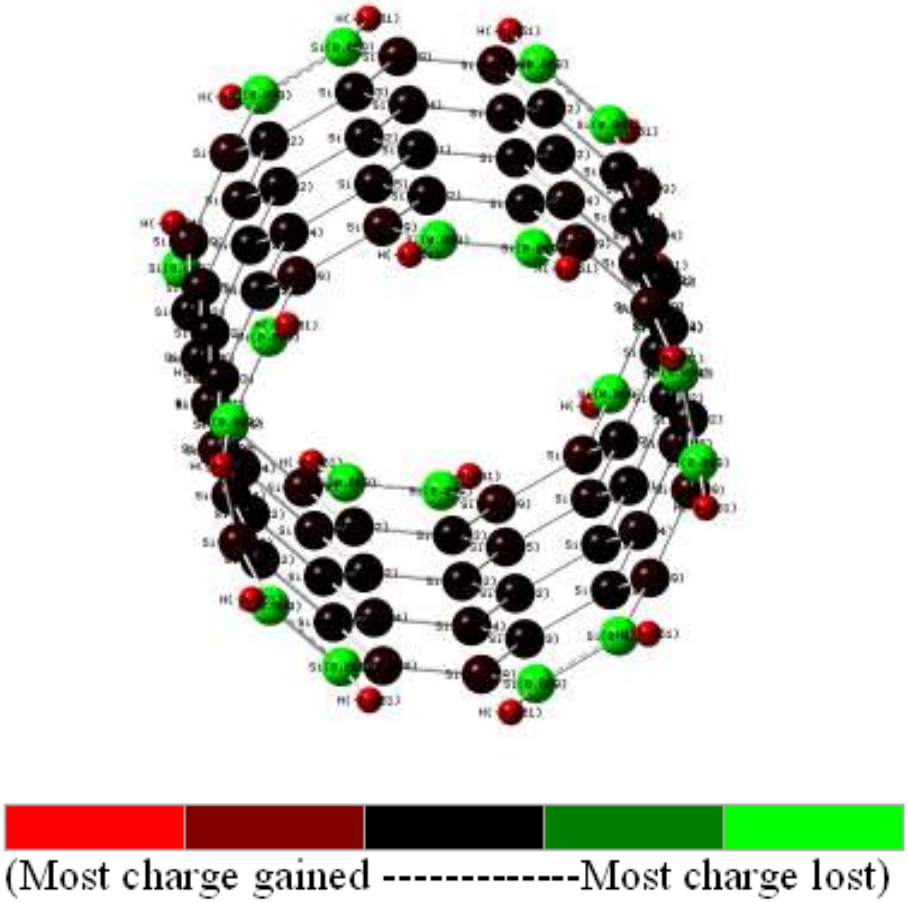

Figure 3.14 Mulliken charge distribution for the relaxed armchair (5, 5) nanotube. The scale used is depicted.

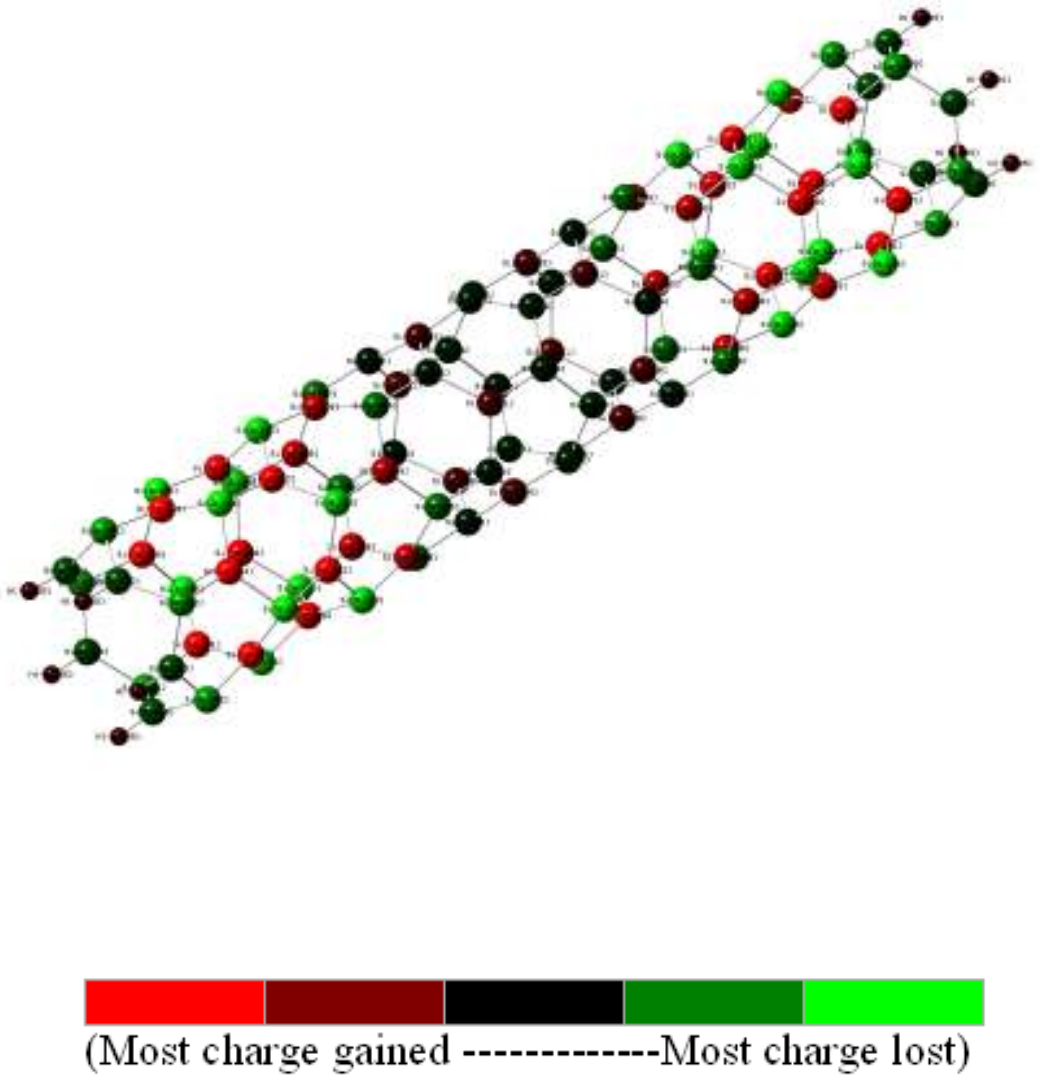

Figure 3.15 Mulliken charge distribution for the relaxed zigzag (5, 0) nanotube. The scale used is depicted.

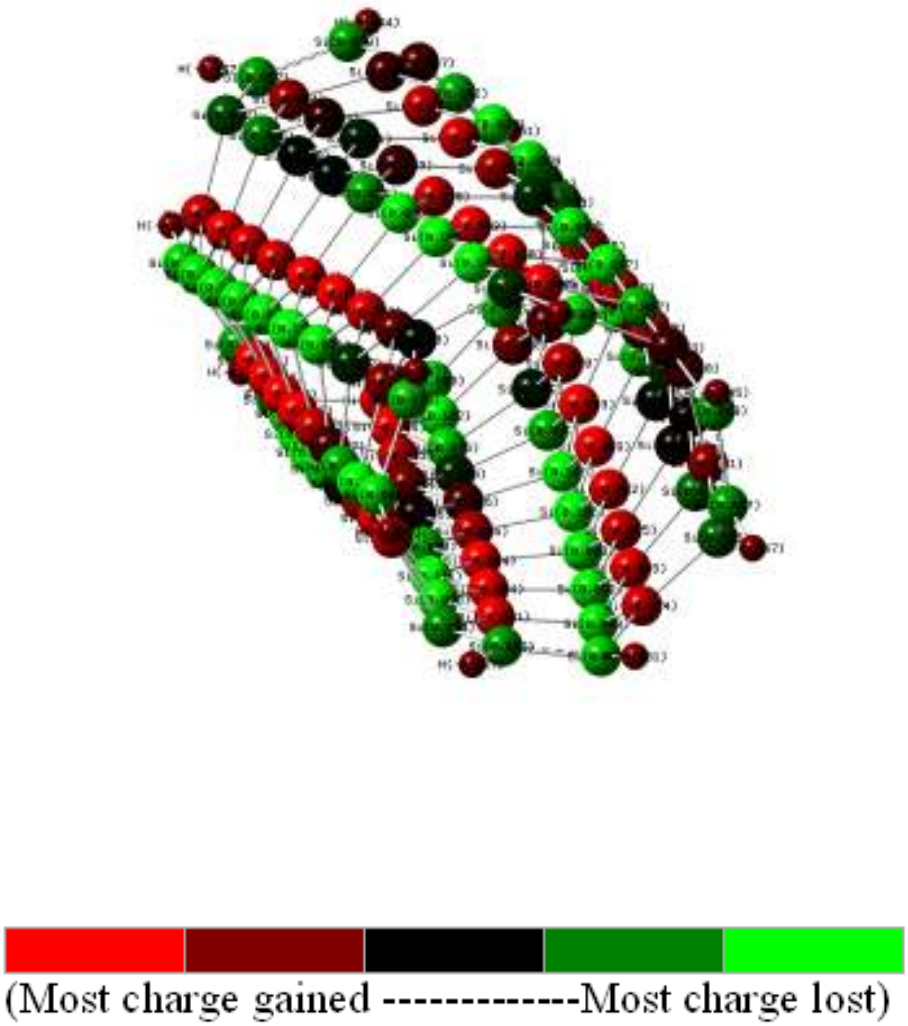

Figure 3.16 Mulliken charge distribution for the relaxed chiral (4, 3) nanotube. The scale used is depicted.

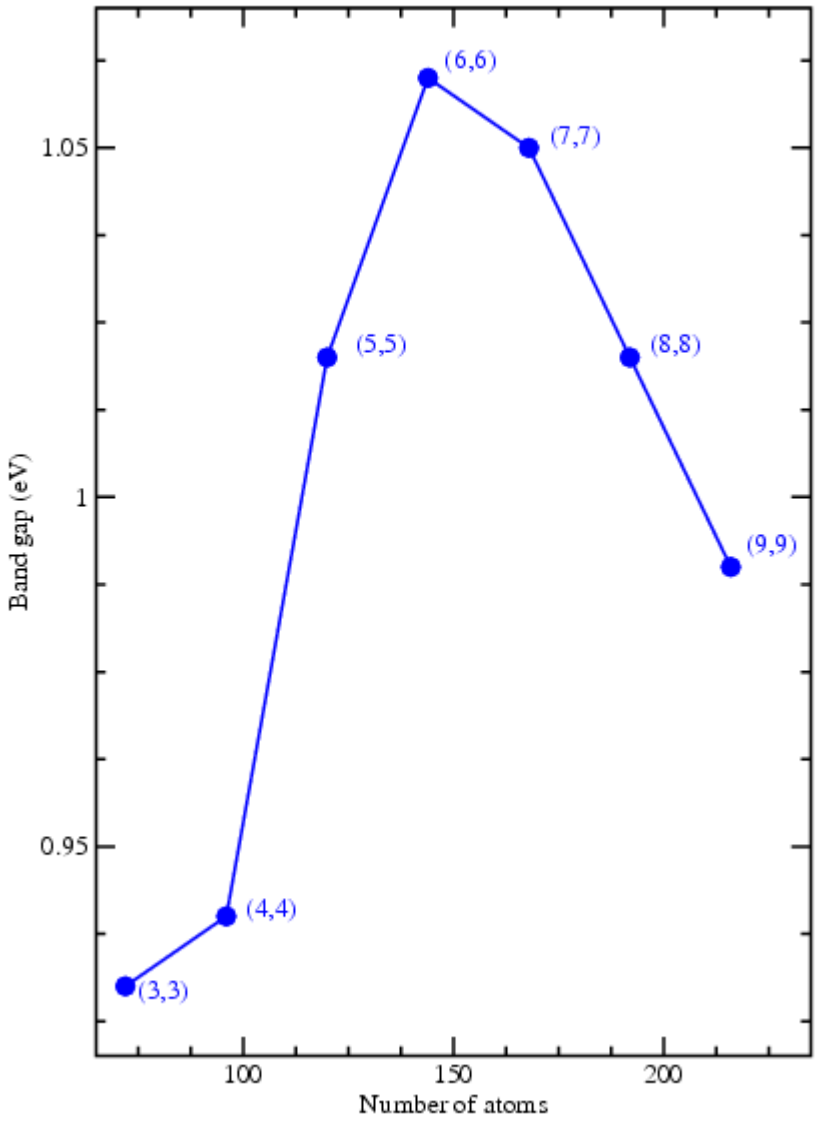

Figure 3.17 Gap as a function of the total number of atoms in the Si armchair nanotubes.

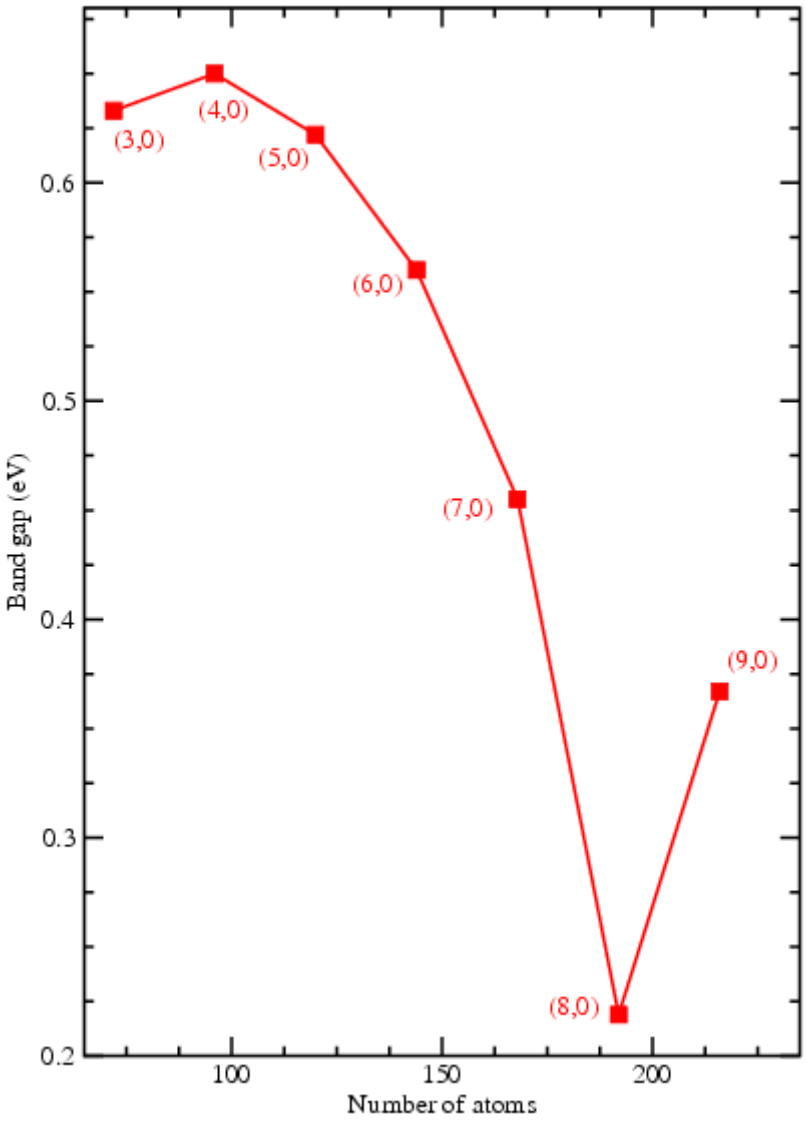

Figure 3.18 Gap as a function of the total number of atoms in the Si zigzag nanotubes.

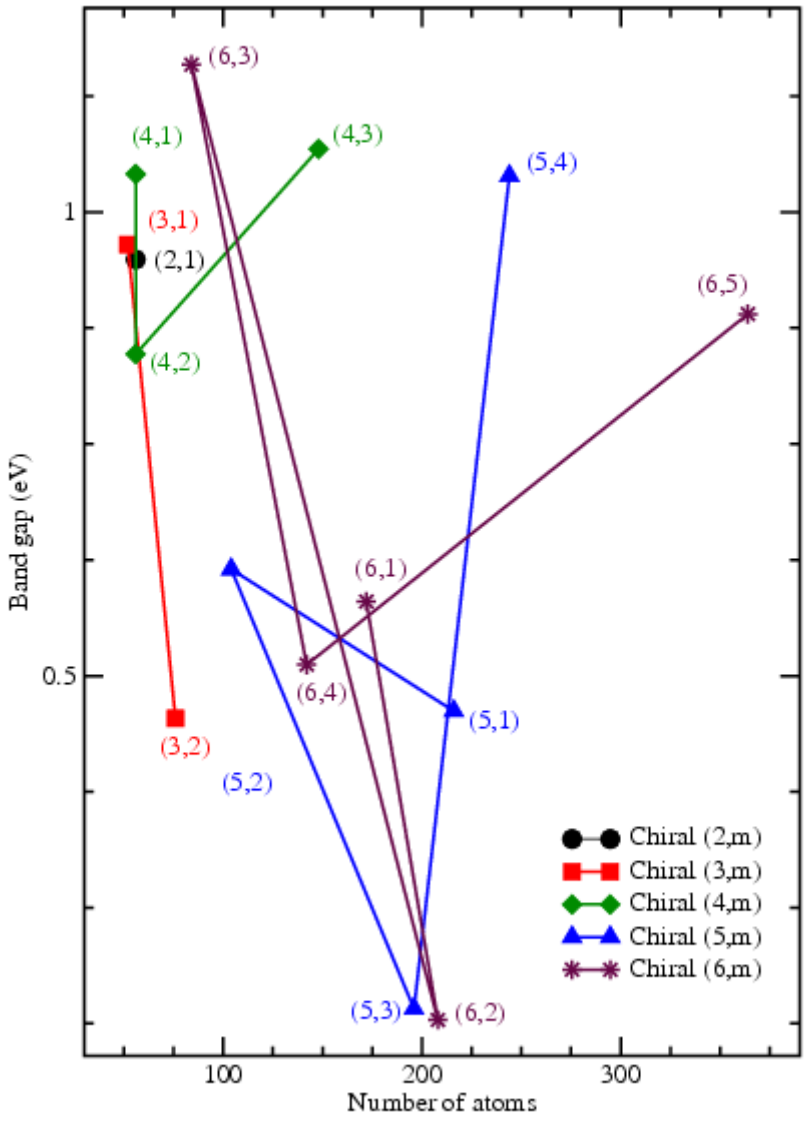

Figure 3.19 Gap as a function of the total number of atoms in the Si chiral nanotubes.

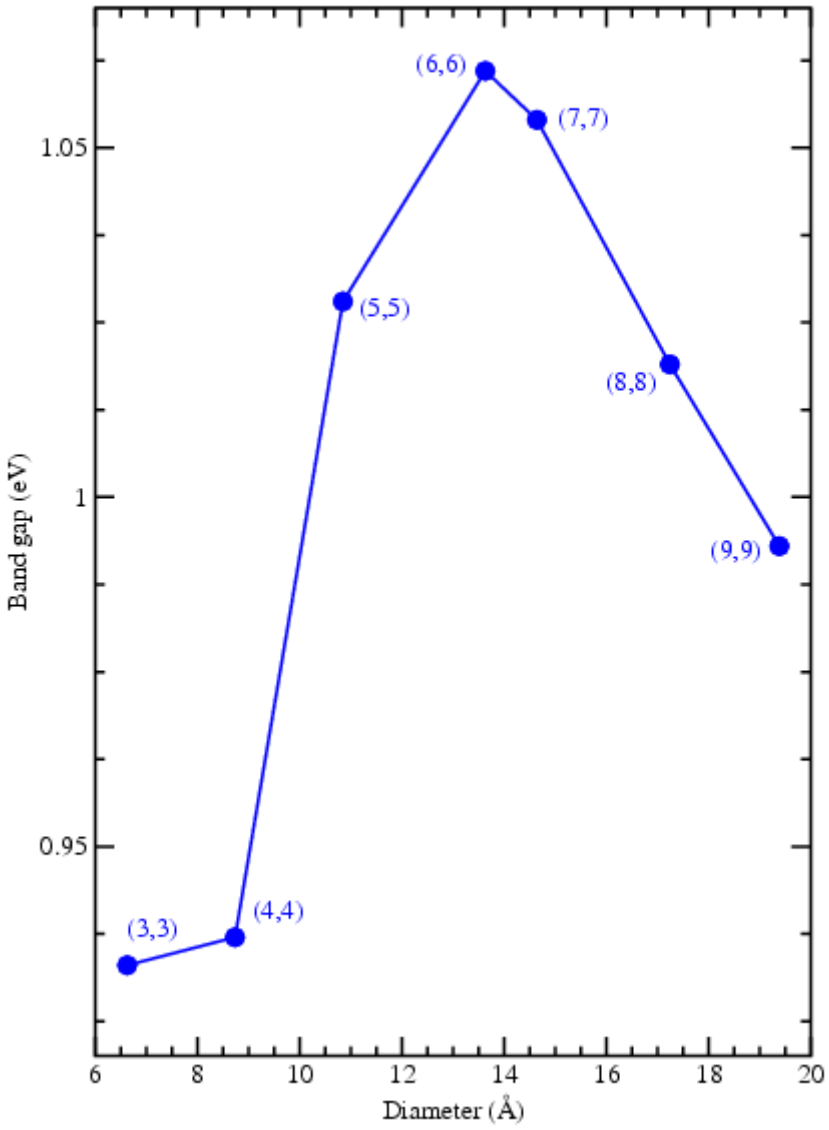

Figure 3.20 Gap as a function of the tube diameter in the Si armchair nanotubes.

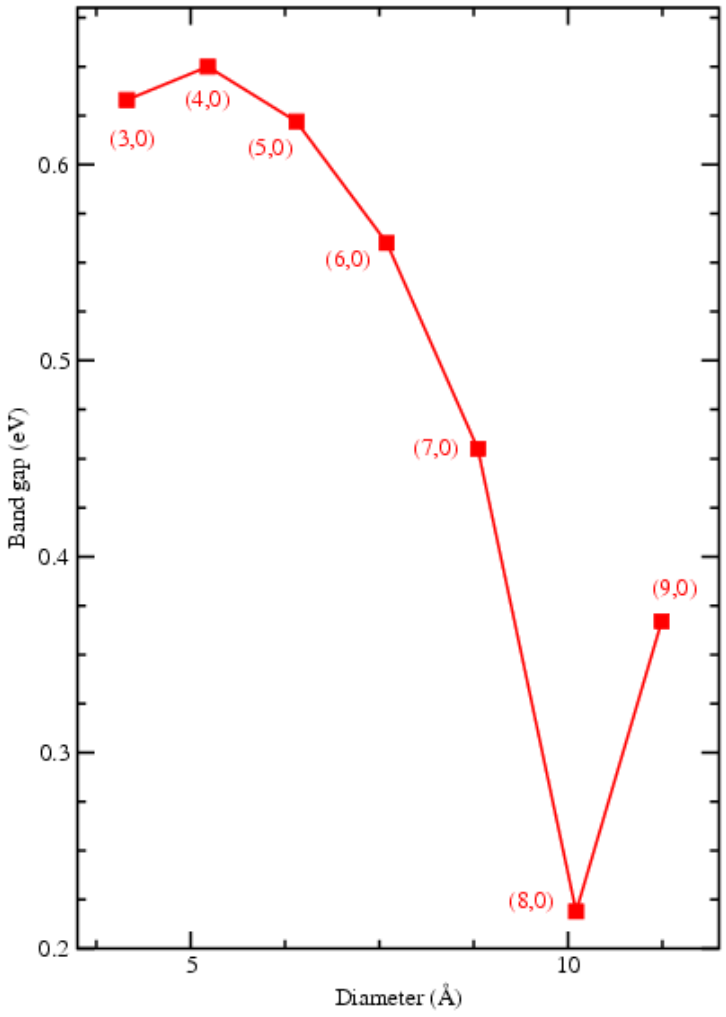

Figure 3.21 Gap as a function of the tube diameter in the Si zigzag nanotubes.

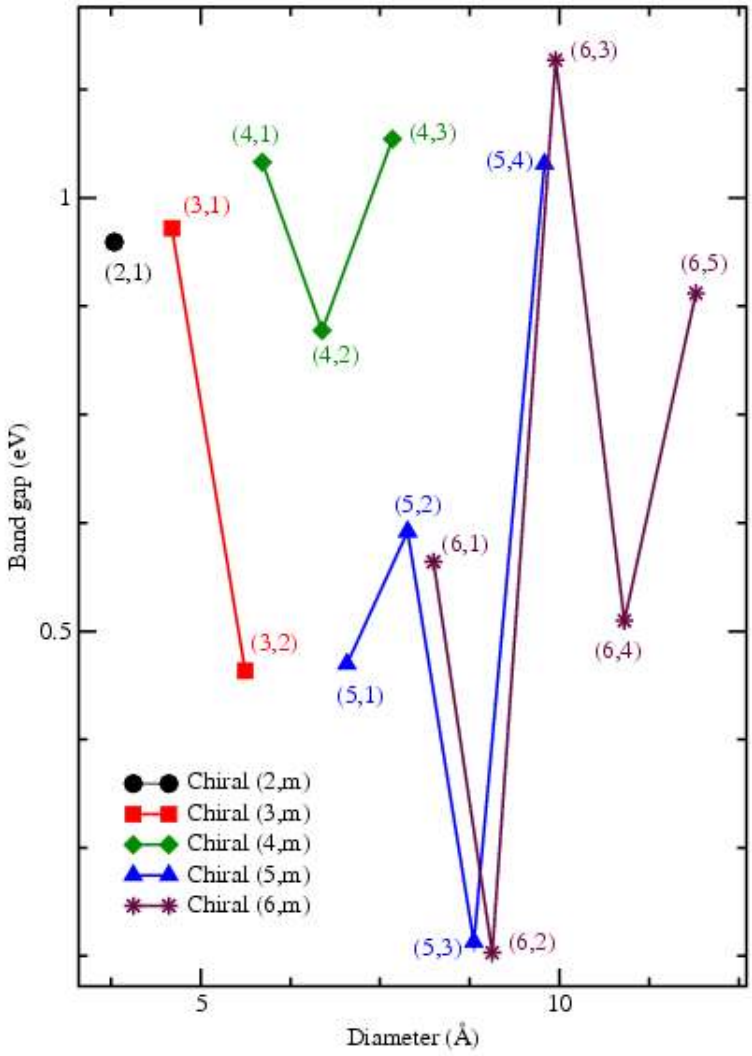

Figure 3.22 Gap as a function of the tube diameter in the Si chiral nanotubes.

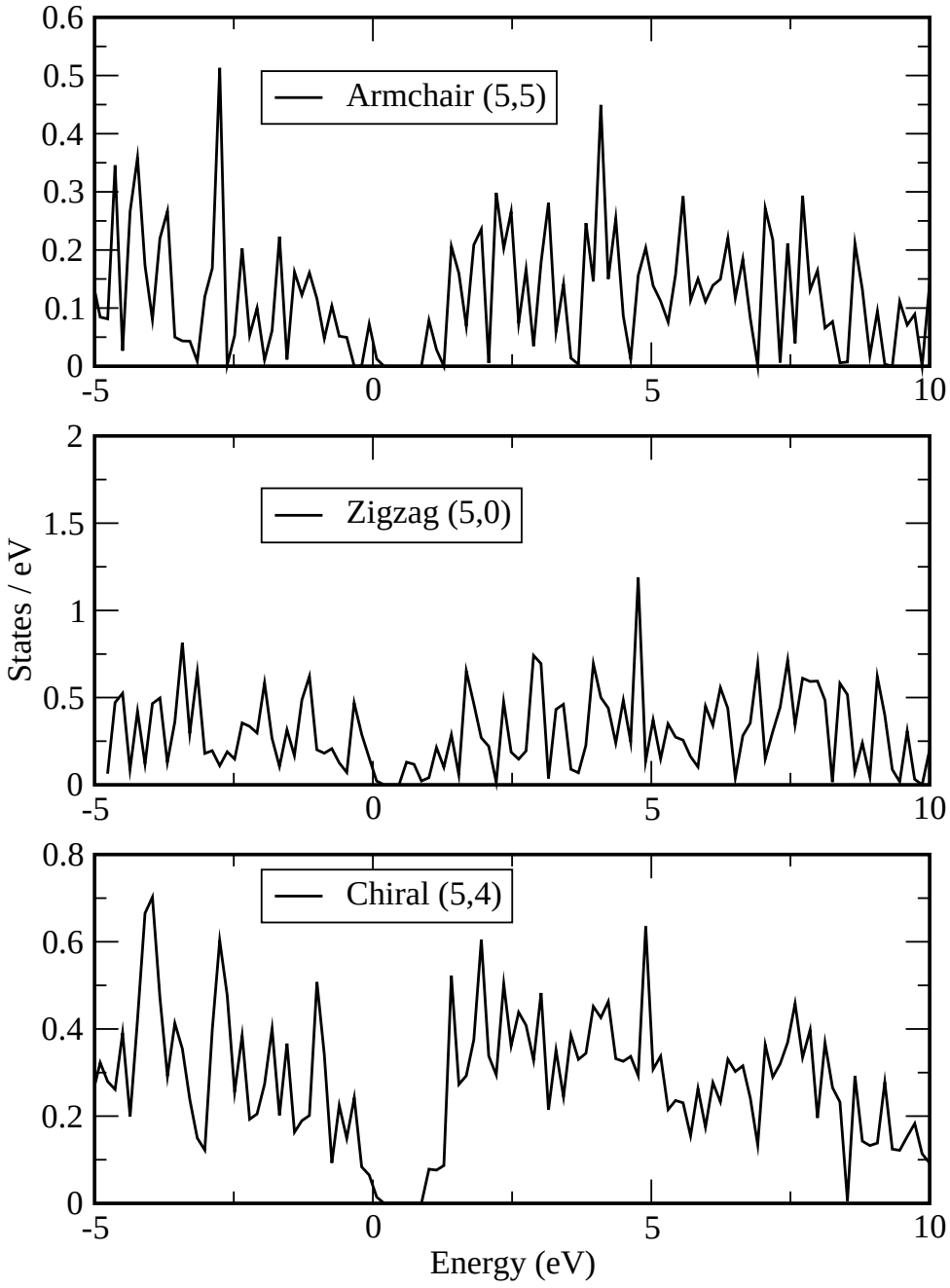

Figure 3.23 Gaussian broadened (σ = 0.05 eV) density of states (DOS) plots for Si nanotubes. HOMO energy is set to zero

Current analysis of band gaps of SiNTs shows the possible application in the field of molecular electronics where Si based nanotubes are more desirable over CNTs. Figures 3.23 is showing the energy density of state for armchair (5, 5), zigzag (5, 0) and chiral (5, 4), the respective band gaps are reflectedin plot. DOS was convoluted with a gaussian of width 0.05 eV and Homo is adjusted at zero.

3.3 Results and discussions for pure Ge nanotubes

In this section we present a detailed analysis of pure Ge nanotubes in both armchair and zigzag configurations for dimensions from (3, 3) to (11, 11) and (3, 0) to (11, 0), respectively. In terms of diameter the smallest armchair nanotube studied is (3, 3) tube with stoichiometry $Ge_{60}H_{12}$, and the largest structure is $Ge_{220}H_{44}$ (11, 11) (figure 3.24), for zigzag nanotube smallest is $Ge_{66}H_6$ (3, 0) and largest is $Ge_{242}H_{22}$ (11, 0) (figure 3.25).

We know the fact that carbon and germanium fall under the same group in the periodic table still their chemical behavior is quite different from each other, the reason to this difference is the type of hybridization they form. C prefers sp^2 while Ge prefers sp^3 hybridization state. We have calculated the binding energy per atom using the formula:

$$E_C = \frac{1}{(a+b)}[aE(Ge) + bE(H) - E(Ge_aH_b)] \qquad (3.2)$$

where a and b are number of Ge and H atoms respectively ,E(Ge) and E(H) are ground state energies of Ge and H atoms respectively and E(Ge_aH_b) is the total energy of the optimized clusters representing the nanotubes. Tables 3.7 to 3.8 show the binding energies per atom for all different nanotubes. Figure 3.26 shows the per atom variations of binding energies of germanium with diameter. Average value of binding energy of armchair nanotubes is found to be 2.56 eV per atom with the largest GeNT studied (11, 11). In zigzag nanotubes the smallest structure (3, 0) gave a binding energy of 2.47 eV per atom and biggest structure (11, 0) yielded 2.61 eV per atom with average binding energy as 2.56 eV per atom. Clearly from the figure 3.26 we can predict that the value of binding energies are attaining a saturation level as we increase the number of atoms or increase the diameter of the tubes.

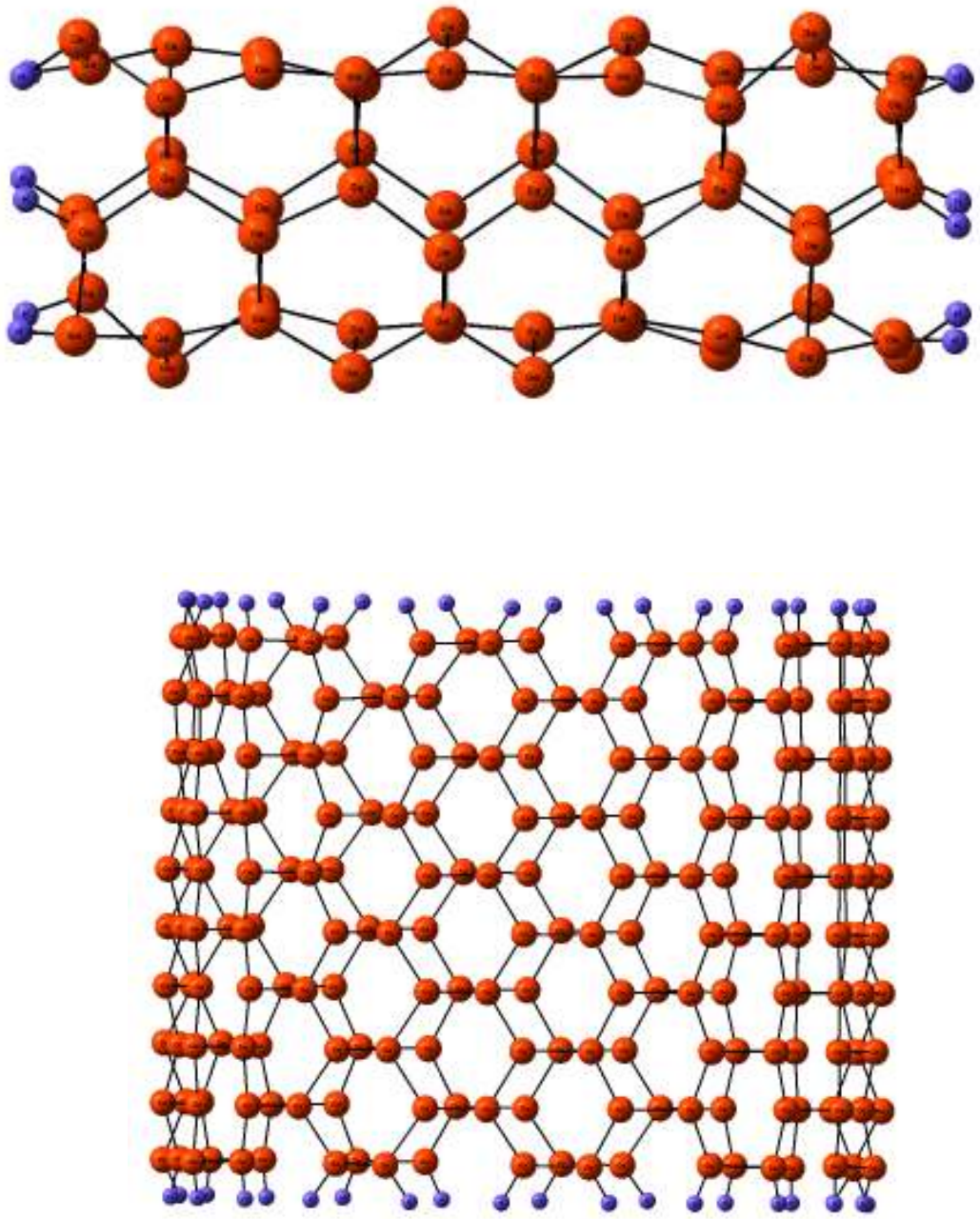

Figure 3.24 (Top) Smallest (3, 3) and (bottom) largest (11, 11) armchair Ge nanotubes.

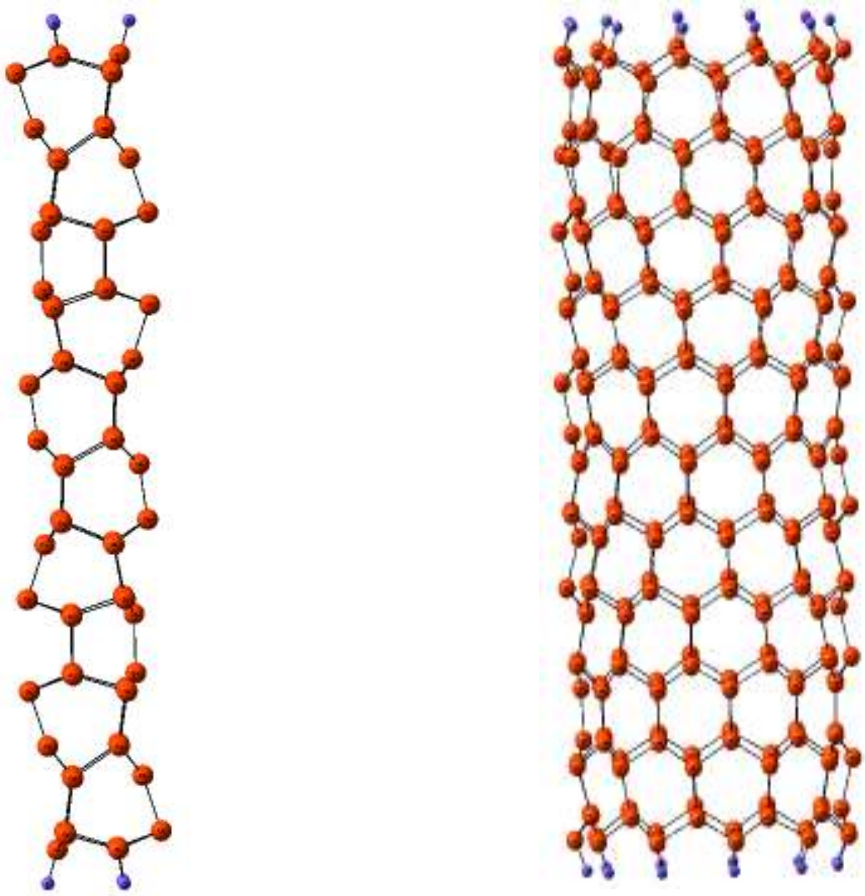

Figure 3.25 (Left) Smallest (3, 0) and (right) largest (11, 0) zigzag Ge nanotubes.

Table 3.7 Electronic States, Binding Energies Per Atom (E_b) in eV, HOMO-LUMO Gaps in eV, Diameters in Å, and Dipole Moments in Debye for Armchair Ge Nanotubes.

Nanotube	Model	State	E_b(eV)	Gap(eV)	Diameter(Å)	Dip.Mnt (Debye)
(3,3)	$Ge_{60}H_{12}$	^3A	2.493	0.698	5.897	0.6217
(4,4)	$Ge_{80}H_{16}$	^1A	2.544	1.084	7.714	0.0568
(5,5)	$Ge_{100}H_{20}$	^3A	2.558	0.755	9.593	0.2321
(6,6)	$Ge_{120}H_{24}$	^3A	2.568	0.744	11.460	0.1701
(7,7)	$Ge_{140}H_{28}$	^3A	2.578	0.489	12.976	1.3922
(8,8)	$Ge_{160}H_{32}$	^1A	2.579	0.752	15.220	0.6419
(9,9)	$Ge_{180}H_{36}$	^3A	2.584	0.327	17.110	6.2446
(10,10)	$Ge_{200}H_{40}$	^3A	2.581	0.317	19.006	4.4916
(11,11)	$Ge_{220}H_{44}$	$^1A_1$	2.588	0.710	20.886	4.4758

Table 3.8 Electronic States, Binding Energies Per Atom (E_b) in eV, HOMO-LUMO Gaps in eV, Diameters in Å, and Dipole Moments in Debye for Zigzag Ge Nanotubes.

Nanotube	Model	State	E_b(eV)	Gap(eV)	Diameter(Å)	Dip.Mnt (Debye)
(3,0)	$Ge_{60}H_{12}$	^3A	2.473	0.642	4.163	0.0000
(4,0)	$Ge_{80}H_{16}$	^3A	2.503	0.581	5.079	0.4310
(5,0)	$Ge_{100}H_{20}$	^3A	2.541	0.345	6.420	0.0029
(6,0)	$Ge_{120}H_{24}$	^3A	2.569	0.465	7.370	0.0000
(7,0)	$Ge_{140}H_{28}$	^3A	2.584	0.693	8.549	0.0000
(8,0)	$Ge_{160}H_{32}$	^3A	2.589	0.232	9.749	0.0000
(9,0)	$Ge_{180}H_{36}$	$^1A_1$	2.591	0.412	11.022	0.0000
(10,0)	$Ge_{200}H_{40}$	^3A	2.594	0.443	12.184	7.3912
(11,0)	$Ge_{220}H_{44}$	$^1A_1$	2.606	0.426	13.336	6.5573

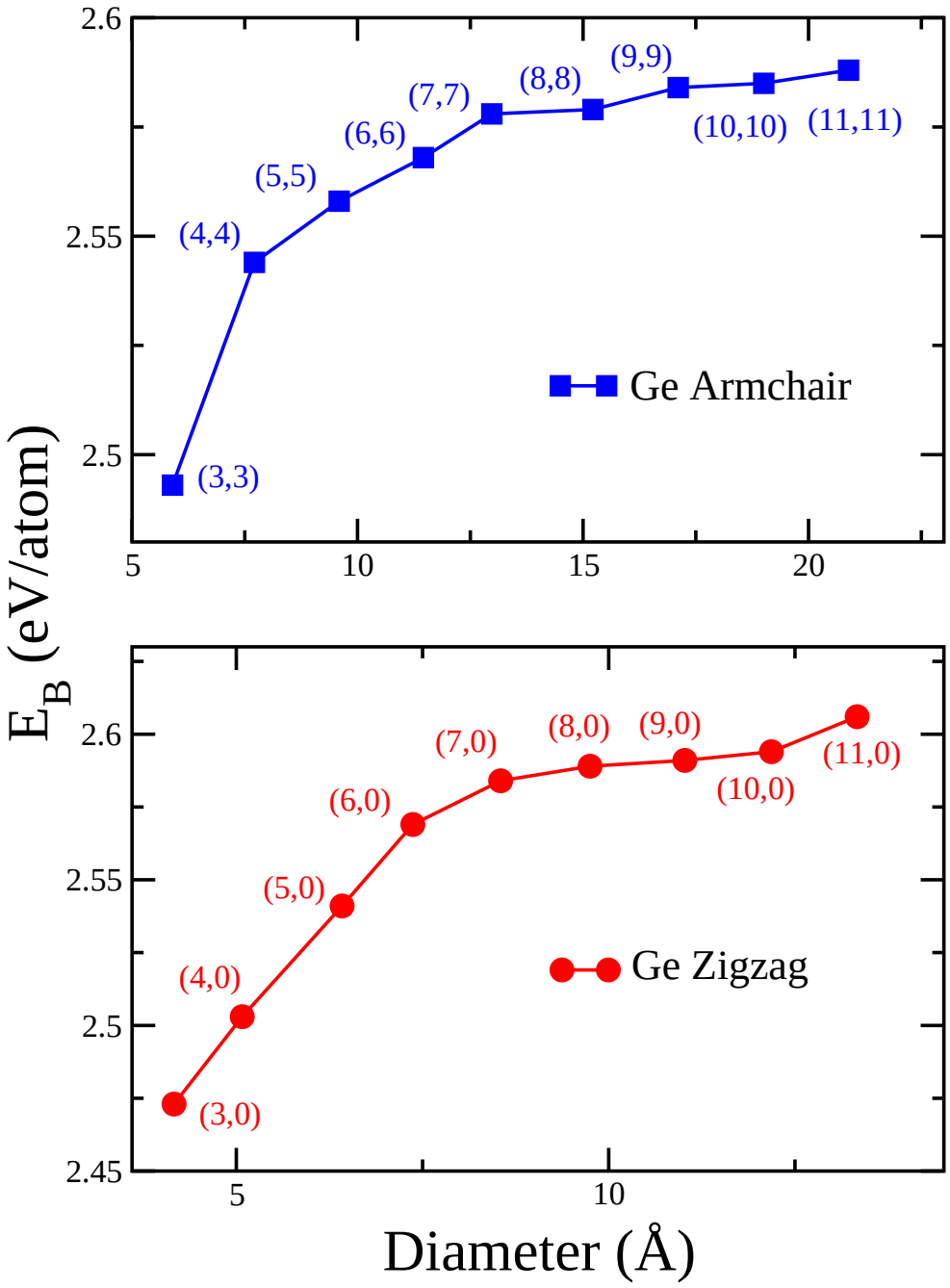

Figure 3.26 Binding energy as a function of the tube diameter in the Ge nanotubes.

The non-linearity in the energy relationship indicates that binding energy is not only purely dependent on diameter but also has contribution from the curvature of the tube. We believe that the binding energy per atom of extremely large nanotube will be close to that of graphene like sheet of Ge. It is interesting to notice that armchair and zigzag nanotubes have very close value of binding energy per atom.

From tables 3.9 and 3.10 it is evident that there is a pattern of distortion among Ge-Ge bond lengths along the length of different Ge nanotubes. In armchair GeNTs the average bond lengths vary from 2.451 (11, 11) to 2.503 Å (3, 3). For zigzag GeNTs these values are from 2.461 (11, 0) to 2.5442 Å (3, 0). The bond lengths are more widely distributed for smaller diameter nanotubes. Also in the both armchair and zigzag average bond lengths are decreasing with the increase in tube diameter. Looking at overall trend, the SiNTS bond lengths gets contracted after the geometry is optimized. Due to high curvature of the smaller diameter nanotubes, the bonds are highly strained in nature. Consequently, the average bond lengths of smaller diameter tubes will have high values. The existence of these strained bonds result in lower binding energy values for smaller diameter tubes. Over all if we compare the structural trends of different GeNTs with SiNTS, we find that the after relaxation higher diameter nanotube surfaces are more rippled in nature, a property which may be exploited while designing nano devices. The rippling in the surface structure caused by bond stretching or bending may also create surface dipoles and significantly modify the surface band structure.

Among all the GeNTs we have studied, smaller diameter tubes have very low or negligible dipole moments (tables 3.7 and 3.8). As mentioned earlier higher diameter tubes showed more puckering of surface, which is a possible reason for significant values of dipole moments. Charge distribution along the tube length is also governing factor for induced dipole moments. It is assumed that the structures with high dipole moments may be expected to be synthesized in nanotube-bundles. One of the most important properties of a cluster or a nanotube is the charge density distribution.

Table 3.9 Average, Minimum, Maximum Bond Lengths (in Å) of Armchair Ge Nanotubes.

Nanotube	Ave.B.L	Min.B.L	Max.B.L
(3,3)	2.503	2.382	2.579
(4,4)	2.483	2.412	2.552
(5,5)	2.468	2.389	2.507
(6,6)	2.463	2.394	2.501
(7,7)	2.460	2.391	2.504
(8,8)	2.453	2.393	2.498
(9,9)	2.454	2.342	2.491
(10,10)	2.449	2.391	2.531
(11,11)	2.451	2.374	2.492

Table 3.10 Average, Minimum, Maximum Bond Lengths (in Å) of Zigzag Ge Nanotubes.

Nanotube	Ave.B.L	Min.B.L	Max.B.L
(3,0)	2.5442	2.4910	2.5923
(4,0)	2.5331	2.4510	2.5693
(5,0)	2.4810	2.4318	2.5076
(6,0)	2.4938	2.4938	2.5148
(7,0)	2.4846	2.4193	2.5089
(8,0)	2.4800	2.4129	2.4984
(9,0)	2.4701	2.4113	2.4891
(10,0)	2.4677	2.3957	2.5389
(11,0)	2.4616	2.3944	2.5368

While designing and incorporating the new nanotube based circuitry it is important to know the regions of high and low electronic charge densities. In order to give a more detailed account of charge distribution in the nanotubes we have performed the Mulliken charge analysis for all types of Ge nanotubes (figures 3.27 and 3.28). For both armchair and zigzag nanotubes a significant amount of charge transfer among Ge atoms has been noticed. Similar to our previously mentioned SiNTs mixed nature of bonding is observed. Some of the smaller diameter Ge tubes are more ionic in nature, whereas higher diameter tubes have essentially covalent type bonding.

In order to predict the conducting properties of nanotube, it is highly important to study the possible metallic or semi-conducting behavior of these nanotubes. Therefore we have calculated the highest-occupied-molecular-orbital to lowest-unoccupied-molecular-orbital (HOMO-LUMO) gaps for all the GeNTs under considerations. The gaps for armchair GeNTs are in the range of 0.317 eV to 1.084 eV. For zigzag tubes this range is from 0.232 to 0.693 eV. The calculated values of gaps for pure Ge nanotubes depict an irregular pattern. In both the cases this trend is observed in figure 3.29. Interactions of atoms beyond the neighboring atoms can be one possible reason for this oscillatory trend of band gap values with respect to tube diameter. Figure 3.30 shows the energy density of states (DOS) for (4, 4) armchair and (6, 0) zigzag Ge nanotubes, respectively. The DOS is convoluted with a Gaussian of width 0.05 eV and HOMO is adjusted to zero. The large gaps of armchair tubes compared to the gaps in the zigzag tubes are clearly visible. Finally, further into the future, we expect the Ge nanotubes to open up many unique avenues in the field of nanoelectronics and related device features.

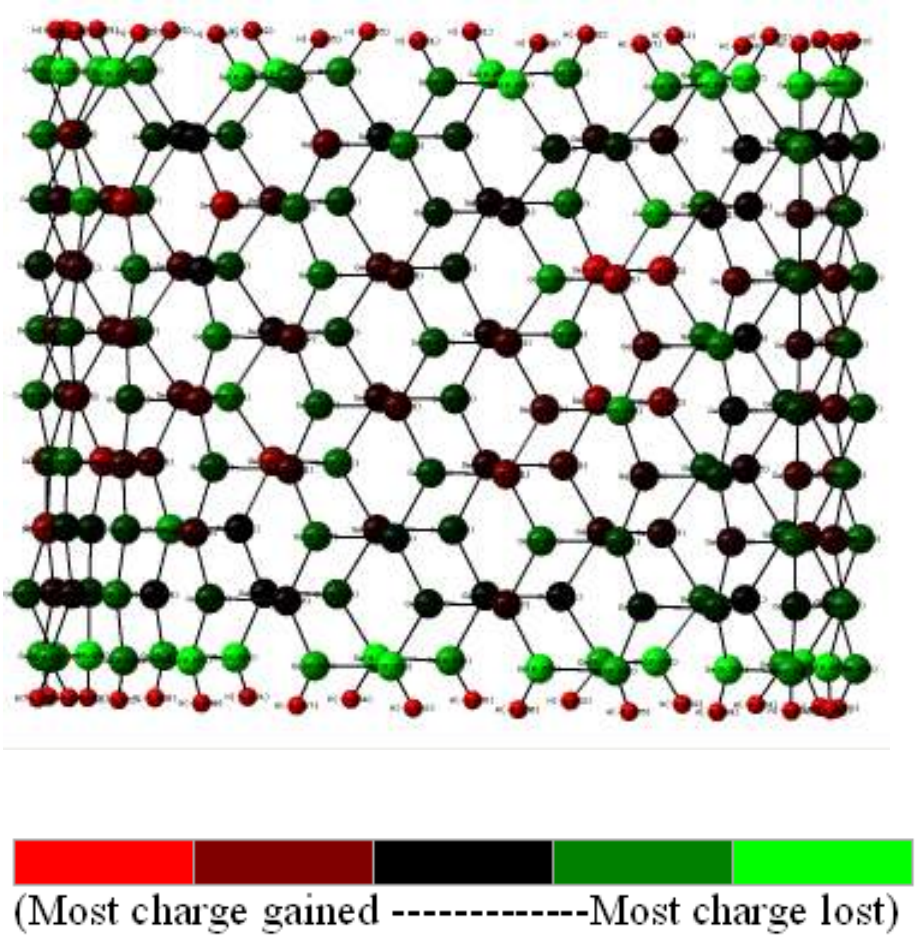

Figure 3.27 Mulliken charge distribution for the relaxed GeNT (11, 11) nanotube. The scale used is depicted.

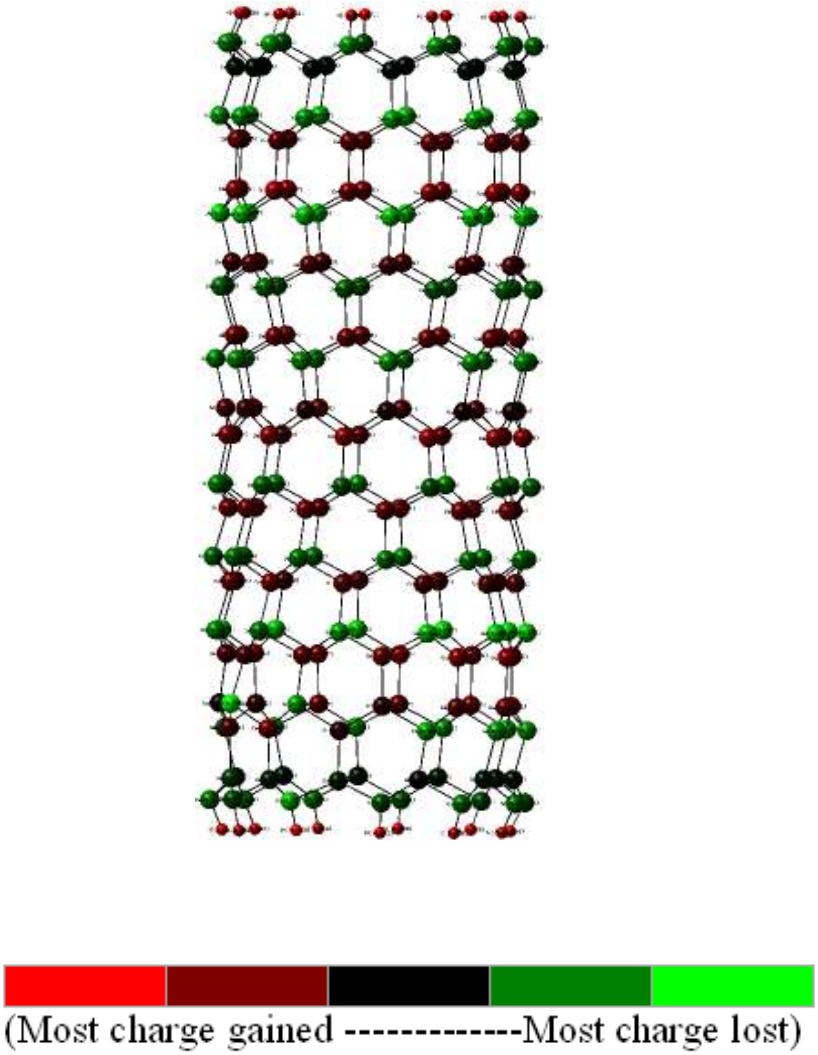

Figure 3.28 Mulliken charge distribution for the relaxed GeNT (11, 0) nanotube. The scale used is depicted.

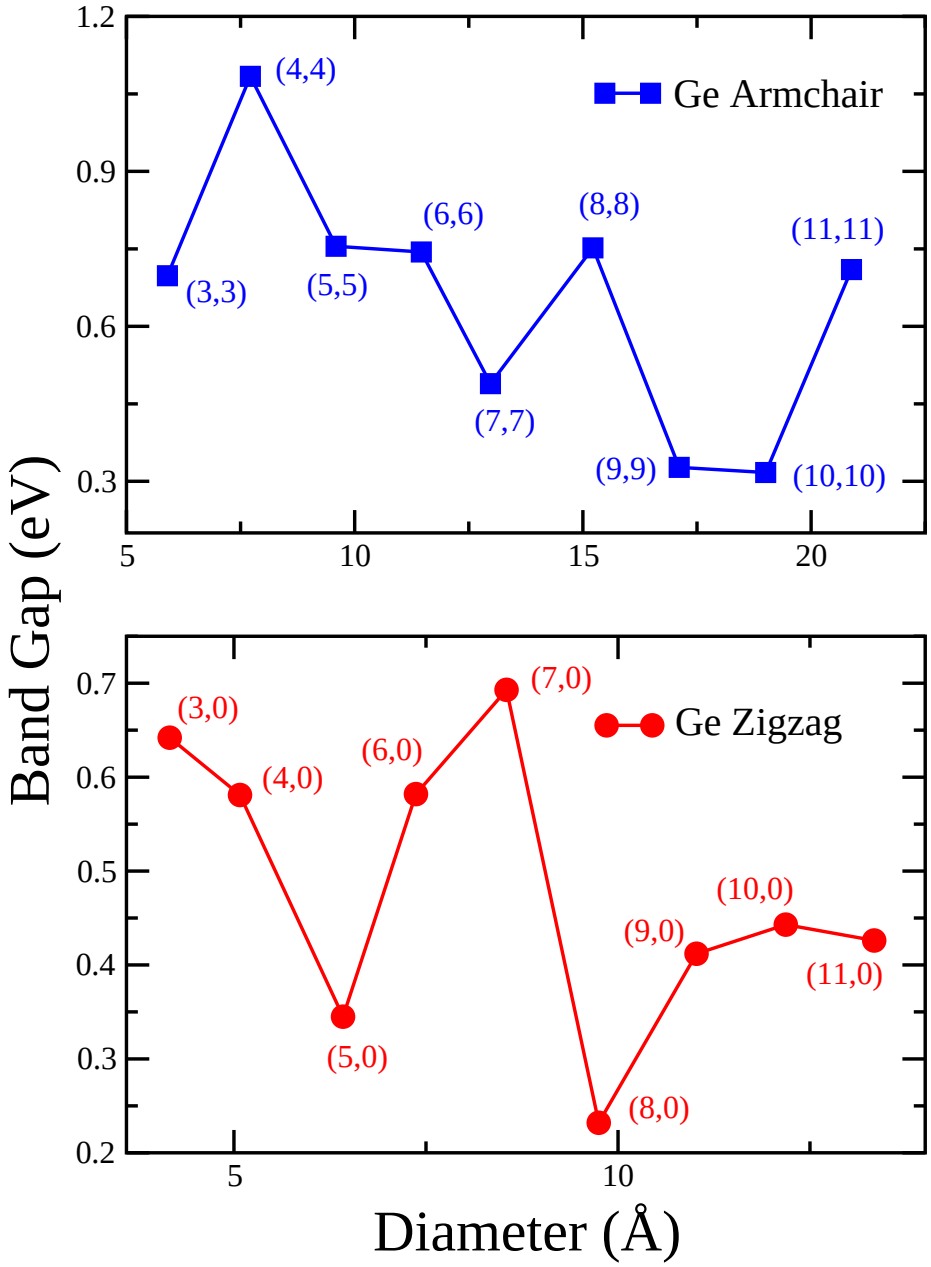

Figure 3.29 Band gap as a function of the tube diameter in the Ge nanotubes.

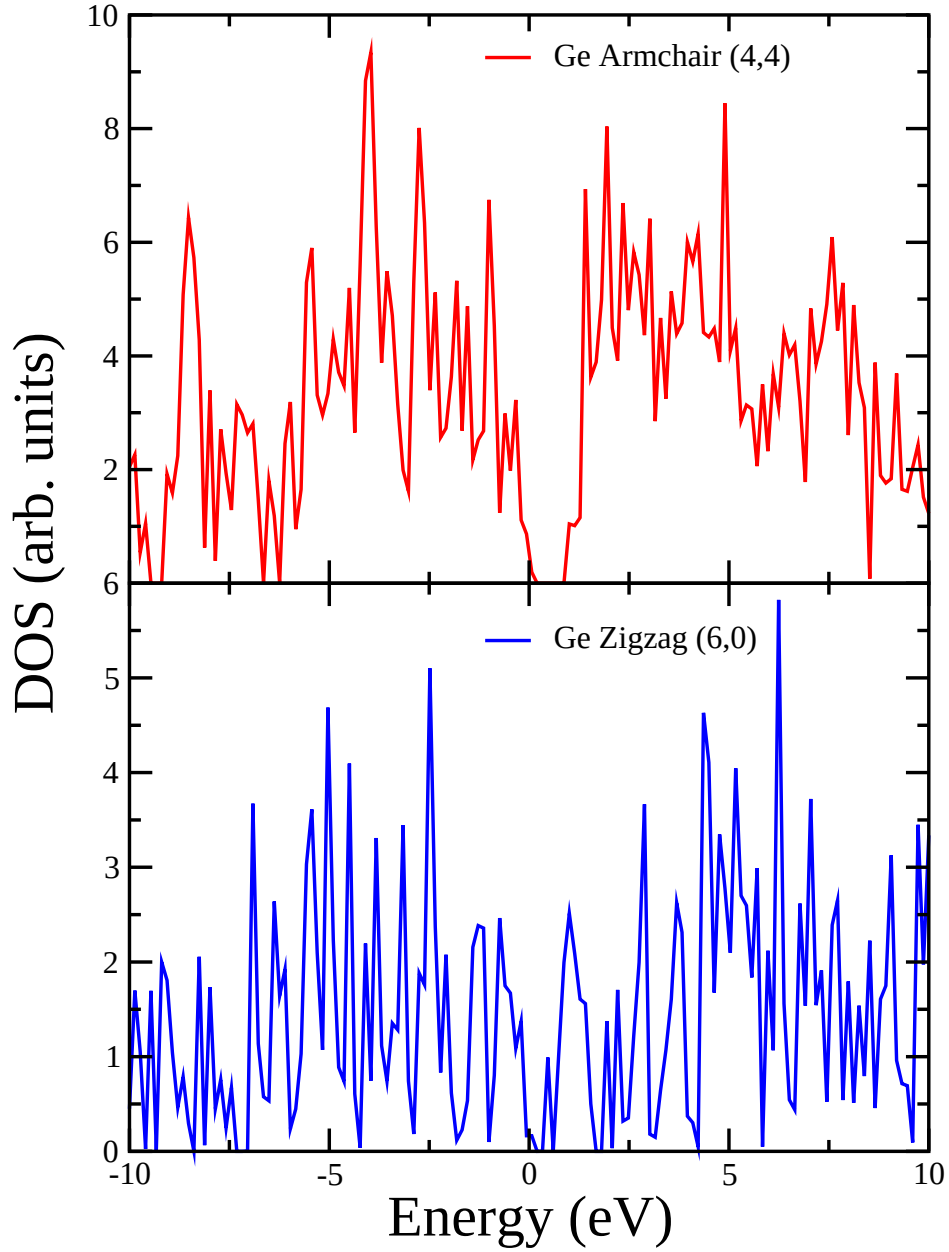

Figure 3.30 Gaussian broadened (σ = 0.05 eV) density of states (DOS) plots for Ge nanotubes. HOMO energy is set to zero.

CHAPTER 4

GERMANIUM CARBIDE NANOTUBES

4.1 Construction of Nanotubes

It is clear that, any compound with a propensity for forming graphite-like sheets can be a modeled into a nanotube structure. Therefore all the tubes reported in the present study are constructed using carbon nanotube template and are also isostructural to our structures in previous chapters. The starting geometries of these tubular structures have been obtained by simply rolling of graphene like sheet of C and Ge atoms placed at different nodes of the *honeycomb* lattice along a given chiral vector. So characterized by the roll up vector (*n, m*) three types of nanotubes are possible namely armchair, zigzag and chiral. It is well known fact that whenever a new family nanotubes is investigated the most two important cases (armchair and zigzag) are studies first. The reason for this being their simple translational symmetric nature in comparison to the broad range of chiral nanotubes. Therefore, in the present report we have restricted our calculations to the armchair and zigzag structures only. Simpler in construction, the (*n, n*) armchair tubes have the two sides of each hexagons are perpendicular to the tubular axis, whereas in *(n*, 0) zigzag, the two sides of each hexagons are parallel to the tube axis [112].

We have studied an array of single walled GeC nanotubes both in armchair and zigzag configurations. With distinct atomic arrangements, these nanotubular morphologies are categorized in three “types” namely Type I, Type II and Type III, which can be distinguished by looking at their respective atomic arrangements (Figs. 4.1 to 4.3). In type I arrangement, alternating C and Ge atoms have only Ge or C atoms as nearest neighbors. In type II and type III arrangements, the nearest neighbors surrounding each C atom consists of two Ge atoms and another C atom and vice-versa. The difference between type II and type III GeC nanotubes lies in the fact that in type II nanotubes, any layer (ring of atoms) perpendicular to the nanotube axis

contains only one kind of atoms, either C or Ge. But in type III, the same kind of layer will contain alternating C and Ge atoms. Also in the case of armchair nanotubes each layer comprises 2*n* atoms for the (*n, n*) nanotube but for zigzag nanotubes this layer has only *n* atoms per layer. For this reason type III zigzag nanotubes can only be formed when the chiral vector *n* is an even number. Finally, from atomic bond type perspective, type I has one kind of bond present throughout the nanotube, namely Ge-C bond, whereas types II and III have also Ge-Ge and C-C bonds (figures. 4.1 to 4.3).

In the armchair family of nanotubes, the smallest GeC conformation is a (3, 3) tube, represented by a cluster of $Ge_{30}C_{30}H_{12}$, and the largest (11, 11) represented by $Ge_{110}C_{110}H_{44}$. The smallest and largest GeC nanotubes in zigzag configuration studied are (3, 0) and (11, 0) tube, which can be denoted by $Ge_{33}C_{33}H_6$ and $Ge_{121}C_{121}H_{22}$, respectively.

4.2 Results and Discussions for GeC Nanotubes.

When instead of graphene, hybrid structures like GeC nanotubes are studied, a best possible way to calculate the relative thermodynamic stability of these structures is to compare the binding energy or cohesive energy per atom of different nanotubes. The cohesive energy or the binding energy per atom for each system is computed from the following equation:

$$E_b = \{[a\,E(Ge) + b\,E(C) + c\,E(H)] - [E(Ge_a C_b H_c)]\}/(a + b + c) \quad (4.1)$$

where *a, b,* and *c* are the numbers of Ge, C, and H atoms respectively. *E(Ge), E (C)* and *E(H)* are the spin-optimized ground state total energies of Ge, C and H atoms, respectively, and $E(Ge_aC_bH_c)$ is the total energy of the geometry and spin-optimized optimized clusters representing the nanotubes. Tables 4.1 to 4.6 summarize the electronic states, the binding energies per atom, the HOMO-LUMO or the “band” gaps, the diameters, and the dipole moments of the three different types of GeC nanotubes. In type I armchair nanotubes, the smallest value of cohesive energy obtained is 3.881eV/atom (3, 3) and the largest is 4.092eV/atom (11, 11).

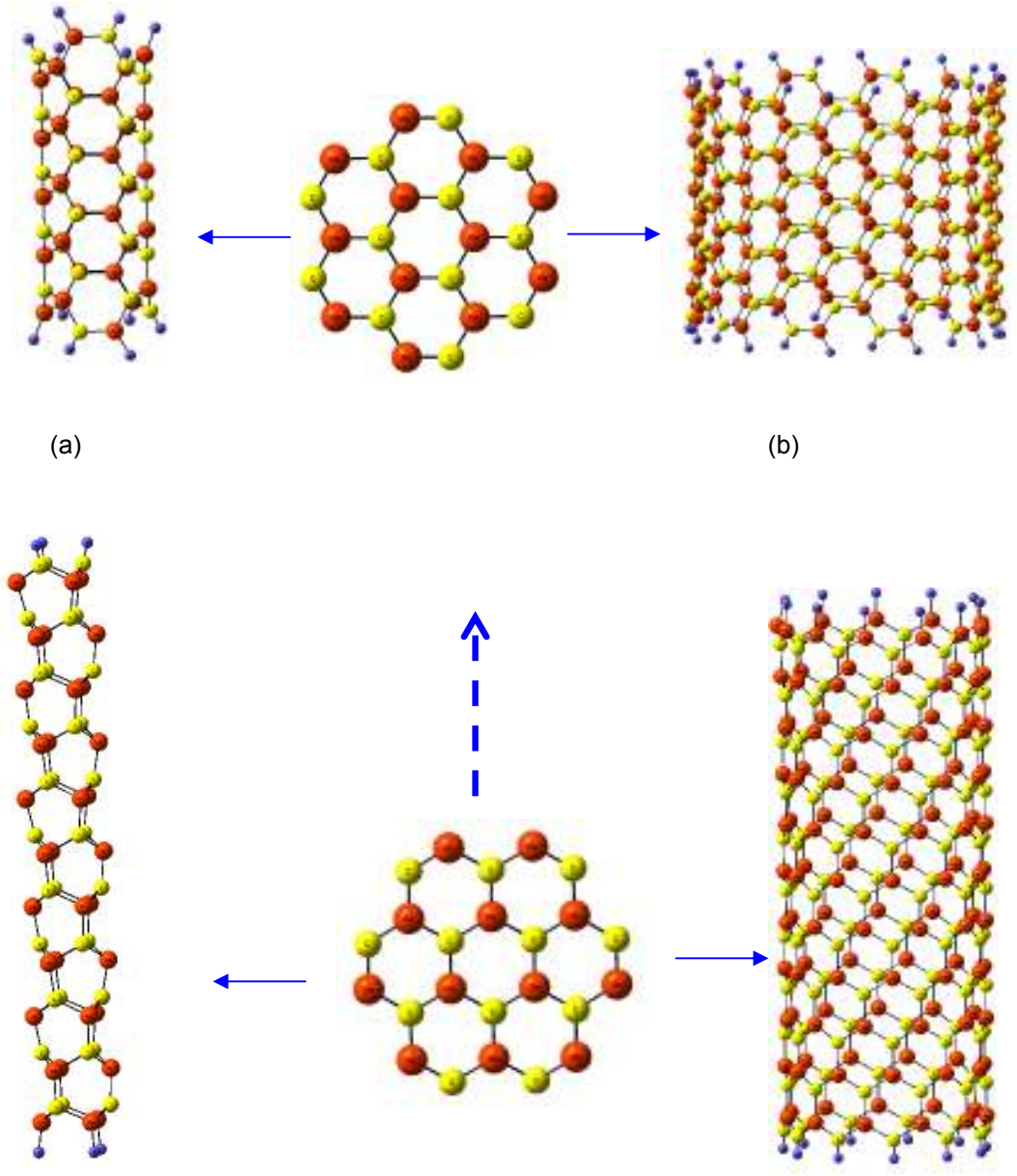

Figure 4.1 Atomic arrangements for (a) type I (3, 3) (b) type I (11, 11) (c) type I (3, 0) (d) type I (11, 0) GeC nanotubes. The carbon atoms are yellow and germanium atoms are red. The dashed line represents the orientation of tube axis.

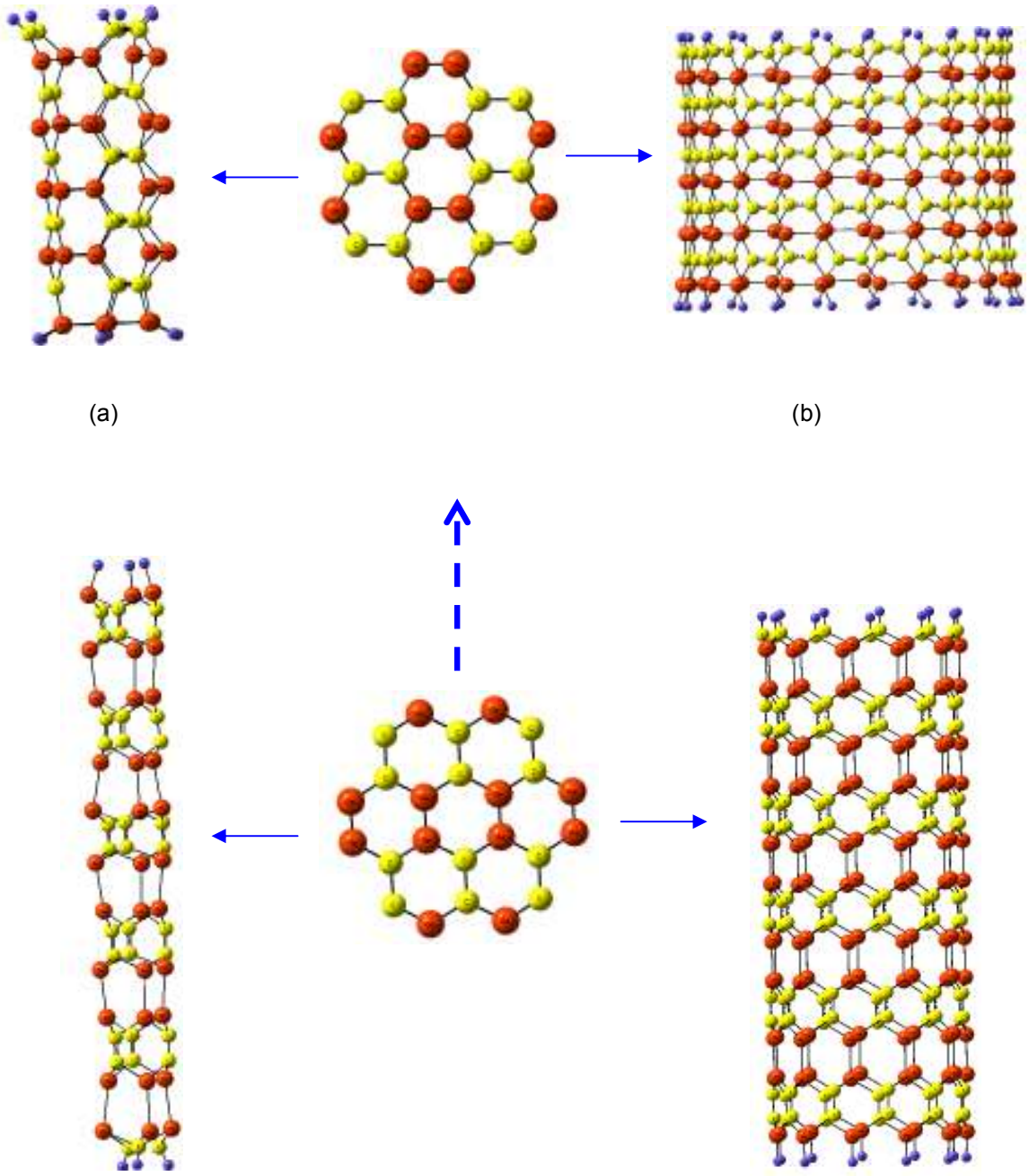

Figure 4.2 Atomic arrangements for (a) type II (3, 3) (b) type II (11, 11) (c) type II (3, 0) (d) type II (11, 0) GeC nanotubes. The carbon atoms are yellow and germanium atoms are red. The dashed line represents the orientation of tube axis.

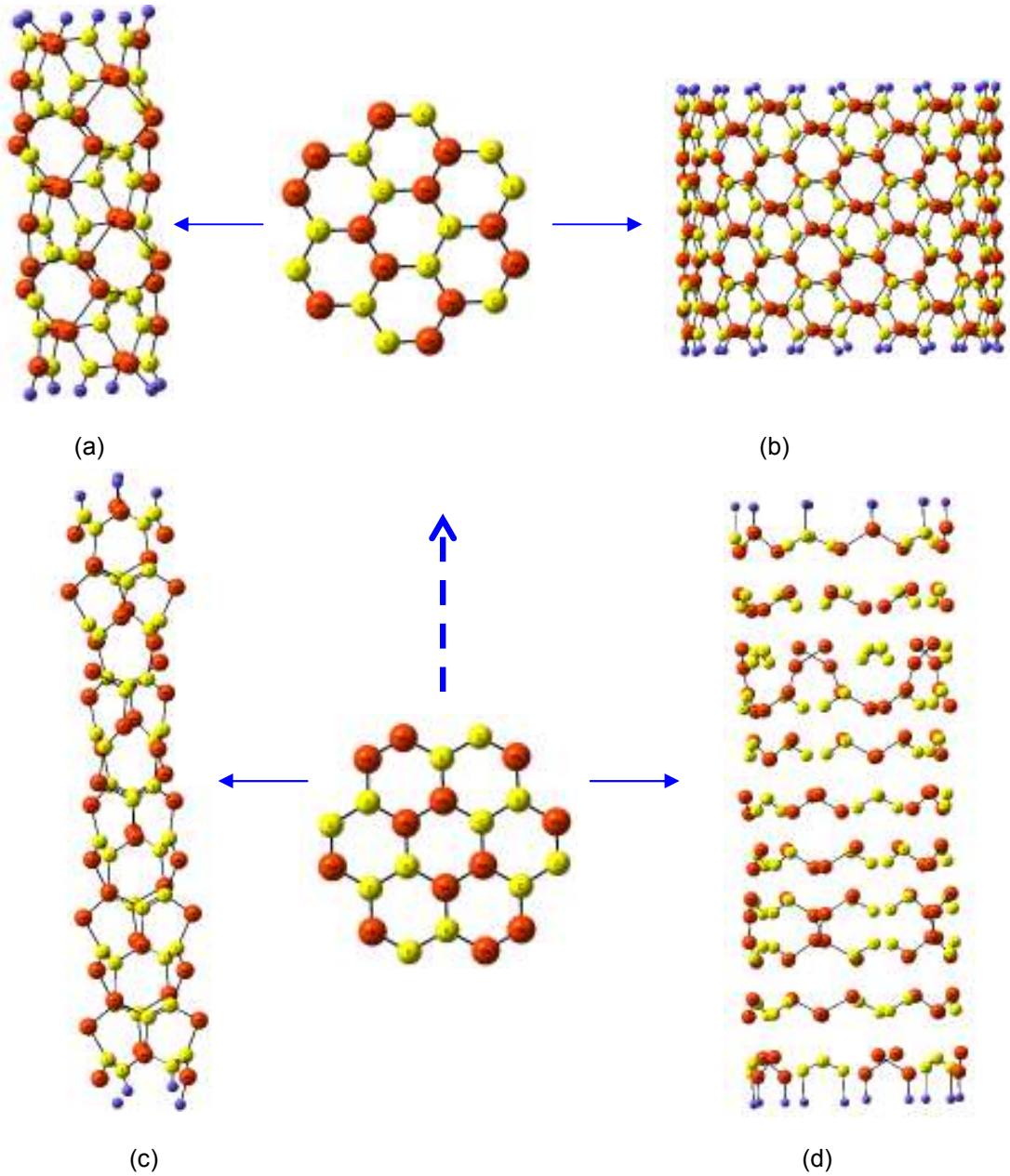

Figure 4.3 Atomic arrangements for (a) type III (3, 3) (b) type III (11, 11) (c) type II (4, 0) (d) type III (10, 0) GeC nanotubes. The carbon atoms are yellow and germanium atoms are red. The dashed line represents the orientation of tube axis.

Table 4.1 Electronic States, Binding Energies per Atom (E_b) in eV, HOMO-LUMO Gaps in eV, Diameters in Å, and Dipole Moments in Debye for Type I Armchair GeC Nanotubes.

Nanotube	Model	State	E_b(eV)	Gap(eV)	Diameter(Å)	Dip.Mnt (Debye)
(3,3)	$Ge_{30}C_{30}H_{12}$	$^1A_1$	3.881	2.666	4.603	0.0897
(4,4)	$Ge_{40}C_{40}H_{16}$	$^1A_1$	3.977	2.785	6.088	0.1085
(5,5)	$Ge_{50}C_{50}H_{20}$	$^1A_1$	4.019	2.988	7.576	0.1131
(6,6)	$Ge_{60}C_{60}H_{24}$	$^1A_1$	4.050	3.016	9.066	0.0798
(7,7)	$Ge_{70}C_{70}H_{28}$	$^1A_1$	4.066	3.003	10.561	0.0000
(8,8)	$Ge_{80}C_{80}H_{32}$	$^1A_1$	4.077	3.003	12.054	0.0000
(9,9)	$Ge_{90}C_{90}H_{36}$	$^1A_1$	4.084	2.999	13.550	0.0000
(10,10)	$Ge_{100}C_{100}H_{40}$	$^1A_1$	4.089	2.995	15.050	0.0005
(11,11)	$Ge_{120}C_{120}H_{44}$	$^1A_1$	4.092	2.995	16.547	0.0005

Table 4.2 Electronic States, Binding Energies per Atom (E_b) in eV, HOMO-LUMO Gaps in eV, Diameters in Å, and Dipole Moments in Debye for Type II Armchair GeC Nanotubes.

Nanotube	Model	State	E_b(eV)	Gap(eV)	Diameter (Å)	Dip.Mnt (Debye)
(3,3)	$Ge_{30}C_{30}H_{12}$	^1A	3.964	1.247	4.591	2.104
(4,4)	$Ge_{40}C_{40}H_{16}$	^1A	3.941	0.941	6.156	3.942
(5,5)	$Ge_{50}C_{50}H_{20}$	^1A	3.964	0.873	7.670	6.914
(6,6)	$Ge_{60}C_{60}H_{24}$	^1A	3.977	0.834	9.231	6.638
(7,7)	$Ge_{70}C_{70}H_{28}$	^1A	3.986	0.549	10.705	5.703
(8,8)	$Ge_{80}C_{80}H_{32}$	^1A	3.973	0.601	12.319	13.227
(9,9)	$Ge_{90}C_{90}H_{36}$	^1A	3.983	0.690	13.796	14.108
(10,10)	$Ge_{100}C_{100}H_{40}$	^1A	3.987	0.625	15.376	17.502
(11,11)	$Ge_{120}C_{120}H_{44}$	^1A	3.985	0.618	16.913	18.100

Table 4.3 Electronic States, Binding Energies per Atom (E_b) in eV, HOMO-LUMO Gaps in eV, Diameters in Å, and Dipole Moments in Debye for Type III Armchair GeC Nanotubes.

Nanotube	Model	State	E_b(eV)	Gap(eV)	Diameter (Å)	Dip.Mnt (Debye)
(3,3)	$Ge_{30}C_{30}H_{12}$	^1A_g	3.834	1.493	4.672	0.0000
(4,4)	$Ge_{40}C_{40}H_{16}$	^1A_g	3.883	1.296	6.167	0.0408
(5,5)	$Ge_{50}C_{50}H_{20}$	$^1A_1$	3.914	1.379	7.661	0.4732
(6,6)	$Ge_{60}C_{60}H_{24}$	$^1A_1$	3.935	1.236	9.165	0.0000
(7,7)	$Ge_{70}C_{70}H_{28}$	$^1A_1$	3.939	0.882	10.688	1.2098
(8,8)	$Ge_{80}C_{80}H_{32}$	$^1A_1$	3.953	0.906	12.199	0.0111
(9,9)	$Ge_{90}C_{90}H_{36}$	$^1A_1$	3.959	0.909	13.703	0.1417
(10,10)	$Ge_{100}C_{100}H_{40}$	$^1A_1$	3.964	0.918	15.222	0.3824
(11,11)	$Ge_{120}C_{120}H_{44}$	$^1A_1$	3.968	0.954	16.725	0.0222

Table 4.4 Electronic States, Binding Energies per Atom (E_b) in eV, HOMO-LUMO Gaps in eV, Diameters in Å, and Dipole Moments in Debye for Type I Zigzag GeC Nanotubes.

Nanotube	Model	State	E_b(eV)	Gap(eV)	Diameter(Å)	Dip.Mnt (Debye)
(3,0)	$Ge_{33}C_{33}H_6$	$^3A_1$	3.575	0.744	3.180	0.228
(4,0)	$Ge_{44}C_{44}H_8$	$^3B_1$	3.805	0.714	4.049	2.294
(5,0)	$Ge_{55}C_{55}H_{10}$	$^3B_1$	3.971	0.449	4.944	3.931
(6,0)	$Ge_{66}C_{66}H_{12}$	^3B	4.059	0.672	5.856	19.419
(7,0)	$Ge_{77}C_{77}H_{14}$	^3A	4.112	1.022	6.781	37.109
(8,0)	$Ge_{88}C_{88}H_{16}$	^3A	4.143	0.552	7.706	60.527
(9,0)	$Ge_{99}C_{99}H_{18}$	^3A	4.172	0.583	8.646	61.072
(10,0)	$Ge_{110}C_{110}H_{20}$	^3B	4.188	0.326	9.584	19.947
(11,0)	$Ge_{121}C_{121}H_{22}$	^3A	4.208	0.579	10.525	44.634

Table 4.5 Electronic States, Binding Energies per Atom (E_b) in eV, HOMO-LUMO Gaps in eV, Diameters in Å, and Dipole Moments in Debye for Type II Zigzag GeC Nanotubes.

Nanotube	Model	State	E_b(eV)	Gap(eV)	Diameter(Å)	Dip.Mnt (Debye)
(3,0)	$Ge_{33}C_{33}H_6$	$^3A_1$	3.816	0.672	3.268	18.377
(4,0)	$Ge_{44}C_{44}H_8$	^3A	3.876	0.603	4.173	1.072
(5,0)	$Ge_{55}C_{55}H_{10}$	^3A	3.918	0.465	5.060	6.794
(6,0)	$Ge_{66}C_{66}H_{12}$	^3A	3.924	0.402	5.862	4.239
(7,0)	$Ge_{77}C_{77}H_{14}$	^3A	3.981	0.385	6.827	7.827
(8,0)	$Ge_{88}C_{88}H_{16}$	^3A	3.985	0.353	7.617	13.499
(9,0)	$Ge_{99}C_{99}H_{18}$	^3A	3.997	0.202	8.743	15.996
(10,0)	$Ge_{110}C_{110}H_{20}$	^3A	4.075	0.311	9.642	19.350
(11,0)	$Ge_{121}C_{121}H_{22}$	^3A	4.086	0.296	10.594	32.256

Table 4.6 Electronic States, Binding Energies per Atom (E_b) in eV, HOMO-LUMO Gaps in eV, Diameters in Å, and Dipole Moments in Debye for Type III Zigzag GeC Nanotubes.

Nanotube	Model	State	E_b(eV)	Gap(eV)	Diameter(Å)	Dip.Mnt (Debye)
(4,0)	$Ge_{33}C_{33}H_8$	^3A	3.978	0.877	3.936	5.024
(6,0)	$Ge_{66}C_{66}H_{12}$	^3A	2.403	0.498	7.277	4.904
(8,0)	$Ge_{88}C_{88}H_{16}$	^3A	2.364	0.262	8.618	0.000
(10,0)	$Ge_{110}C_{110}H_{20}$	^3B	2.491	0.306	11.985	2.590

The corresponding numbers for type II and III armchair nanotubes are 3.964 and 3.985 eV/atom, and 3.834 and 3.968 eV/atom, respectively. In case of zigzag nanotubes, the smallest value of binding energy for type I (3, 0) is 3.575 eV/atom and largest (11, 0) is 4.208 eV/atom. The corresponding numbers for type II zigzag nanotubes are 3.816 and 4.086 eV/atom. Unlike the armchair nanotubes, the type III zigzag structures are not demonstrating continuous increase in binding energy with the diameter. The smallest nanotube (4, 0) has the maximum cohesive energy of 3.978 eV/atom and the minimum value of 2.364 eV/atom is obtained for (8, 0) nanotube. The average value of the binding energy of type I armchair GeC nanotube is found to be 4.037 eV/ atom. For type II and type III, these values are 3.973 and 3.927 eV/atom, respectively. Zigzag type I nanotubes yield an average binding energy per atom to be 4.026eV. For type II and type III, these values are 3.963 and 2.809 eV/atom, respectively. It is evident that for both armchair and zigzag structures, type I nanotubes have the highest average stability. Similar trend was noticed in our previous study on SiC nanotubes [113]. Furthermore, type I armchair tubes are more stable than type II and III tubes, only exception being the smallest (3, 3) nanotube. In the case of zigzag GeC tubes, similar trend is observed with the exceptions of the smaller (3, 0) and (4, 0) nanotubes.

It is evident from the figures 4.4 and 4.5 for types I and III armchair tubes binding energy per atom tends to increase monotonically achieving near saturation at (11, 11). This monotonous increment in binding energy is also noticed in types I and II GeC zigzag nanotubes. Such increase in binding energies with cluster sizes until saturation point is a well-known phenomenon in cluster calculations. Same saturation tendency, from (3, 3) to (11, 11) is also observed for type II armchair nanotubes with minor fluctuations as we move from (3, 3) to (4, 4) and (7, 7) to (8, 8). The rather small increase in cohesive energy with cluster size in type II is attributed to the geometrical arrangement. From table 4.6 and figure 4.5 it is clear that higher diameter type III zigzag tubular structures are less stable than all the other nanotubes reported.

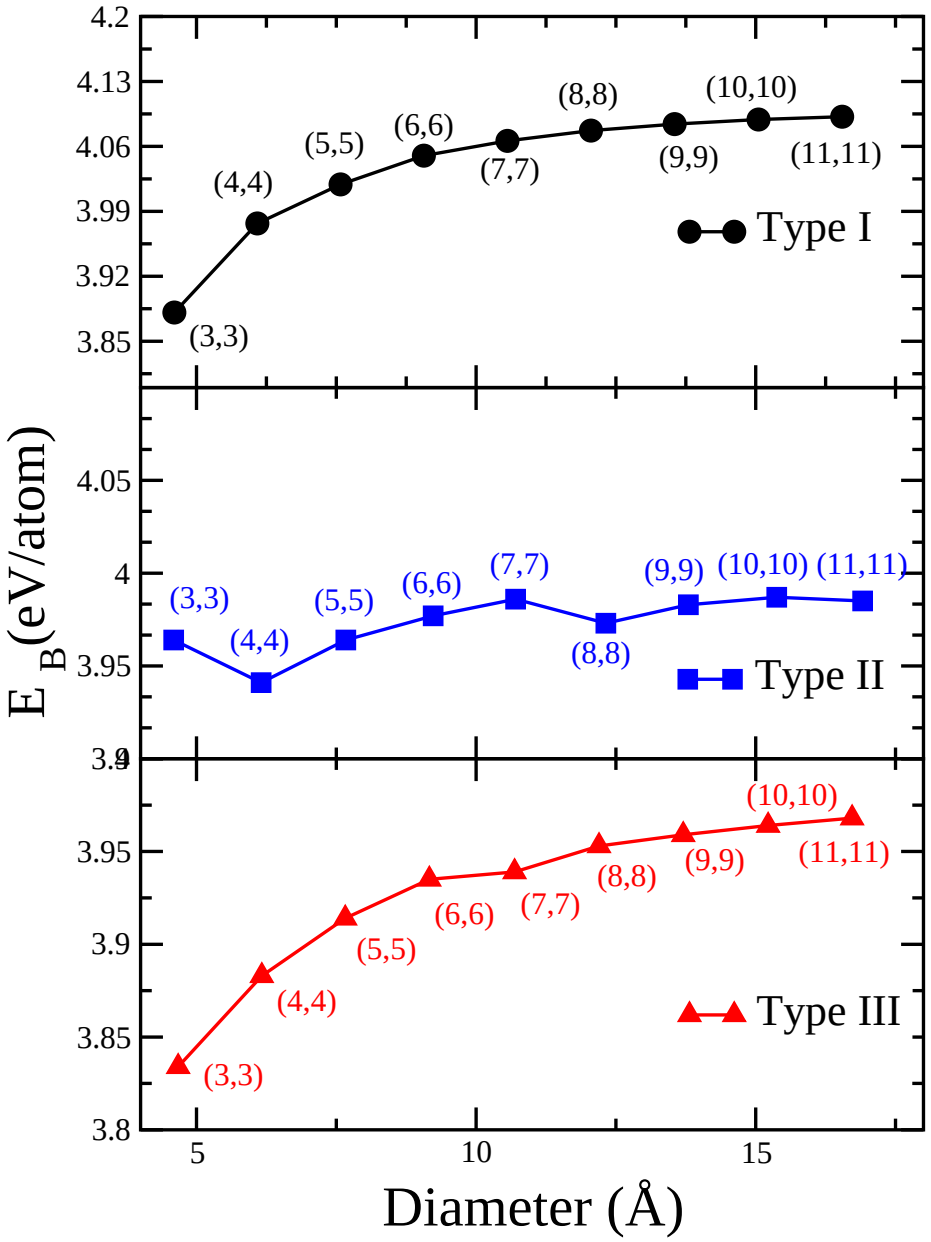

Figure 4.4 Binding energy versus diameter for GeC armchair nanotubes.

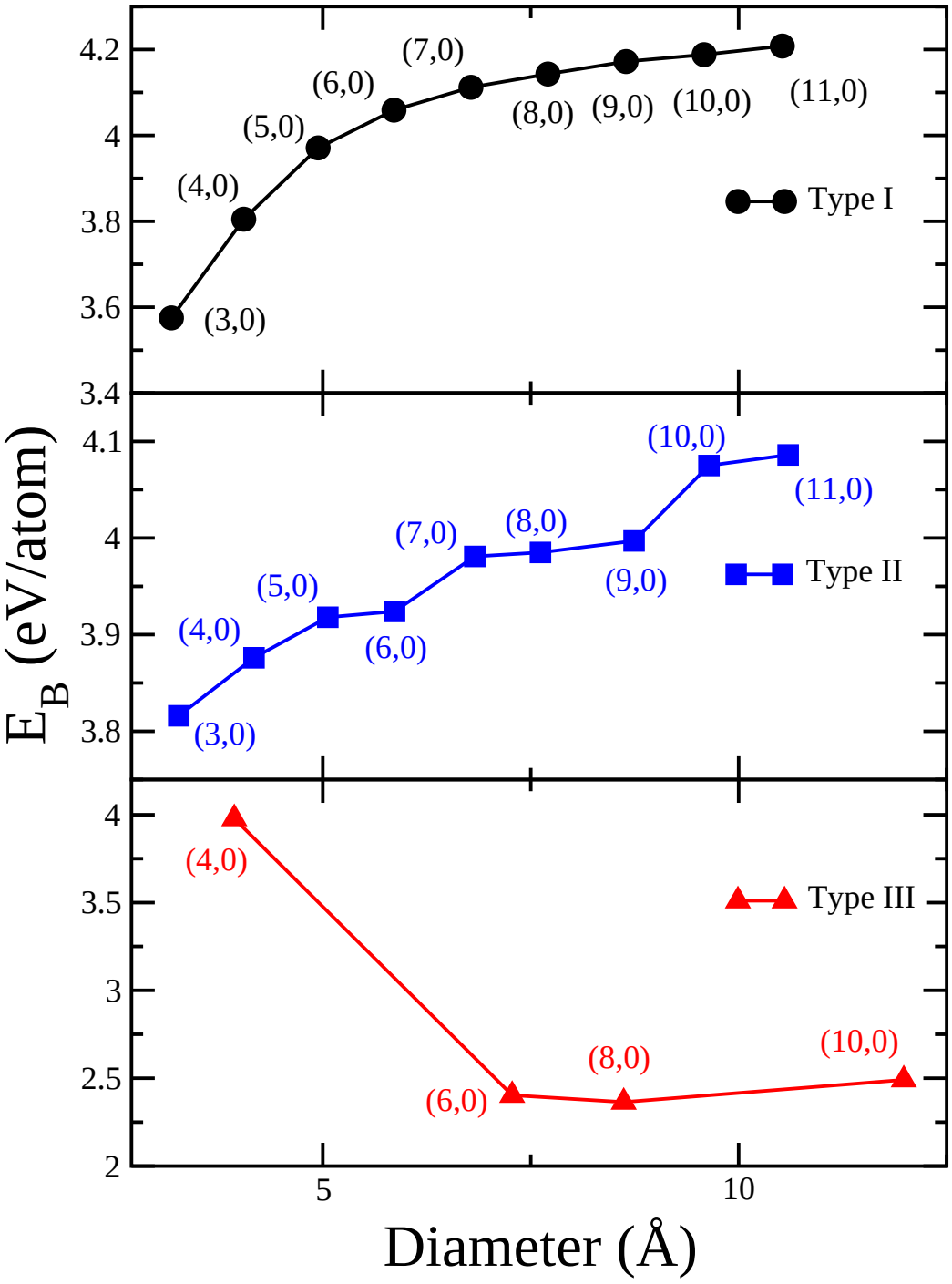

Figure 4.5 Binding energy versus diameter for GeC zigzag nanotubes.

The overall symmetry of type I nanotubes and the presence of only Ge-C bonds in type I structures for both armchair and zigzag nanotubes are responsible for their higher stability. On the other hand type II and III nanotubes have three different types of bonds, namely Ge-C, C-C and Ge-Ge, which might be a possible reason for their lower stability. The unusual trend in stability with respect to the diameter for type III zigzag nanotubes can be possibly linked with the heavy structural distortion for higher diameter tubes (Fig. 4.3). It is worthwhile to note that, in spite of high degree of structural distortion in higher diameter type III zigzag tubes, these nanotubular structures retained their cylindrical geometry which justify the manufacturing of these tubes under suitable conditions. It is expected that these tubes can be further stabilized by either hydrogen passivation or by doping with proper impurity for the specific nano based applications.

Rolling of graphene like sheet into a tubular cylinder induces a strain in the structure, which cause a pattern of bond distortions along the nanotubes. Furthermore, bond distortion also depends on the spatial position of the atoms, which is clearly distinct in the armchair and zigzag tubes. All the relaxed nanotubes reported here are initially built with all atoms equally spaced, and at same radial distance from the axis. In tables 4.7 to 4.12, we report the bond length variations for different nanotubes. For all three types of armchair and zigzag nanotubes the average Ge-C and Ge-Ge bond lengths decrease as the tube diameter increases with some exceptions. Small diameter nanotubes by virtue of their strong curvature are highly strained and to minimize the strain energy Ge-C and Ge-Ge bonds expand. In contrast, C-C bond indicate a mixed behavior in both chiralities. The average Ge-C bond lengths in armchair and zigzag nanotubes are smaller than our calculated Ge-C dimer bond length reported earlier. This contraction of bond length indicates the efficient overlap of the orbitals and a strong binding character of GeC bonds within the nanotube, which is responsible for the overall stability of the type I nanotubes. On the other hand, Ge-C bond lengths have relatively higher values in type II and type III structures, resulting in lower cohesive energy per atom.

Table 4.7 Average, Minimum, Maximum Bond Lengths (in Å) of Type I Armchair GeC Nanotubes.

Nanotube	Ave	Min	Max
(3,3)	1.887	1.824	1.898
(4,4)	1.882	1.828	1.892
(5,5)	1.879	1.828	1.888
(6,6)	1.878	1.830	1.889
(7,7)	1.877	1.829	1.889
(8,8)	1.876	1.830	1.889
(9,9)	1.876	1.830	1.889
(10,10)	1.875	1.829	1.889
(11,11)	1.875	1.829	1.888

Table 4.8 Average, Minimum, Maximum Bond Lengths (in Å) of Type II Armchair GeC Nanotubes.

	Ge-Ge			C-C			Ge-C		
Nanotube	**Ave**	**Min**	**Max**	**Ave**	**Min**	**Max**	**Ave**	**Min**	**Max**
(3,3)	2.525	2.487	2.557	1.391	1.364	1.409	1.996	1.918	2.068
(4,4)	2.458	2.379	2.499	1.402	1.378	1.413	1.970	1.914	2.025
(5,5)	2.426	2.374	2.474	1.409	1.375	1.428	1.953	1.912	2.006
(6,6)	2.414	2.372	2.448	1.423	1.400	1.446	1.950	1.908	1.988
(7,7)	2.408	2.372	2.428	1.411	1.376	1.425	1.948	1.913	1.985
(8,8)	2.349	2.300	2.377	1.429	1.387	1.443	1.913	1.895	1.928
(9,9)	2.394	2.352	2.444	1.418	1.380	1.441	1.935	1.906	1.973
(10,10)	2.349	2.294	2.379	1.430	1.387	1.445	1.911	1.892	1.926
(11,11)	2.348	2.292	2.380	1.430	1.388	1.445	1.911	1.892	1.926

Table 4.9 Average, Minimum, Maximum Bond Lengths (in Å) of Type III Armchair GeC Nanotubes.

	Ge-Ge			C-C			Ge-C		
Nanotube	**Ave**	**Min**	**Max**	**Ave**	**Min**	**Max**	**Ave**	**Min**	**Max**
(3,3)	2.541	2.521	2.560	1.394	1.391	1.397	1.983	1.820	2.091
(4,4)	2.442	2.419	2.465	1.412	1.411	1.412	1.955	1.826	2.051
(5,5)	2.400	2.380	2.421	1.420	1.395	1.443	1.937	1.831	2.022
(6,6)	2.382	2.368	2.396	1.424	1.417	1.432	1.927	1.832	1.998
(7,7)	2.352	2.347	2.362	1.437	1.429	1.456	1.909	1.819	1.942
(8,8)	2.350	2.347	2.353	1.433	1.422	1.444	1.907	1.837	1.937
(9,9)	2.347	2.344	2.354	1.434	1.422	1.445	1.906	1.838	1.944
(10,10)	2.348	2.346	2.349	1.435	1.425	1.445	1.906	1.838	1.934
(11,11)	2.349	2.346	2.352	1.434	1.423	1.444	1.906	1.837	1.940

Table 4.10 Average, Minimum, Maximum Bond Lengths (in Å) of Type I Zigzag GeC Nanotubes.

Nanotube	Ave	Min	Max
(3,0)	1.950	1.868	1.990
(4,0)	1.908	1.858	1.933
(5,0)	1.895	1.866	1.910
(6,0)	1.889	1.865	1.903
(7,0)	1.886	1.876	1.899
(8,0)	1.884	1.853	1.898
(9,0)	1.882	1.866	1.897
(10,0)	1.882	1.866	1.897
(11,0)	1.882	1.832	1.966

Table 4.11 Average, Minimum, Maximum Bond Lengths (in Å) of Type II Zigzag GeC Nanotubes.

	Ge-Ge			C-C			Ge-C		
Nanotube	**Ave**	**Min**	**Max**	**Ave**	**Min**	**Max**	**Ave**	**Min**	**Max**
(3,0)	2.751	2.612	2.966	1.415	1.350	1.657	2.048	1.987	2.121
(4,0)	2.561	2.452	2.994	1.380	1.376	1.382	1.986	1.912	2.035
(5,0)	2.641	2.468	2.966	1.387	1.355	1.414	1.976	1.867	2.040
(6,0)	2.498	1.999	2.965	1.419	1.374	1.491	1.947	1.433	2.165
(7,0)	2.370	2.346	2.428	1.421	1.413	1.428	1.925	1.854	1.944
(8,0)	2.365	2.345	2.414	1.430	1.424	1.436	1.917	1.858	1.933
(9,0)	2.354	2.352	2.358	1.647	1.629	1.678	1.893	1.847	1.912
(10,0)	2.397	2.355	2.478	1.423	1.411	1.434	1.927	1.835	2.022
(11,0)	2.364	2.354	2.397	1.441	1.434	1.454	1.909	1.860	1.922

Table 4.12 Average, Minimum, Maximum Bond Lengths (in Å) of Type III Zigzag GeC Nanotubes.

	Ge-Ge			C-C			Ge-C		
Nanotube	**Ave**	**Min**	**Max**	**Ave**	**Min**	**Max**	**Ave**	**Min**	**Max**
(4,0)	2.610	2.588	2.650	1.383	1.360	1.395	2.012	1.921	2.119
(6,0)	2.450	2.379	2.603	1.414	1.387	1.439	1.985	1.525	2.179
(8,0)	2.412	2.283	2.592	1.468	1.425	1.511	1.952	1.791	2.068
(10,0)	2.310	1.783	2.696	1.513	1.491	1.545	1.947*	1.702	1.993

We note that Ge-C bonds have mixed sp^2-sp^3 nature, whereas Ge-Ge and C-C bonds are dominantly sp^3 and sp^2 in character respectively, which also accounts for the observed behavior in the bond length variations.

Also structure relaxation leads to a change in the radial geometry of cylindrical structures, which is characterized by two concentric cylindrical tubes, one consisting of Ge atoms and another one formed of C atoms. The radial buckling β is calculated as an absolute value of the difference between average radial distances of germanium and carbon atoms from the tube axis:

$$\beta = | \langle r_{Ge} \rangle - \langle r_C \rangle | \qquad (4.2)$$

where $\langle r_{Ge} \rangle$ and $\langle r_C \rangle$ are the average radial distances of Ge and C atoms, respectively. In tables 4.13 and 4.14 and figures 4.6 and 4.7, we report the variations of buckling values with respect to different tube diameters. For type I armchair nanotubes, there is a very small outward relaxation of C atoms while Ge atoms slightly move inwards and therefore the amount of buckling can be considered as negligible.

Table 4.13 Tube Diameters (in Å) and Radial Bucklings (in Å) for Types I, II and III Armchair GeC Nanotubes.

	Type I		Type II		Type III	
Nanotube	**Diameter(Å)**	**β (Å)**	**Diameter(Å)**	**β (Å)**	**Diameter(Å)**	**β (Å)**
(3,3)	4.603	0.0068	4.591	0.1823	4.672	0.3749
(4,4)	6.088	0.0078	6.156	0.3074	6.167	0.2597
(5,5)	7.576	0.0077	7.670	0.2280	7.661	0.1790
(6,6)	9.066	0.0090	9.231	0.1999	9.165	0.1248
(7,7)	10.561	0.0080	10.705	0.1949	10.688	0.0518
(8,8)	12.054	0.0071	12.319	0.1219	12.199	0.0401
(9,9)	13.550	0.0078	13.796	0.1389	13.703	0.0330
(10,10)	15.050	0.0059	15.376	0.1186	15.222	0.0256
(11,11)	16.547	0.0060	16.913	0.1086	16.725	0.0411

Table 4.14 Tube Diameters (in Å) and Radial Bucklings (in Å) for Types I, II and III Zigzag GeC Nanotubes.

	Type I		Type II		Type III	
Nanotube	**Diameter(Å)**	**β (Å)**	**Diameter(Å)**	**β (Å)**	**Diameter(Å)**	**β (Å)**
(3,0)	3.180	0.3024	3.268	0.3272		
(4,0)	4.049	0.0377	4.173	0.1859	3.936	0.6399
(5,0)	4.944	0.0041	5.060	0.1696		
(6,0)	5.856	0.0012	5.862	0.2805	7.277	0.0257
(7,0)	6.781	0.0017	6.827	0.0523		
(8,0)	7.706	0.0017	7.617	0.0626	8.618	0.1142
(9,0)	8.646	0.0006	8.743	0.0032		
(10,0)	9.584	0.0058	9.642	0.0557	11.985	0.0566
(11,0)	10.525	0.0006	10.594	0.0266		

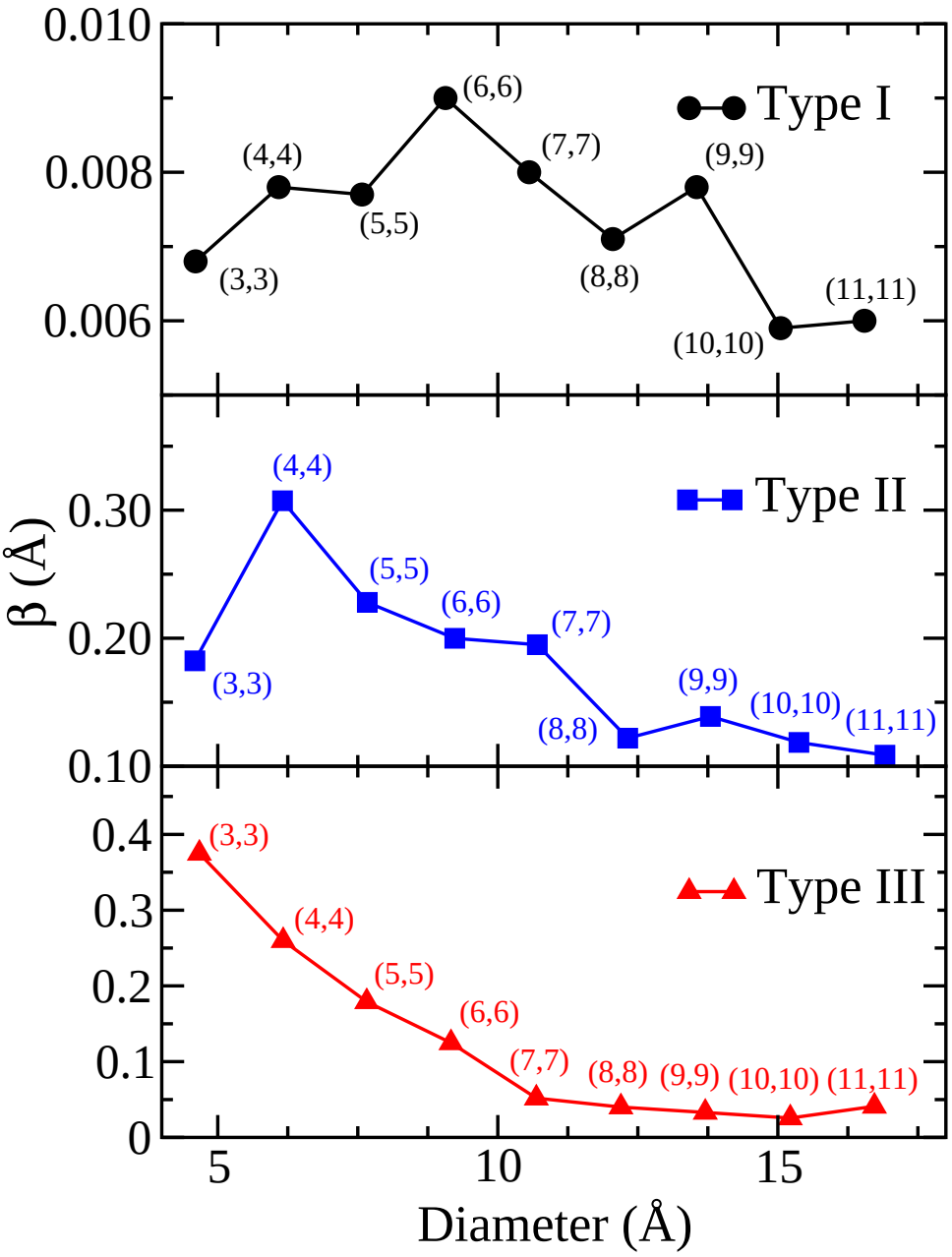

Figure 4.6 Tube buckling versus diameter for GeC armchair nanotubes.

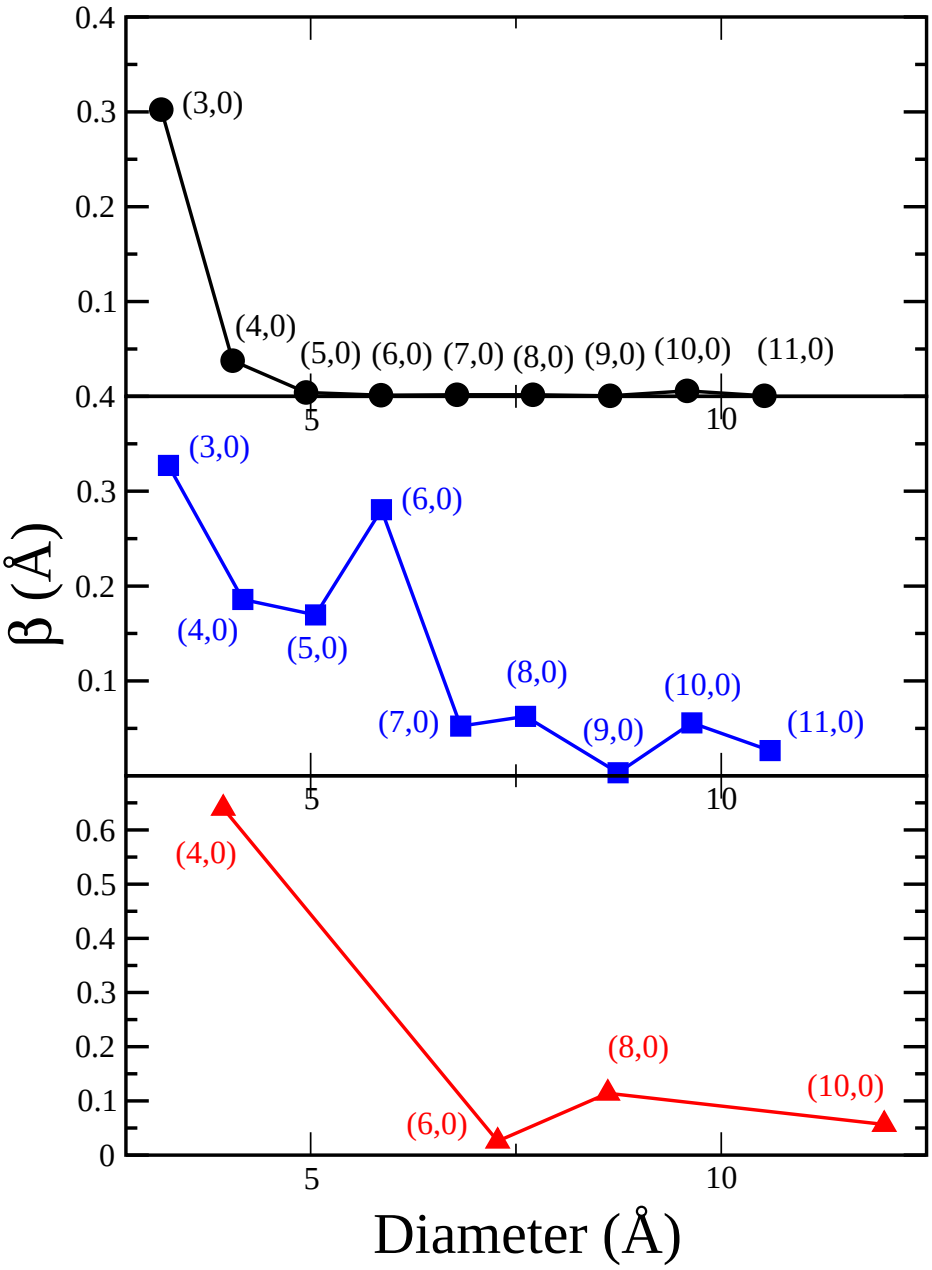

Figure 4.7 Tube buckling versus diameter for GeC zigzag nanotubes.

In case of type I zigzag nanotubes, this buckling direction is reversed, with Ge atoms moving away from the tube axis and C atoms moving toward the axis the axis. Nonetheless, the amounts of buckling in the zigzag structures have almost negligible values like armchair nanotubes. This rather small buckling is attributed to the fact that type I nanotubes are highly symmetric in nature, with only one type of bonds. In types II and III for both armchair and zigzag, the Ge atoms shift outwards and C atoms tend to move towards the axis of the nanotubes resulting in significant radial buckling. Hence types II and III nanotubes may be considered as Ge coated nanotubes with the reconstructions of the tube surfaces being quite prominent. It is worth mentioning that in our previous investigation on SiC nanotubes, similar type of behavior was observed [113]. Buckling does appear to be a minor effect, specifically for type I due to the overall symmetry and might possibly be a manifestation of the finite lengths of the tubes. In general for both the chiralities, lesser surface reconstructions are noted with increasing the tube diameters. The puckered surface structure caused by bond bending may also induce surface dipoles and modify the surface band structure, indicating some relevant potential chemical applications of GeC nanotubes.

From tables 4.1 to 4.6, we note that type I armchair nanotubes have almost negligible net dipole moments, which can again be attributed to the over all symmetry of the structures. High values of net dipole moment after relaxation for type II armchair and zigzag and type I zigzag nanotubes can be explained from the fact that these nanotubes have alternate layers of either Ge or C atoms and thus two ends of nanotubes will always be populated by different kinds of atoms. Though type III nanotubes in both chiralities do not have only either Ge or C atoms at the ends of the tubes, asymmetry in the structures in comparison to type I tubes induces the small values of the dipole moments.

We have performed the Mulliken charge analysis for all three types of GeC. As expected, these structures show a significant charge transfer from Ge to C atoms since C is more electronegative than Ge.

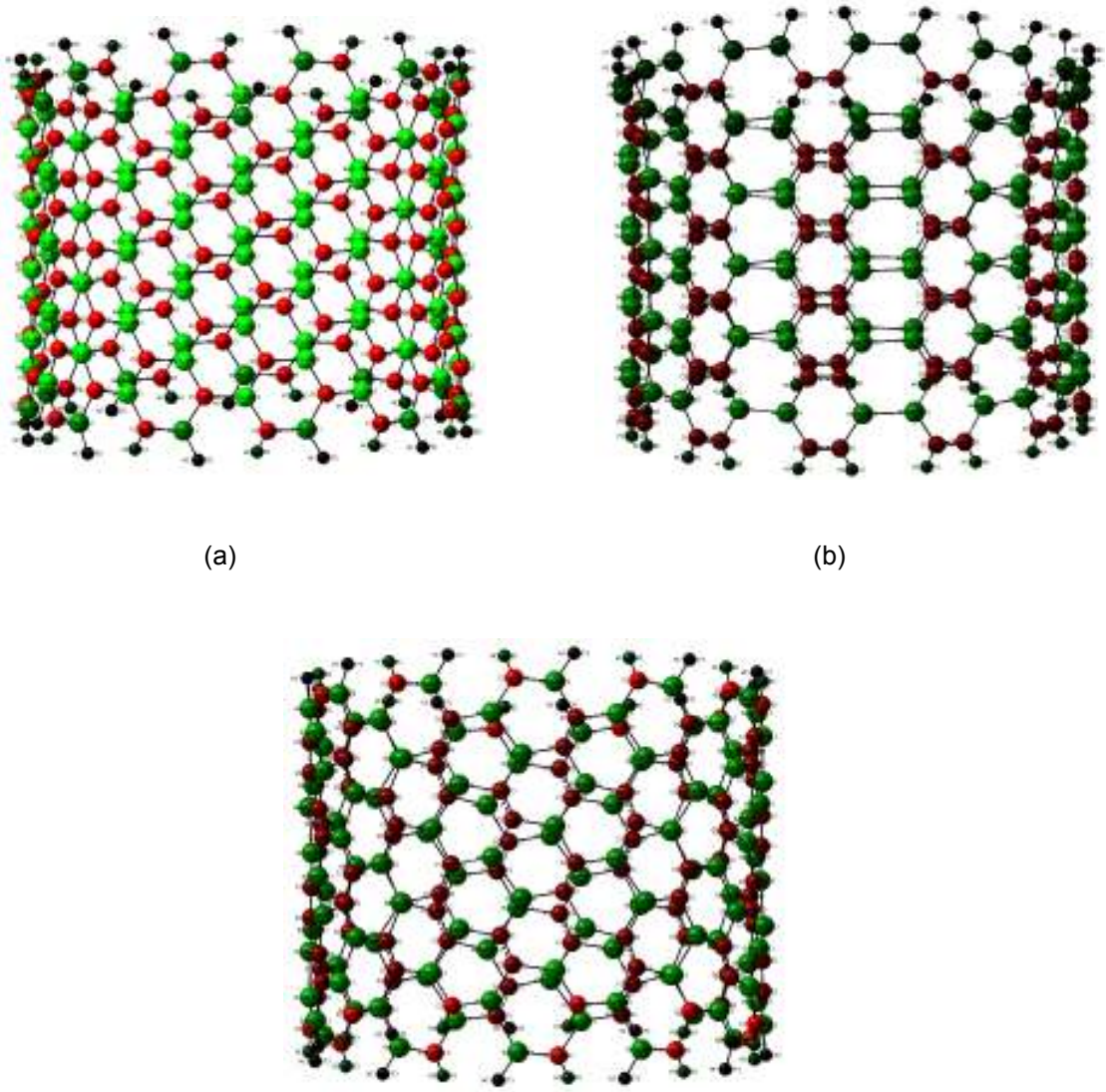

Figure 4.8 Mulliken charge distributions for (11, 11) nanotubes. (a) type I, (b) type II and (c) type III. Carbon atoms gained and germanium atoms, lost charge.

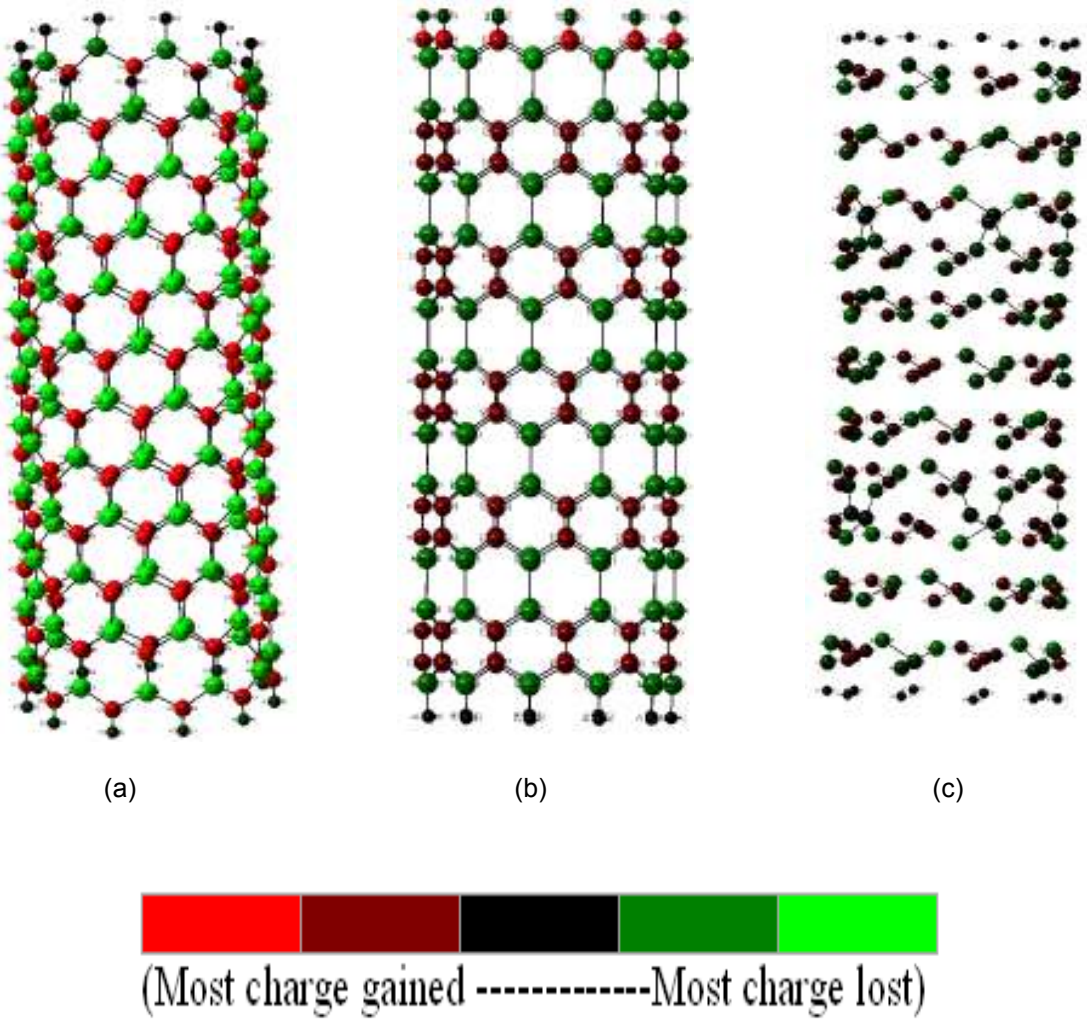

Figure 4.9 Mulliken charge distributions for (a) type I (11, 0), (b) type II (11, 0) and (c) type III (10, 0) nanotubes.

Figures 4.8 and 4.9 indicate that type I structures exhibit more ionic bonding characteristics than types II and III, in other words more charge transfer occurs from Ge atom to carbon atoms. Carbon atoms gained and germanium atoms, lost charge to C atoms in type I nanotubes. This is due to the fact that only Ge-C bonds are present in type I. Since types II and III contain C-C, Ge-C, and Ge-Ge bonds, the nature of the bonding is a mixture of ionic and covalent bonds. Thus, to an extent, we can say that the mechanism of charge transfer among the atoms influence the stability of the nanotubes. The larger the charge transfer, stronger is the hybridization of Ge-C bonds and thus higher is the nanotube stability.

To investigate the possible metallic or semi-conducting behavior of the nanotubes, we have calculated the highest-occupied-molecular-orbital to lowest-unoccupied-molecular-orbital (HOMO-LUMO) gaps or the “band gaps’ of all the nanotubes reported in this work. Tables 4.1 to 4.6 and figures 4.10 to 4.11 show the calculated gaps as a function of the diameters of the corresponding nanotubes. The results suggest that all GeC nanotubes are semi-conducting in nature, with a wide spectrum of band gaps ranging from 0.549 eV to 3.016 eV for armchair, 0.262 eV to 1.022 eV for zigzag nanotubes and 0.232 eV to 0.693 eV for pure Ge zigzag nanotubes. Type I armchair nanotubes have the largest gaps, with smallest (3, 3) structure having a band gap of 2.666 eV and the largest (11, 11) structure with a band gap of 2.995 eV, with convergence achieved around (7, 7). Type I armchair nanotubes have band gaps which are systematically larger than previously studied the two bulk structures [77, 78]. Type I zigzag nanotubes also yield relatively higher band gap values than the other two types. Strong ionic nature of type I nanotubes may be responsible for localizing electronic states which results in wide band gap values. A similar result was reported for SiC nanotubes [113]. The band gaps for types II and III nanotubes are significantly lower than type I nanotubes in armchair configuration. Furthermore type II armchair nanotubes have comparatively lower gaps than corresponding type III nanotubes, with gaps indicating a downward trend with increasing diameter. Similar behavior has also been noted before for SiC nanotubes [113].

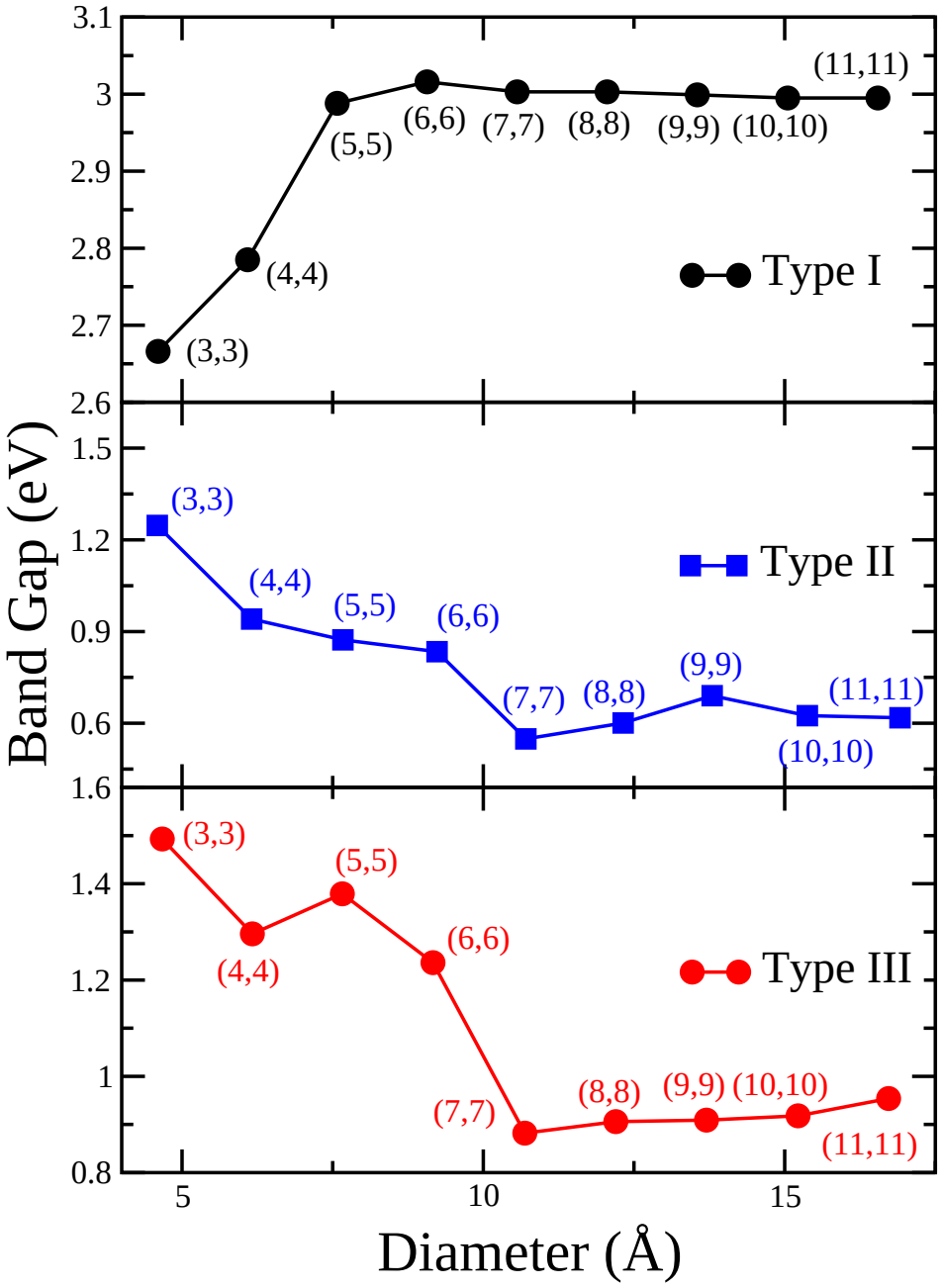

Figure 4.10 HOMO-LUMO gaps versus diameter for GeC armchair nanotubes.

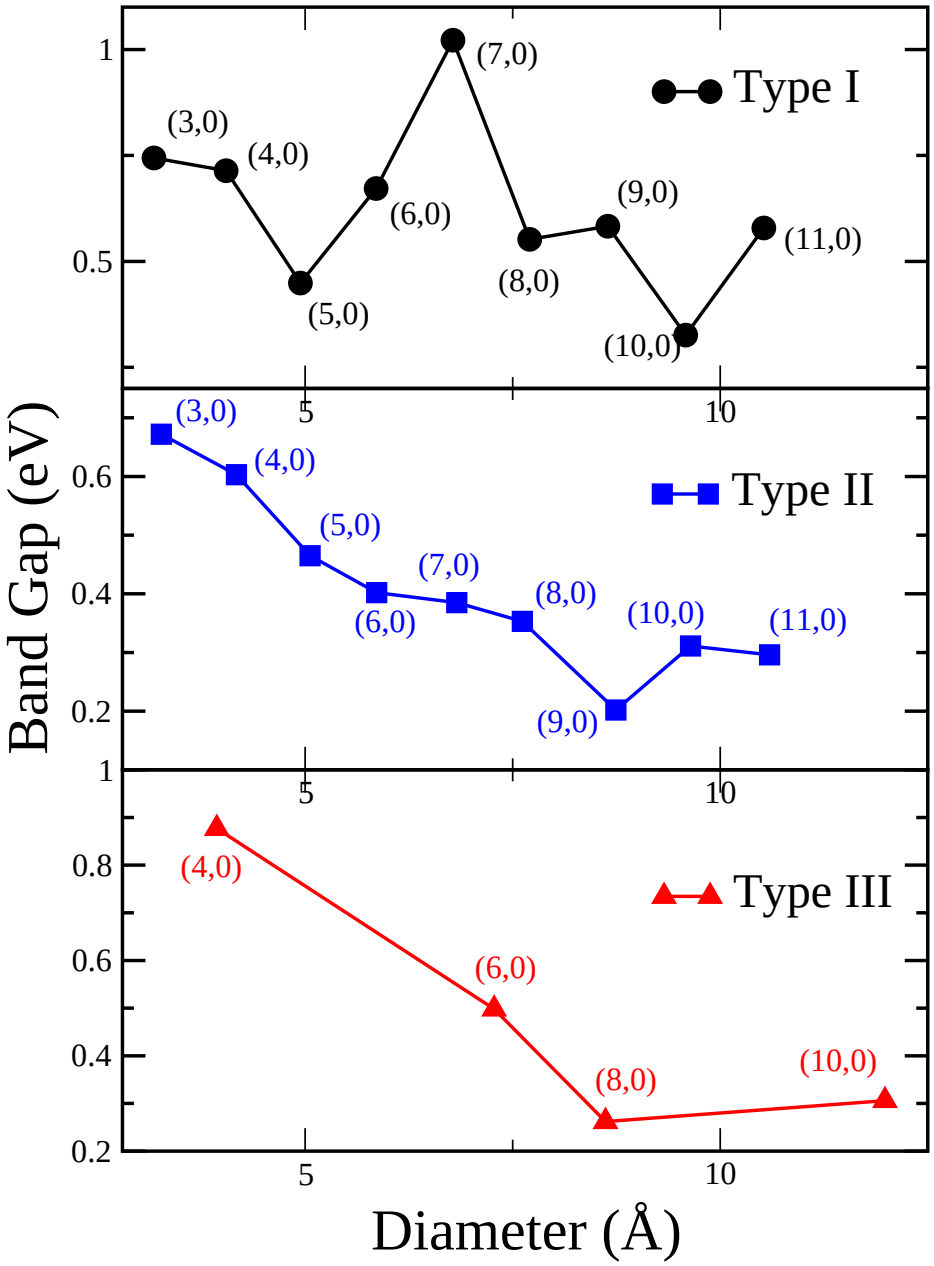

Figure 4.11 HOMO-LUMO gaps versus diameter for GeC zigzag nanotubes

On the other hand type I zigzag nanotubes show an oscillatory behavior in band gap values with increasing the tube diameters. For both types II and III armchair nanotubes, the band gaps decrease from (3, 3) to (7, 7) with minor oscillatory pattern noted thereafter. The irregularities in gap values for these zigzag tubes can possibly be a manifestation of smaller diameters, which ultimately gives rise to atomic interactions well beyond the nearest neighbors. Band gaps for nanotubes with higher diameter are expected to approach the limiting values of the corresponding graphene like sheets. GeC nanotubes with wide spectrum of band gaps can potentially be used in some nano-optical based applications and in the low voltage based nanoelectronics circuits as insulators where the excitation energy is not enough to overcome the gap barrier.

The highest occupied molecular orbitals (HOMO) and lowest unoccupied molecular orbitals (LUMO) of the three types of nanotubes are shown in figures 4.12 to 4.17. It is evident from the figures that HOMO is localized to C atoms in type I armchair and zigzag nanotubes consistent with the higher charge transfer from Ge to C atoms. The delocalized nature of the electrons is clearly visible for types II and III armchair and zigzag nanotubes which is a manifestation of the aromatic behavior of C-C bonds and the mixed ionic and covalent behavior of the nanotubes. This delocalization of the orbital is a reminiscent of the lower stabilities of type II and III nanotubes discussed earlier.

Figures 4.18 and 4.19 show the energy density of states (DOS) for GeC armchair (6, 6), and zigzag (6, 0) nanotubes, respectively. The DOS is convoluted with a Gaussian of width 0.05 eV and HOMO is adjusted to zero. The large gaps of type I tubes as compared to the gaps in the other two types is clearly visible. Further on the application side, we expect the properties of GeC tubes can be selectively modified by the adsorption of external functionalized groups. Wide band gap spectrum of three different types of GeC nanotubes also opens up an arena for bandgap selective engineered for nano optoelectronic devices.

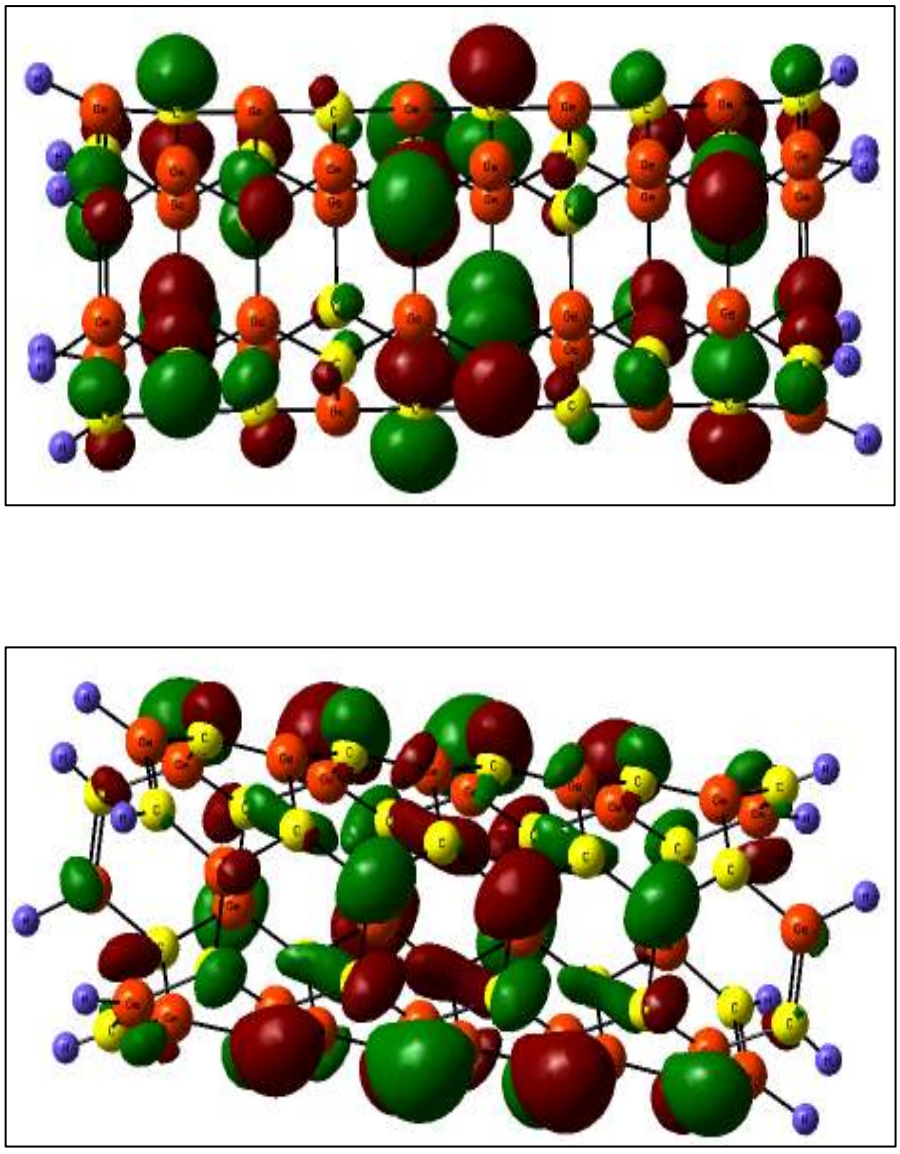

Figure 4.12 Type I (3, 3) HOMO (top) and LUMO (bottom).

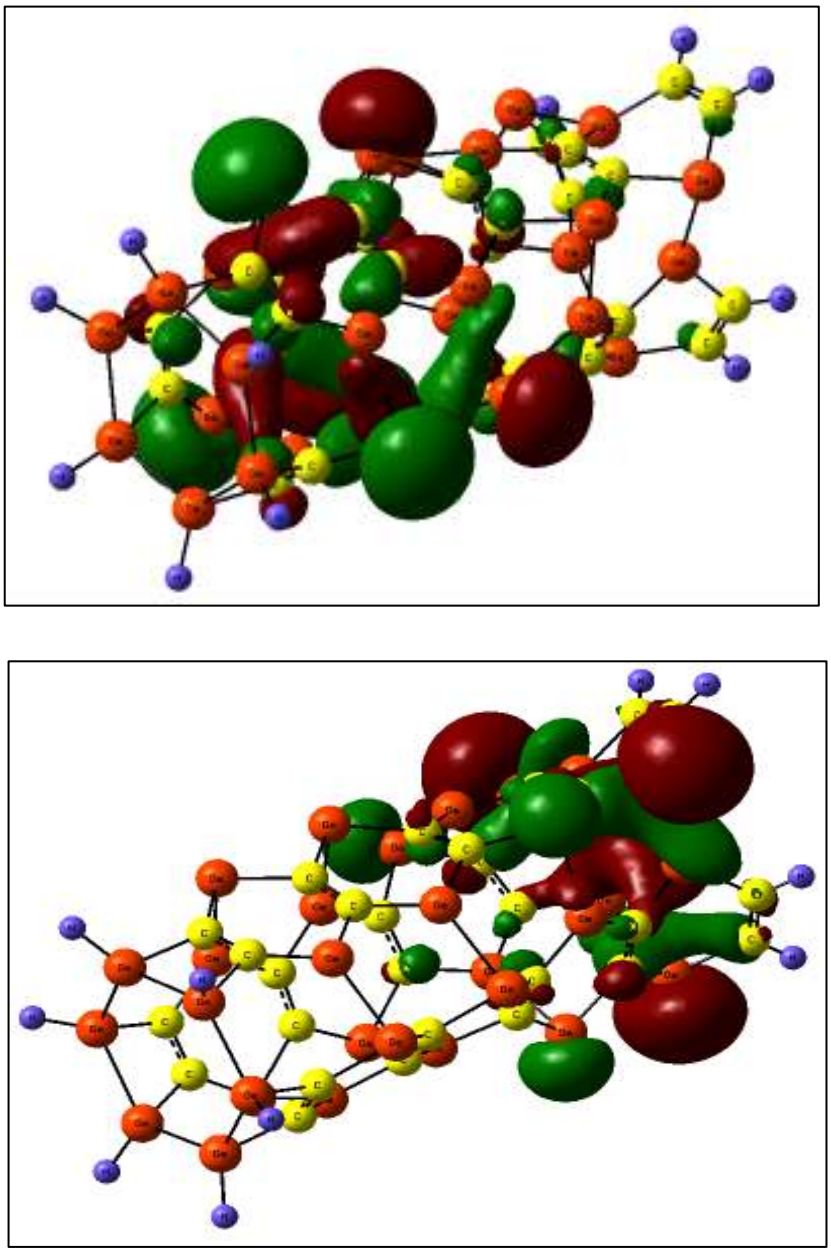

Figure 4.13 Type II (3, 3) HOMO (top) and LUMO (bottom).

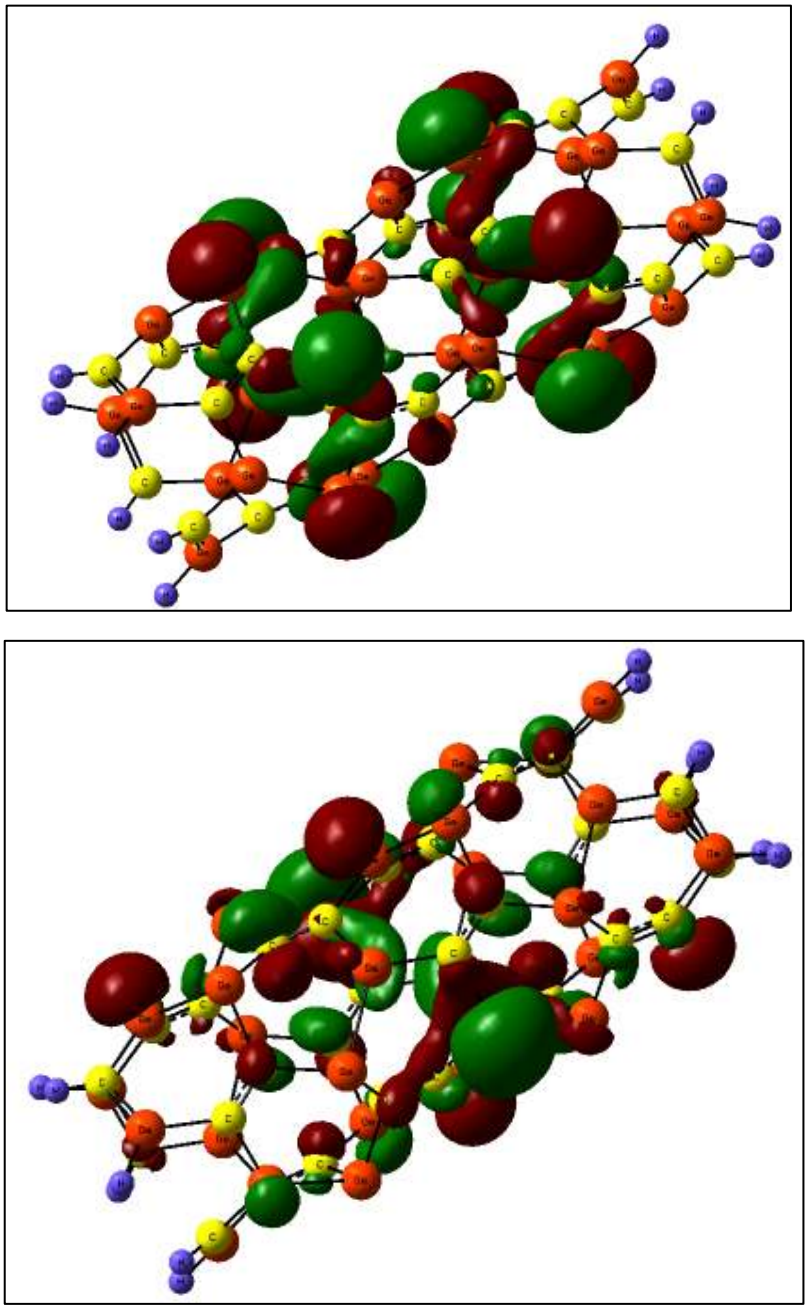

Figure 4.14 Type III (3, 3) HOMO (top) and LUMO (bottom).

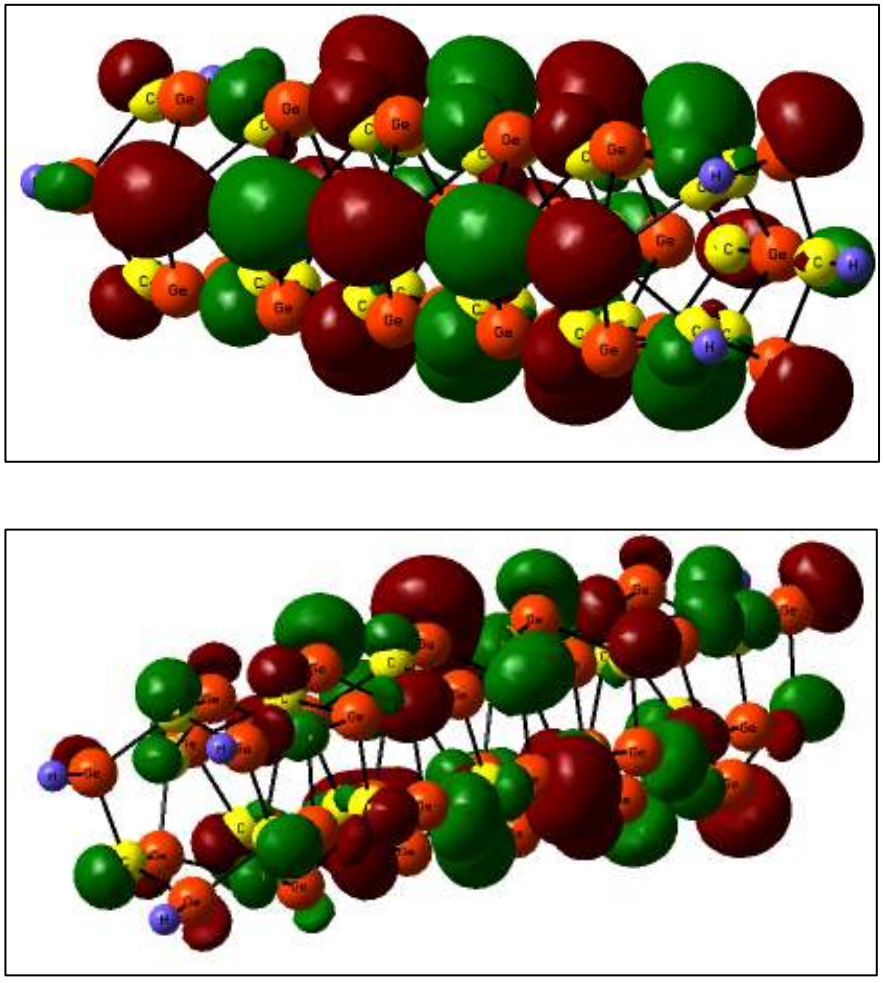

Figure 4.15 Type I (3, 0) HOMO (top) and LUMO (bottom).

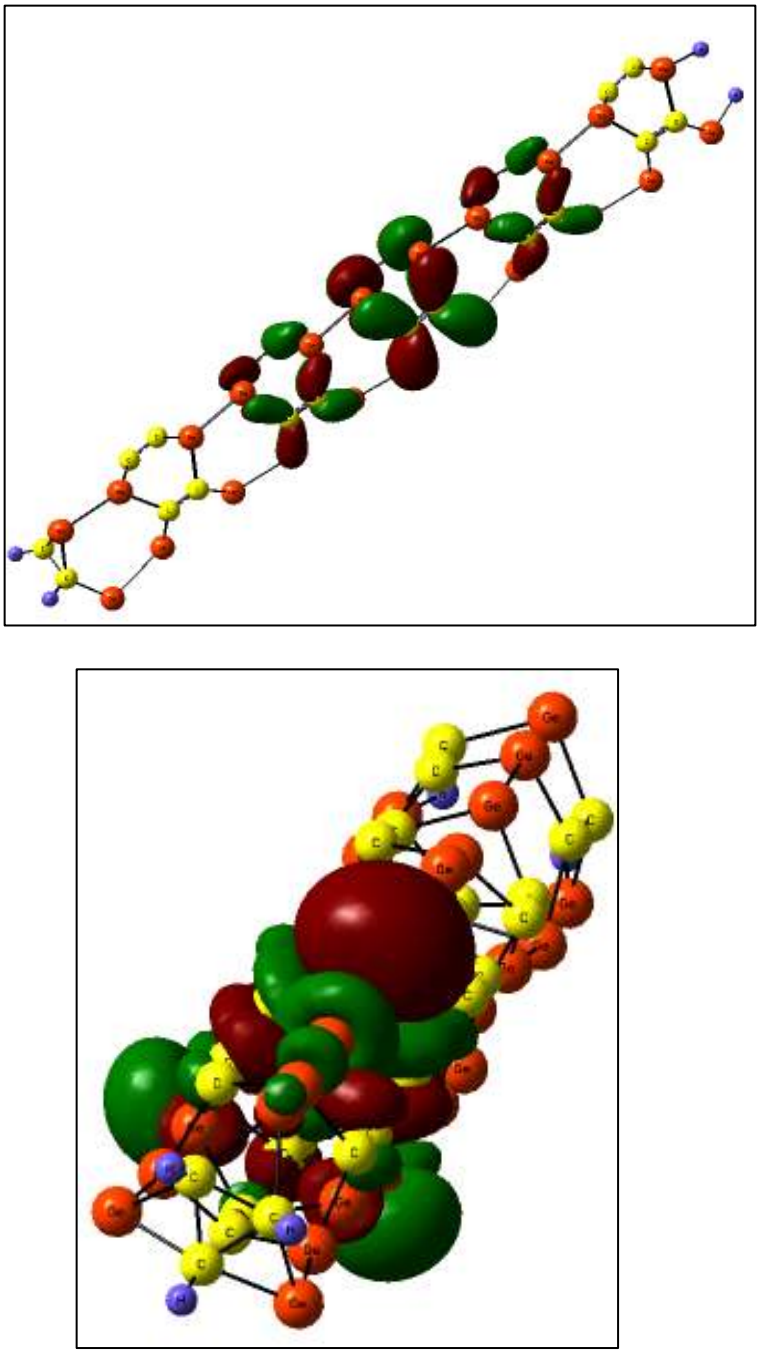

Figure 4.16 Type II (3, 0) HOMO (top) and LUMO (bottom).

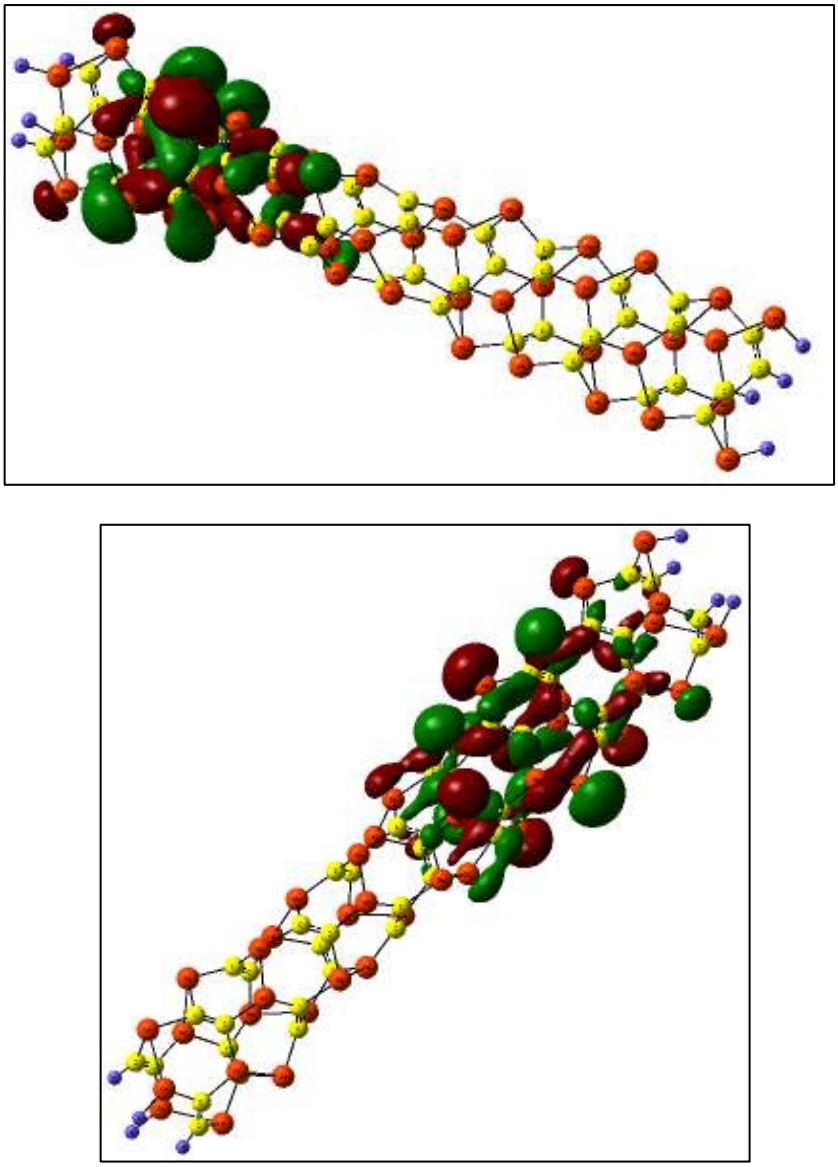

Figure 4.17 Type III (4, 0) HOMO (top) and LUMO (bottom).

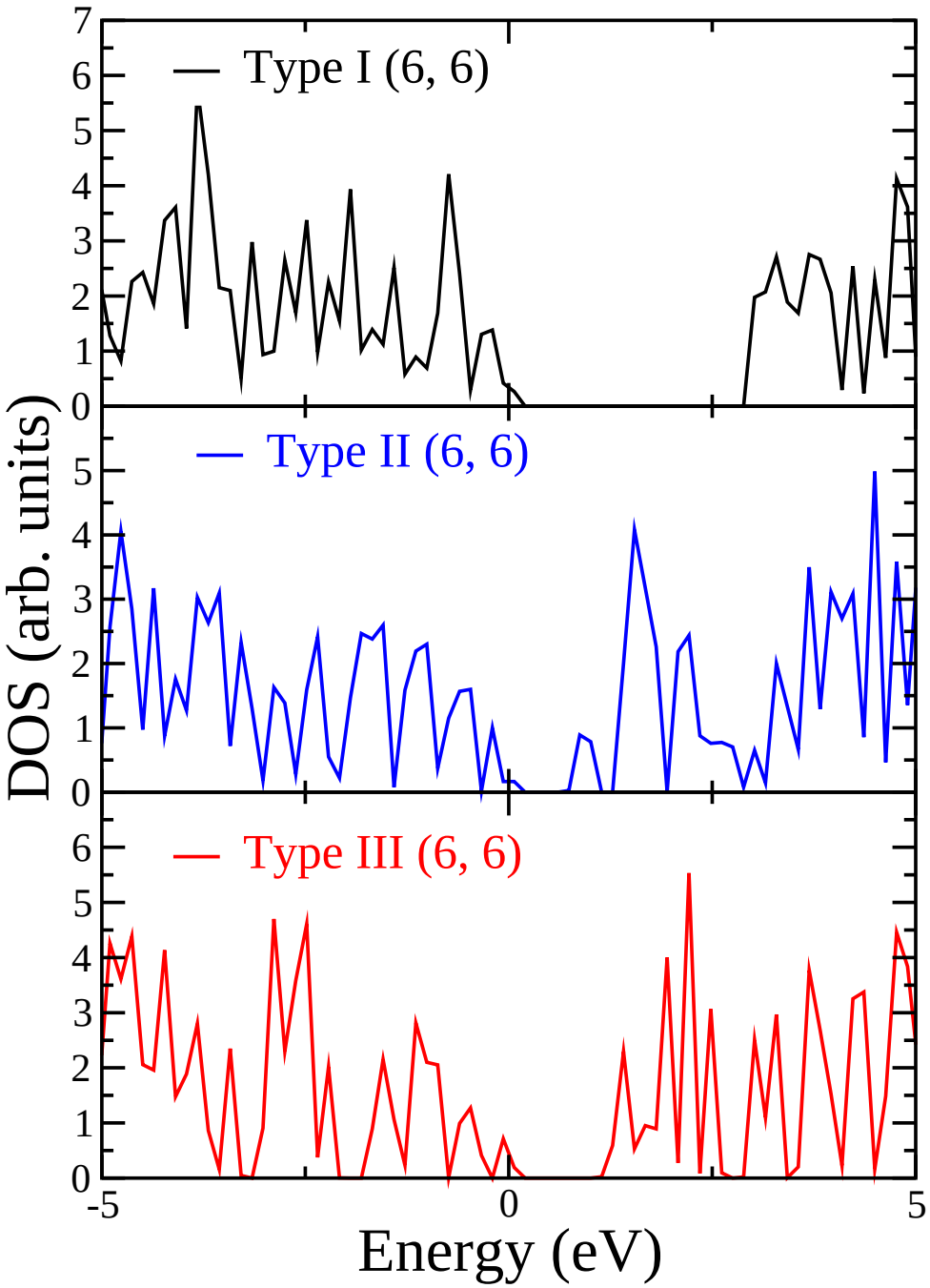

Figure 4.18 Gaussian broadened (width = 0.05 eV) density of states (DOS) plots for (6, 6) armchair GeC nanotubes. HOMO energy is set to zero.

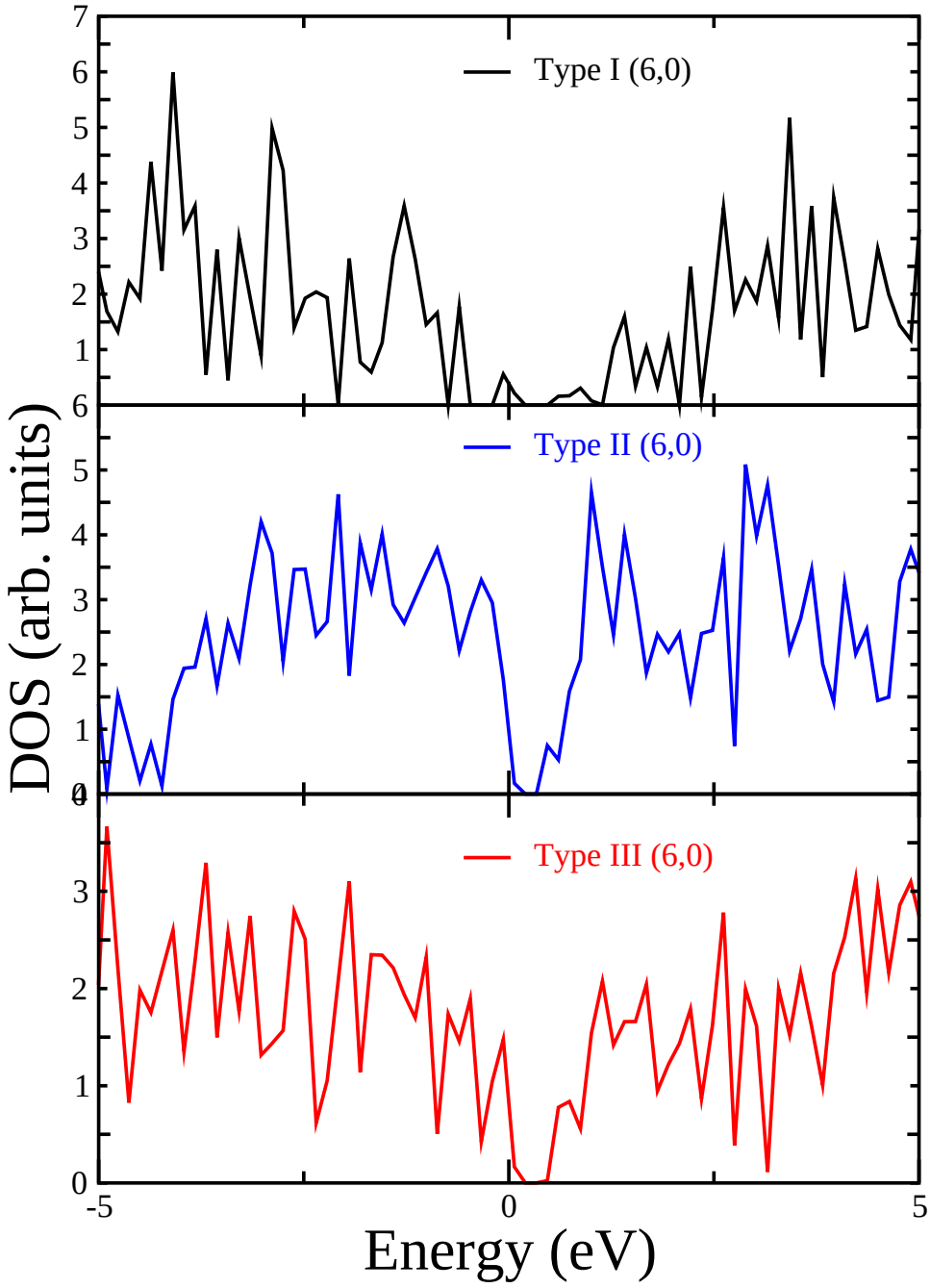

Figure 4.19 Gaussian broadened (width = 0.05 eV) density of states (DOS) plots for (6, 0) zigzag GeC nanotubes. HOMO energy is set to zero.

CHAPTER 5

SILICON GERMANIUM NANOTUBES

5.1 Nanotube Construction

With development of advanced theoretical and experimental tools, it is natural to imagine that tubes based on graphene like structures can be replicated or replaced by other materials and compounds. A more complicated atomic arrangement of Si and Ge in one dimensional tubular forms, which are known as SiGe nanotubes (a hybrid structure) have also been focus of scientific community lately. The tubes reported in the present study are all constructed in a fashion similar to carbon nanotubes and are analogous in geometry to our previous calculations on nanotubes [113, 114].

We have designed an array of single walled SiGe nanotubes both in armchair and zigzag configurations. Furthermore, with distinct atomic arrangements, these nanotubular morphologies are categorized in three “types” namely Type I, Type II and Type III, which can be distinguished by looking at their respective atomic arrangements (figures. 5.1 to 5.3). In type I arrangement, alternating Si and Ge atoms have only Ge or Si atoms as nearest neighbors. In type II and type III arrangements, the nearest neighbors surrounding each Si atom consists of two Ge atoms and another Si atom and vice-versa. The difference between type II and type III SiGe nanotubes lies in the fact that in type II nanotubes, any layer (ring of atoms) perpendicular to the nanotube axis contains only one kind of atoms, either Si or Ge. But in type III, the same kind of layer will contain alternating Si and Ge atoms. Also in the case of armchair nanotubes each layer comprises 2*n* atoms for the (*n, n*) nanotube but for zigzag nanotubes this layer has only *n* atoms per layer. For this reason type III zigzag nanotubes can only be formed when the chiral vector *n* is an even number.

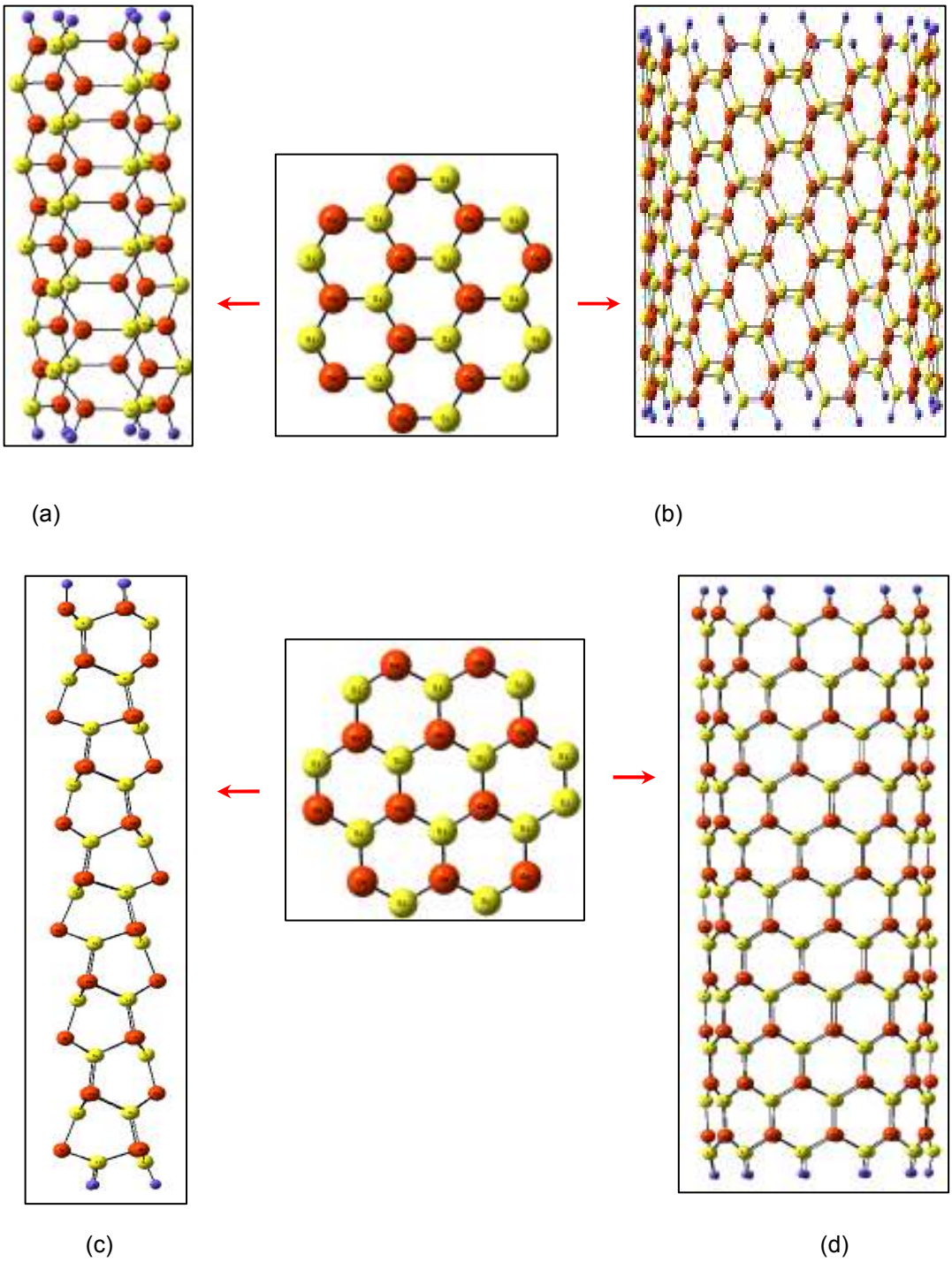

Figure 5.1 Atomic arrangements for (a) type I (3, 3) (b) type I (11, 11) (c) type I (3, 0) (d) type I (11, 0) SiGe nanotubes. The silicon atoms are yellow and germanium atoms are red.

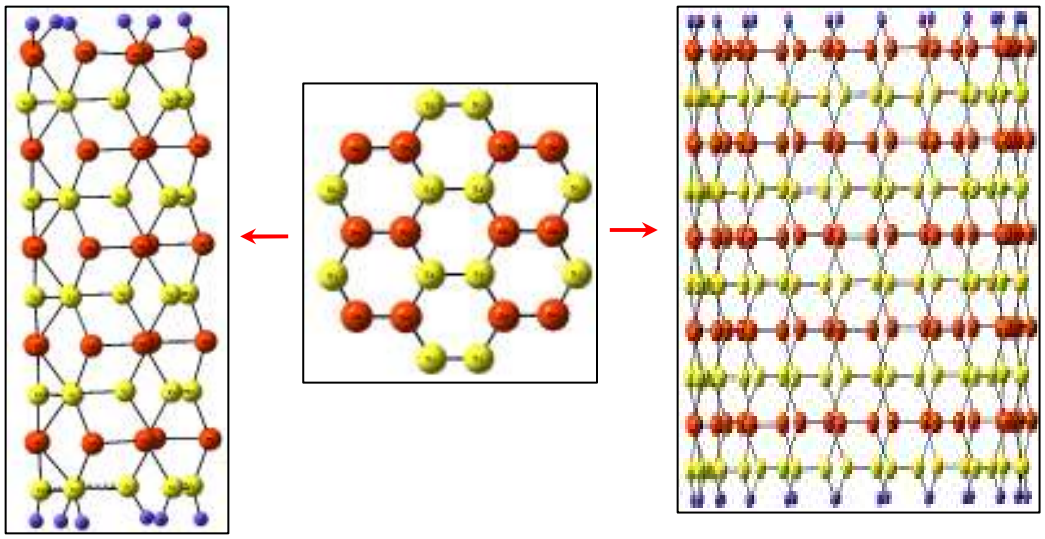

(a) (b)

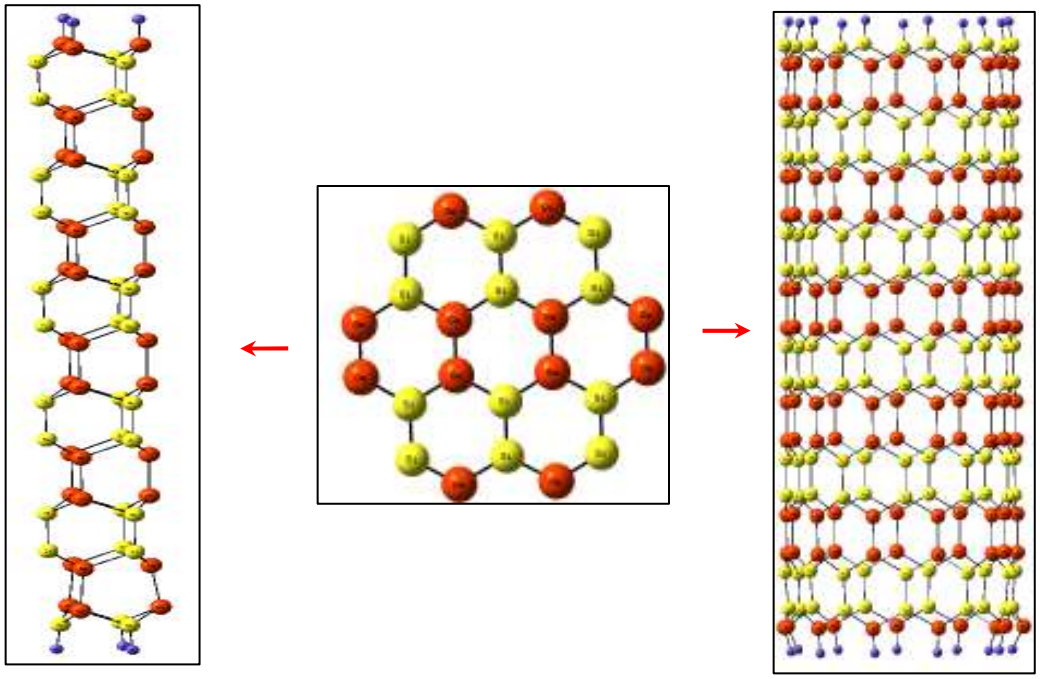

(c) (d)

Figure 5.2 Atomic arrangements for (a) type II (3, 3) (b) type II (11, 11) (c) type II (3, 0) (d) type II (11, 0) SiGe nanotubes. The silicon atoms are yellow and germanium atoms are red.

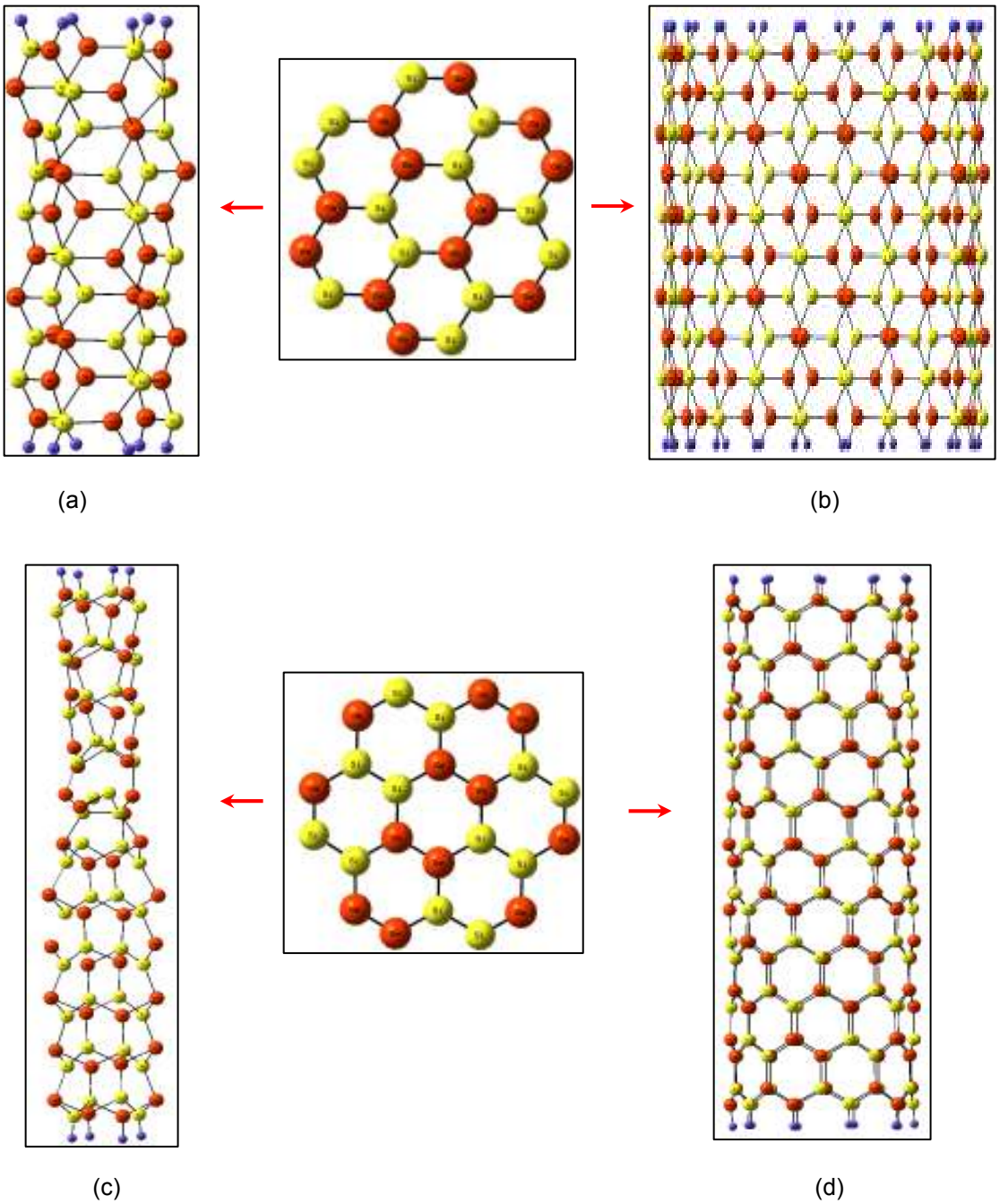

Figure 5.3 Atomic arrangements for (a) type III (3, 3) (b) type III (11, 11) (c) type III (4, 0) (d) type III (10, 0) SiGe nanotube.The silicon atoms are yellow and germanium atoms are red.

In the armchair family of nanotubes, the smallest SiGe conformation is a (3, 3) tube, represented by a cluster of $Si_{30}Ge_{30}H_{12}$, and the largest (11, 11) represented by $Si_{110}Ge_{110}H_{44}$. The smallest and largest SiGe nanotubes in zigzag configuration studied are (3, 0) and (11, 0) tube, which can be denoted by $Si_{33}Ge_{33}H_6$ and $Si_{121}Ge_{121}H_{22}$, respectively.

5.2 Results and Discussions

In order to calculate the relative stability of these structures, binding or cohesive energy calculation has been done. Moreover, the identical chemical composition of these structures, allows us to compare their energies per atom directly. Tables 5.1 to 5.6 enlist the stoichiometry and respective binding or cohesive energy per atom for all the three types of armchair and zigzag SiGe nanotubes. The cohesive energy or the binding energy per atom for each system is computed from:

$$E_b = \{[a\,E(Si) + b\,E(Ge) + c\,E(H)] - [E(Si_a\,Ge_b\,H_c)]\} / (a + b + c) \qquad (5.1)$$

where *a, b,* and *c* are the numbers of Si, Ge, and H atoms respectively. *E(Si), E(Ge)* and *E(H)* are the spin-optimized ground state total energies of Si, Ge and H atoms, respectively, and $E(Si_aGe_bH_c)$ is the total energy of the geometry and spin-optimized clusters representing the nanotubes. For type I armchair nanotubes, the smallest value of cohesive energy obtained is 2.733 eV/atom (3, 3) and the largest is 2.844 eV/atom (11, 11). The corresponding numbers for types II and III armchair tubes are 2.758 and 2.851 eV/atom, and 2.761 and 2.848 eV/atom, respectively. In case of zigzag nanotubes, the smallest value of binding energy for type I (3, 0) is 2.663 eV/atom and largest (11, 0) is 2.855 eV/atom. The corresponding numbers for type II and type III zigzag nanotubes are 2.624 and 2.852 eV/atom and 2.769 and 2.841 eV/atom, respectively. Among armchair SiGe nanotubes the overall highest stability is reported for type II tubes, whereas type I zigzag tubes have the highest cohesive energy values among the zigzag family, only exception being the smaller (4, 0) and (6, 0) nanotubes.

Table 5.1 Electronic States, Binding Energies per Atom (E_b) in eV, HOMO-LUMO Gaps in eV, Diameters in Å, and Dipole Moments in Debye for Type I Armchair SiGe Nanotubes.

Nanotube	Model	State	E_b(eV)	Gap(eV)	Diameter(Å)	Dip.Mnt (Debye)
(3,3)	$Si_{30}Ge_{30}H_{12}$	$^1A_1$	2.733	1.630	5.670	0.510
(4,4)	$Si_{40}Ge_{40}H_{16}$	$^1A_1$	2.768	1.388	7.474	0.051
(5,5)	$Si_{50}Ge_{50}H_{20}$	$^1A_1$	2.807	1.296	9.287	0.041
(6,6)	$Si_{60}Ge_{60}H_{24}$	$^1A_1$	2.822	1.226	11.108	0.161
(7,7)	$Si_{70}Ge_{70}H_{28}$	$^1A_1$	2.830	1.146	13.189	0.355
(8,8)	$Si_{80}Ge_{80}H_{32}$	$^1A_1$	2.836	1.094	14.762	0.059
(9,9)	$Si_{90}Ge_{90}H_{36}$	$^1A_1$	2.839	1.054	16.593	0.033
(10,10)	$Si_{100}Ge_{100}H_{40}$	$^1A_1$	2.842	1.024	18.422	0.175
(11,11)	$Si_{120}Ge_{120}H_{44}$	$^1A_1$	2.844	1.006	20.314	0.045

Table 5.2 Electronic States, Binding Energies per Atom (E_b) in eV, HOMO-LUMO Gaps in eV, Diameters in Å, and Dipole Moments in Debye for Type II Armchair SiGe Nanotubes.

Nanotube	Model	State	E_b(eV)	Gap(eV)	Diameter (Å)	Dip.Mnt (Debye)
(3,3)	$Si_{30}Ge_{30}H_{12}$	^1A	2.758	1.635	5.658	0.614
(4,4)	$Si_{40}Ge_{40}H_{16}$	^1A	2.763	1.196	7.463	0.209
(5,5)	$Si_{50}Ge_{50}H_{20}$	^1A	2.774	0.980	9.319	0.314
(6,6)	$Si_{60}Ge_{60}H_{24}$	^1A	2.792	1.022	11.130	0.389
(7,7)	$Si_{70}Ge_{70}H_{28}$	^1A	2.804	0.986	12.577	0.339
(8,8)	$Si_{80}Ge_{80}H_{32}$	^1A	2.843	1.032	14.753	1.213
(9,9)	$Si_{90}Ge_{90}H_{36}$	^1A	2.847	0.995	16.586	1.873
(10,10)	$Si_{100}Ge_{100}H_{40}$	^1A	2.849	0.971	18.418	0.783
(11,11)	$Si_{120}Ge_{120}H_{44}$	^1A	2.851	0.944	20.251	1.816

Table 5.3 Electronic States, Binding Energies per Atom (E_b) in eV, HOMO-LUMO Gaps in eV, Diameters in Å, and Dipole Moments in Debye for Type III Armchair SiGe Nanotubes.

Nanotube	Model	State	E_b(eV)	Gap(eV)	Diameter (Å)	Dip.Mnt (Debye)
(3,3)	$Si_{30}Ge_{30}H_{12}$	^1A	2.761	1.318	5.669	0.549
(4,4)	$Si_{40}Ge_{40}H_{16}$	^1A	2.791	1.288	7.467	0.157
(5,5)	$Si_{50}Ge_{50}H_{20}$	^1A	2.814	1.209	10.860	0.312
(6,6)	$Si_{60}Ge_{60}H_{24}$	^1A	2.826	1.104	11.672	0.310
(7,7)	$Si_{70}Ge_{70}H_{28}$	^1A	2.834	1.044	12.533	0.238
(8,8)	$Si_{80}Ge_{80}H_{32}$	^1A	2.840	0.981	14.759	1.647
(9,9)	$Si_{90}Ge_{90}H_{36}$	^1A	2.843	0.937	16.589	0.111
(10,10)	$Si_{100}Ge_{100}H_{40}$	^1A	2.846	0.905	18.422	0.242
(11,11)	$Si_{120}Ge_{120}H_{44}$	^1A	2.848	0.905	20.246	0.311

Table 5.4 Electronic States, Binding Energies per Atom (E_b) in eV, HOMO-LUMO Gaps in eV, Diameters in Å, and Dipole Moments in Debye for Type I Zigzag SiGe Nanotubes.

Nanotube	Model	State	E_b(eV)	Gap(eV)	Diameter(Å)	Dip.Mnt (Debye)
(3,0)	$Si_{33}Ge_{33}H_6$	^3A	2.663	0.413	3.977	0.3623
(4,0)	$Si_{44}Ge_{44}H_8$	^3A	2.727	0.338	4.898	8.9124
(5,0)	$Si_{55}Ge_{55}H_{10}$	^3A	2.772	0.671	6.001	5.5598
(6,0)	$Si_{66}Ge_{66}H_{12}$	^3B	2.779	0.486	7.242	11.6279
(7,0)	$Si_{77}Ge_{77}H_{14}$	^3A	2.835	0.681	8.308	26.9628
(8,0)	$Si_{88}Ge_{88}H_{16}$	^3A	2.847	0.138	9.471	8.0597
(9,0)	$Si_{99}Ge_{99}H_{18}$	^3A	2.851	0.358	10.608	22.1378
(10,0)	$Si_{110}Ge_{110}H_{20}$	^3A	2.854	0.643	11.787	11.6471
(11,0)	$Si_{121}Ge_{121}H_{22}$	^3A	2.855	0.228	12.938	27.3387

Table 5.5 Electronic States, Binding Energies per Atom (E_b) in eV, HOMO-LUMO Gaps in eV, Diameters in Å, and Dipole Moments in Debye for Type II Zigzag SiGe Nanotubes.

Nanotube	Model	State	E_b(eV)	Gap(eV)	Diameter(Å)	Dip.Mnt (Debye)
(3,0)	$Si_{33}Ge_{33}H_6$	^3A	2.624	0.638	4.058	9.0545
(4,0)	$Si_{44}Ge_{44}H_8$	^3A	2.656	0.397	5.122	3.4061
(5,0)	$Si_{55}Ge_{55}H_{10}$	^3A	2.708	0.584	6.013	9.5329
(6,0)	$Si_{66}Ge_{66}H_{12}$	^3A	2.714	0.326	7.277	4.4765
(7,0)	$Si_{77}Ge_{77}H_{14}$	^3A	2.731	0.427	8.316	34.6908
(8,0)	$Si_{88}Ge_{88}H_{16}$	^3A	2.761	0.407	9.703	15.6026
(9,0)	$Si_{99}Ge_{99}H_{18}$	^3A	2.802	0.475	10.640	3.0211
(10,0)	$Si_{110}Ge_{110}H_{20}$	^3A	2.838	0.579	11.784	3.3500
(11,0)	$Si_{121}Ge_{121}H_{22}$	^3A	2.852	0.532	12.949	13.5679

Table 5.6 Electronic States, Binding Energies per Atom (E_b) in eV, HOMO-LUMO Gaps in eV, Diameters in Å, and Dipole Moments in Debye for Type III Zigzag SiGe Nanotubes.

Nanotube	Model	State	E_b(eV)	Gap(eV)	Diameter(Å)	Dip.Mnt (Debye)
(4,0)	$Si_{44}Ge_{44}H_8$	^3A	2.769	0.680	4.871	2.298
(6,0)	$Si_{66}Ge_{66}H_{12}$	^3A	2.801	0.304	7.197	2.846
(8,0)	$Si_{88}Ge_{88}H_{16}$	$^3B_1$	2.837	0.401	9.472	1.228
(10,0)	$Si_{110}Ge_{110}H_{20}$	^3A	2.841	0.164	11.792	1.928

The stability trend reported here is different from our previous calculations on SiC and GeC nanotubes [113, 114], where type I nanotubes were found to be energetically more favorable.

It is evident from figure 5.4 that for armchair tubes binding energy per atom tends to increase monotonically achieving near saturation at (11, 11). This monotonous increment in binding energy is also noticed in SiGe zigzag nanotubes (Fig. 5.5). It is well known fact that distances between the atoms play a major role in stabilizing the tubes, which is evident in smaller diameter nanotubes. But as we increase the tube diameter, interaction between diametrically opposite atoms decreases and thus stabilizes the tubes. Also the higher diameter tube surfaces are more planar in comparison to highly curved smaller diameter tubes; this flatness of surface reduces the σ-π hybridizations thus increasing the stability of higher diameter nanotubes. As mentioned earlier, all the different types of nanotubes have different atomic arrangements which results in distinct geometries of these tubes. The presence of only one kind of bond (Si-Ge) in type I tubes, layered configurations of atoms in type II tubes, and alternative atom placement in type III can also affect the overall stability of these nanotubes.

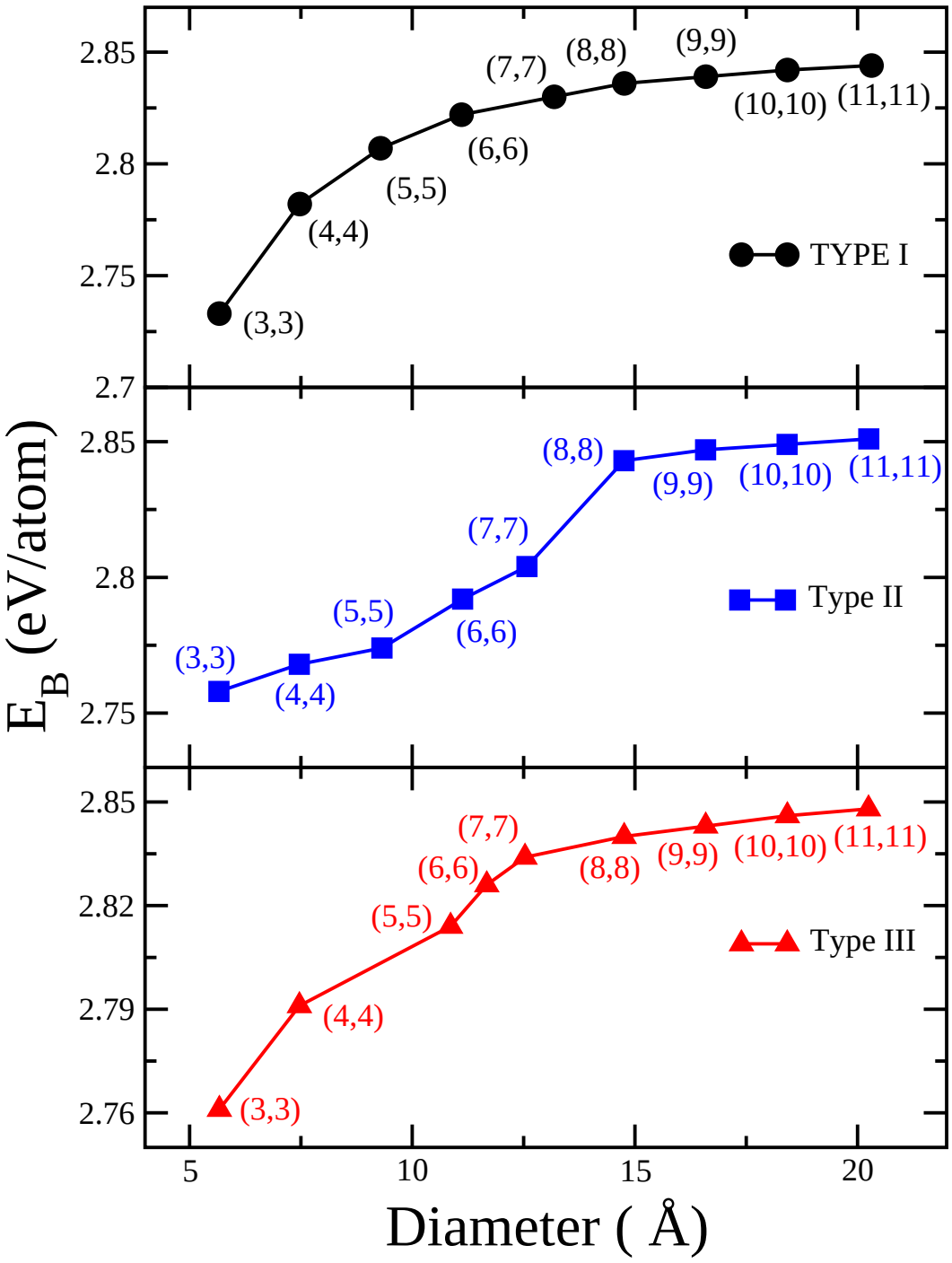

Figure 5.4 Binding energy versus diameter for SiGe armchair nanotubes.

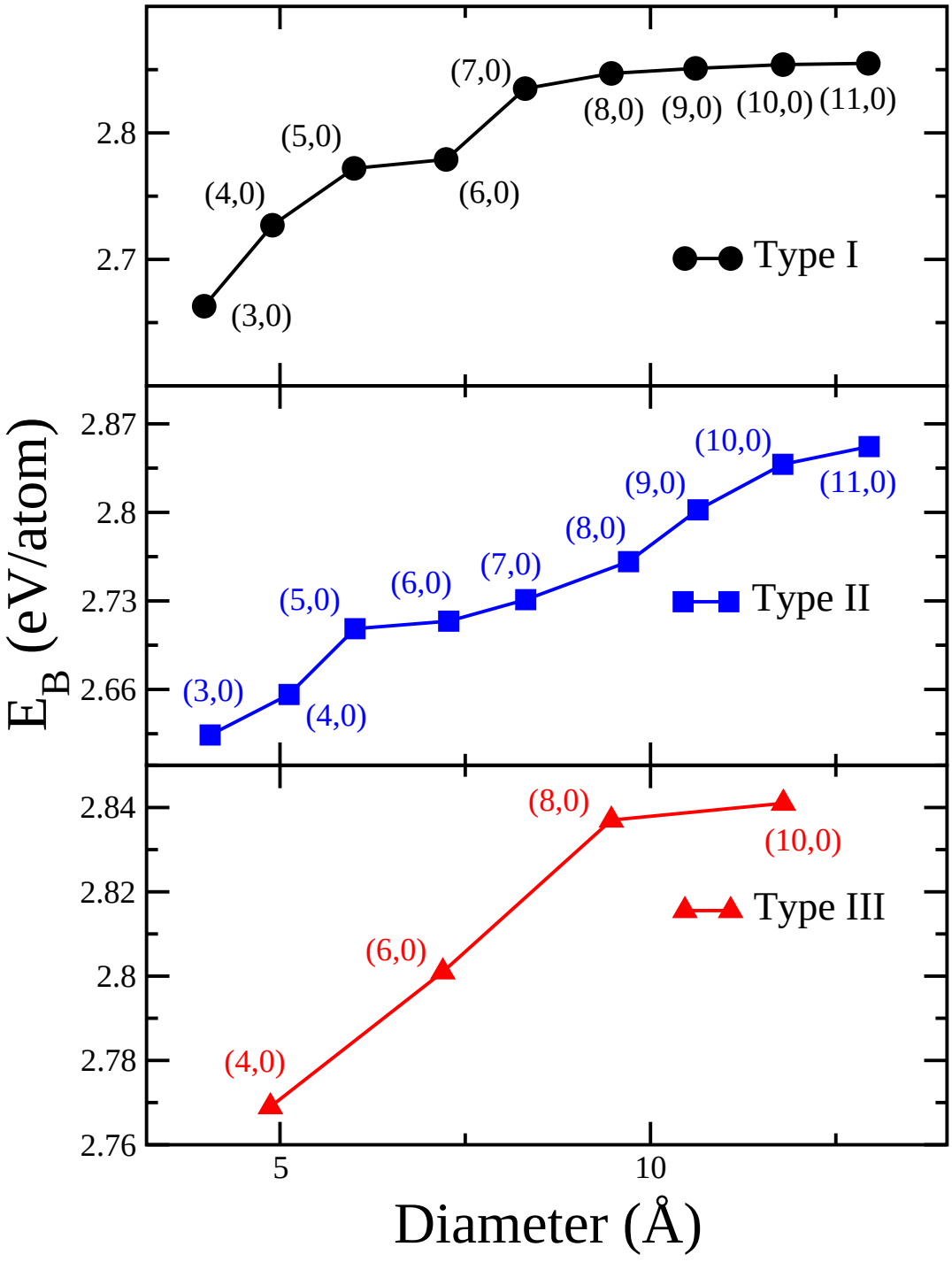

Figure 5.5 Binding energy versus diameter for SiGe zigzag nanotubes.

As suggested by Cabria and group members [115], comparatively less stable smaller diameter tubes can be neatly anchored over the vacancy in the wall of larger diameter tubes to form different nano-junctions. This technique of anchoring the tubes can be very promising in not only stabilizing the smaller diameter less stable SiGe tubes but also in designing the nano interconnect junctions in the circuitry. It also helps to saturate some of the dangling bonds which play a major role in cluster calculations. Doping with proper impurity (p-type or n-type) or hydrogen passivation along the length of tube is also well sought alternative in increasing the stability of nanotubes.

When a graphene like sheet is rolled into a tubular cylinder, the corresponding bonds between the atoms are strained and distorted. The degree of the distortion also depends on the spatial position of the atoms, which is clearly distinct in the armchair and zigzag tubes. All the relaxed nanotubes reported here are initially built with all atoms equally spaced, and at same radial distance from the axis. In tables 5.7 to 5.12, we report the bond length variations for different nanotubes. For all three types of armchair and zigzag nanotubes the average Si-Ge, Ge-Ge and Si-Si bond lengths show a mixed pattern as the tube diameter changes. In case of type I armchair and types II and III zigzag tubes Si-Ge bonds tend to contract as diameter is increased. Ge-Ge bond lengths in type II armchair decrease initially as we move from (3, 3) to (7, 7) then increase as we approach largest (11, 11) nanotube. But for type III in armchair configuration and types II and III in zigzag format a declining trend for Ge-Ge bond lengths is observed with some exceptions. An oscillatory pattern is reported in Si-Si bonds for all different types of nanotubes. It is known that both Si and Ge atoms favor sp^3 hybridization, whereas all the nanotubes presented here are based on the graphite templates which make the atoms essentially three fold coordinated or sp^2 hybridized. During the relaxation of nanotubes, these atoms try to retain their preferred sp^3 hybridization state which not only accounts for distortion in the tubular structure but also for the differences in bond length values for different nanotubes.

Table 5.7 Average, Minimum, Maximum Bond Lengths (in Å) of Type I Armchair SiGe Nanotubes.

Nanotube	Ave.B.L	Min.B.L	Max.B.L
(3,3)	2.372	2.301	2.399
(4,4)	2.370	2.302	2.397
(5,5)	2.362	2.303	2.387
(6,6)	2.357	2.304	2.387
(7,7)	2.355	2.297	2.375
(8,8)	2.351	2.295	2.371
(9,9)	2.350	2.296	2.370
(10,10)	2.349	2.296	2.369
(11,11)	2.308	2.252	2.331

Table 5.8 Average, Minimum, Maximum Bond Lengths (in Å) of Type II Armchair SiGe Nanotubes.

	Si-Si			Ge-Ge			Si-Ge		
Nanotube	**Ave**	**Min**	**Max**	**Ave**	**Min**	**Max**	**Ave**	**Min**	**Max**
(3,3)	2.252	2.199	2.287	2.523	2.462	2.556	2.365	2.339	2.373
(4,4)	2.257	2.205	2.306	2.477	2.419	2.510	2.361	2.337	2.390
(5,5)	2.244	2.191	2.271	2.372	2.314	2.401	2.315	2.305	2.329
(6,6)	2.239	2.176	2.276	2.373	2.322	2.412	2.312	2.295	2.329
(7,7)	2.242	2.191	2.270	2.370	2.313	2.402	2.312	2.300	2.326
(8,8)	2.268	2.213	2.294	2.436	2.394	2.456	2.361	2.331	2.382
(9,9)	2.268	2.213	2.294	2.433	2.390	2.451	2.359	2.330	2.378
(10,10)	2.268	2.213	2.294	2.430	2.388	2.448	2.358	2.330	2.376
(11,11)	2.268	2.213	2.293	2.429	2.389	2.447	2.357	2.330	2.376

Table 5.9 Average, Minimum, Maximum Bond Lengths (in Å) of Type III Armchair SiGe Nanotubes.

	Si-Si			Ge-Ge			Si-Ge		
Nanotube	**Ave**	**Min**	**Max**	**Ave**	**Min**	**Max**	**Ave**	**Min**	**Max**
(3,3)	2.294	2.275	2.324	2.518	2.478	2.565	2.346	2.270	2.391
(4,4)	2.310	2.303	2.319	2.455	2.449	2.462	2.367	2.312	2.397
(5,5)	2.285	2.277	2.292	2.457	2.457	2.457	2.365	2.305	2.395
(6,6)	2.282	2.274	2.290	2.445	2.443	2.448	2.386	2.303	2.359
(7,7)	2.280	2.272	2.288	2.439	2.436	2.442	2.359	2.301	2.394
(8,8)	2.279	2.271	2.288	2.435	2.430	2.439	2.357	2.300	2.389
(9,9)	2.278	2.270	2.287	2.432	2.427	2.437	2.355	2.300	2.385
(10,10)	2.277	2.269	2.285	2.430	2.426	2.435	2.353	2.298	2.383
(11,11)	2.280	2.274	2.285	2.429	2.422	2.436	2.352	2.293	2.374

Table 5.10 Average, Minimum, Maximum Bond Lengths (in Å) of Type I Zigzag SiGe Nanotubes.

Nanotube	Ave.B.L	Min.B.L	Max.B.L
(3,0)	2.331	2.327	2.351
(4,0)	2.382	2.366	2.395
(5,0)	2.339	2.339	2.399
(6,0)	2.329	2.308	2.344
(7,0)	2.374	2.339	2.383
(8,0)	2.367	2.331	2.384
(9,0)	2.346	2.312	2.386
(10,0)	2.317	2.292	2.324
(11,0)	2.316	2.278	2.329

Table 5.11 Average, Minimum, Maximum Bond Lengths (in Å) of Type II Zigzag SiGe Nanotubes.

	Si-Si			Ge-Ge			Si-Ge		
Nanotube	**Ave**	**Min**	**Max**	**Ave**	**Min**	**Max**	**Ave**	**Min**	**Max**
(3,0)	2.279	2.275	2.282	2.561	2.547	2.583	2.402	2.391	2.429
(4,0)	2.249	2.230	2.268	2.461	2.425	2.482	2.383	2.364	2.397
(5,0)	2.296	2.263	2.330	2.499	2.487	2.526	2.374	2.351	2.393
(6,0)	2.293	2.266	2.317	2.470	2.483	2.507	2.371	2.355	2.385
(7,0)	2.284	2.261	2.302	2.454	2.426	2.471	2.368	2.334	2.398
(8,0)	2.289	2.274	2.326	2.423	2.388	2.447	2.333	2.319	2.365
(9,0)	2.265	2.255	2.278	2.376	2.359	2.385	2.320	2.295	2.334
(10,0)	2.251	2.246	2.259	2.377	2.369	2.392	2.317	2.293	2.328
(11,0)	2.248	2.237	2.265	2.378	2.369	2.394	2.318	2.274	2.388

Table 5.12 Average, Minimum, Maximum Bond Lengths (in Å) of Type III Zigzag SiGe Nanotubes.

	Si-Si			Ge-Ge			Si-Ge		
Nanotube	**Ave**	**Min**	**Max**	**Ave**	**Min**	**Max**	**Ave**	**Min**	**Max**
(4,0)	2.307	2.288	2.340	2.555	2.503	2.593	2.370	2.333	2.396
(6,0)	2.259	2.227	2.278	2.494	2.431	2.537	2.348	2.310	2.391
(8,0)	2.266	2.246	2.288	2.466	2.399	2.512	2.354	2.320	2.399
(10,0)	2.251	2.232	2.263	2.383	2.375	2.389	2.317	2.280	2.326

It is worthwhile to notice, that the layered type construction is favored by both Si-Si and Ge-Ge atoms which is evident from the relatively higher stability of the type II armchair and types I and II single walled SiGe nanotubes. These nanotubes while constructed in multiwalled manner also had similar kind of layered configurations [81, 82].

Furthermore, structure relaxation leads to a change in the radial geometry of the cylindrical structures, which is characterized by two concentric cylindrical tubes, one consisting of Si atoms and another one formed by Ge atoms. The radial buckling 'β' is calculated as an absolute value of the difference between average radial distances of silicon and germanium atoms from the tube axis:

$$\beta = | \langle r_{Si} \rangle - \langle r_{Ge} \rangle \quad (5.2)$$

where $\langle r_{Si} \rangle$ and $\langle r_{Ge} \rangle$ are the average radial distances of Si and Ge atoms, respectively. In type I armchair tubes Si atoms which are slightly more electronegative in nature as compared to Ge atoms tend to shift away from the tubular axis, whereas Ge atoms move towards the axis. For types II and III tubes, there is a very small outward relaxation of Ge atoms while Si atoms slightly move inward. In case of zigzag nanotubes, except type I (6, 0), (7, 0) tubular structures and smaller (3, 0) and (4, 0) type II tubes Ge atoms relax away from the nanotube axis with

small shift of Si atoms in the opposite direction. Hence, depending on the relative positions of the Ge and Si atoms, type I armchair tubes can be considered Si coated, while types II and III armchair nanotubes and all three zigzag tubes (with some exceptions) can be considered as Ge coated. It is worth mentioning that in our previous investigation on GeC and SiC nanotubes, similar type of behavior was observed where atoms with different electronegativities tend to displace from their initial positions [113, 114]. From tables 5.13 and 5.14 it is clear that, the amount of buckling in the SiGe structures is small and value decreases as the tubes grow in diameter. It is illustrated from figures 5.6 and 5.7 that in type I armchair and type III zigzag nanotubes buckling value decreases as tube diameter is increased. Types II and III armchair tubes also show the similar behavior but with some oscillatory patterns. For types I and II zigzag tubes, buckling value fluctuates around (5, 0) to (9, 0) but eventually reduces as we increase the tube diameter. In the present investigation, buckling does appear to be a minor effect, and might possibly be a manifestation of the finite lengths of the tubes. Slight differences in the electronegativities of Si and Ge atoms can also contribute to the reconstruction of the surfaces. The puckered surface structure caused by bond stretching or bending may also create surface dipoles and significantly modify the surface band structure.

From tables 5.1 to 5.6, we note that SiGe armchair nanotubes have small net dipole moments, whereas zigzag conformations have relatively significant values of dipole moments. Among armchair tubes type I has the lowest dipole moments which can be attributed to the overall symmetry of the structures and presence of only Si-Ge bonds. Smaller values of net dipole moment after relaxation for type II armchair nanotubes can be explained from the fact that these nanotubes have alternate layers of either Si or Ge atoms and thus two ends of nanotubes will always be populated by different kinds of atoms. Though type III armchair nanotubes do not have only either Si or Ge atoms at the ends of the tubes, asymmetry in the structures in comparison to type I tubes induces the small values of the dipole moments. In summary, alternative layered arrangement for types I and II zigzag tubes, comparatively smaller

diameters with longer tube lengths, and higher bond distortion with bonds stretching along the tube length give rise to significant amount of dipole values in the zigzag tubes.

One of the most important properties of a cluster or a nanotube is the charge density distribution. While designing and incorporating the new nanotube based circuitry it is important to know the regions of high and low electronic charge densities. In order to give a more detailed account of charge distribution in the nanotubes we have performed the Mulliken charge analysis for all types of SiGe nanotubes. As expected, these structures show a significant charge transfer from Ge to Si atoms since Si is relatively more electronegative than Ge. Figure 5.8 clearly indicates that type I armchair structures exhibit more ionic bonding characteristics than types II and III, in other words more charge transfer occurs from Ge to Si atoms in type I nanotubes. This is due to the fact that only Si-Ge bonds are present in type I. Since types II and III contain Si-Si, Si-Ge, and Ge-Ge bonds, the nature of the bonding is a mixture of ionic and covalent bonds which are also evident in the figure 5.8. Investigating the zigzag SiGe structures (Fig. 5.9), the types I and III also show a charge transfer pattern among the Si and Ge atoms. As the size of Si atoms are smaller than the corresponding Ge atoms stronger nuclear forces compel the charge accumulation over these atoms. The main source of charge is the outer shell of Ge atoms which tend to lose the charge to the scavenging Si atoms. Mixed nature of bonding is also reported for zigzag SiGe structures. Type II zigzag structures show a unique spread of charge along the tube. It can be viewed from figure 5.9 that type II structure (11, 0) is divided into positive and negative regions, furthermore irrespective of the electronegativities, Si atoms and Ge atoms loose or gain the charge. This unique feature can be exploited in the developing the p-n junction type devices where different sections have different charge concentrations.

Table 5.13 Tube Diameters (in Å) and Radial Bucklings (in Å) for Types I, II and III Armchair SiGe Nanotubes.

	Type I		Type II		Type III	
Nanotube	**Diameter(Å)**	**β (Å)**	**Diameter(Å)**	**β (Å)**	**Diameter(Å)**	**β (Å)**
(3,3)	5.670	0.596	5.658	0.284	5.669	0.152
(4,4)	7.474	0.555	7.463	0.197	7.467	0.217
(5,5)	9.287	0.527	9.319	0.022	10.860	0.087
(6,6)	11.108	0.513	11.130	0.029	11.672	0.073
(7,7)	13.189	0.488	12.577	0.064	12.533	0.069
(8,8)	14.7628	0.485	14.753	0.064	14.759	0.152
(9,9)	16.593	0.481	16.586	0.053	16.589	0.142
(10,10)	18.422	0.477	18.418	0.048	18.422	0.136
(11,11)	20.314	0.022	20.251	0.045	20.246	0.071

Table 5.14 Tube Diameters (in Å) and Radial Bucklings (in Å) for Types I, II and III Zigzag SiGe Nanotubes.

	Type I		Type II		Type III	
Nanotube	**Diameter(Å)**	**β (Å)**	**Diameter(Å)**	**β (Å)**	**Diameter(Å)**	**β (Å)**
(3,0)	3.977	0.625	4.058	0.175		
(4,0)	4.898	0.286	5.122	0.028	4.871	0.503
(5,0)	6.001	0.288	6.013	0.219		
(6,0)	7.242	0.004	7.277	0.019	7.197	0.328
(7,0)	8.308	0.545	8.316	0.021		
(8,0)	9.471	0.367	9.703	0.016	9.472	0.169
(9,0)	10.608	0.035	10.640	0.056		
(10,0)	11.787	0.045	11.784	0.017	11.792	0.019
(11,0)	12.938	0.009	12.949	0.109		

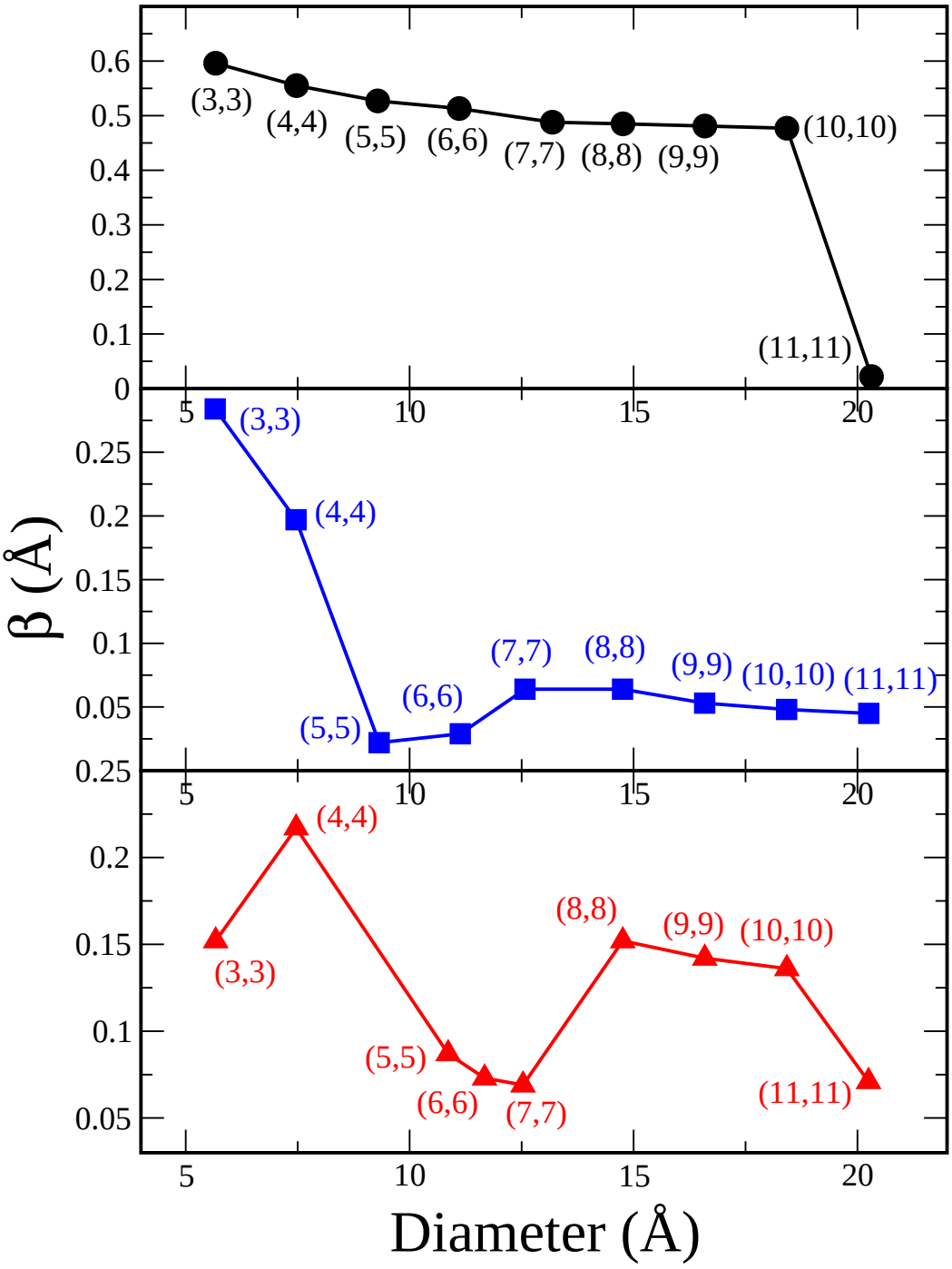

Figure 5.6 Tube buckling versus diameter for SiGe armchair nanotubes.

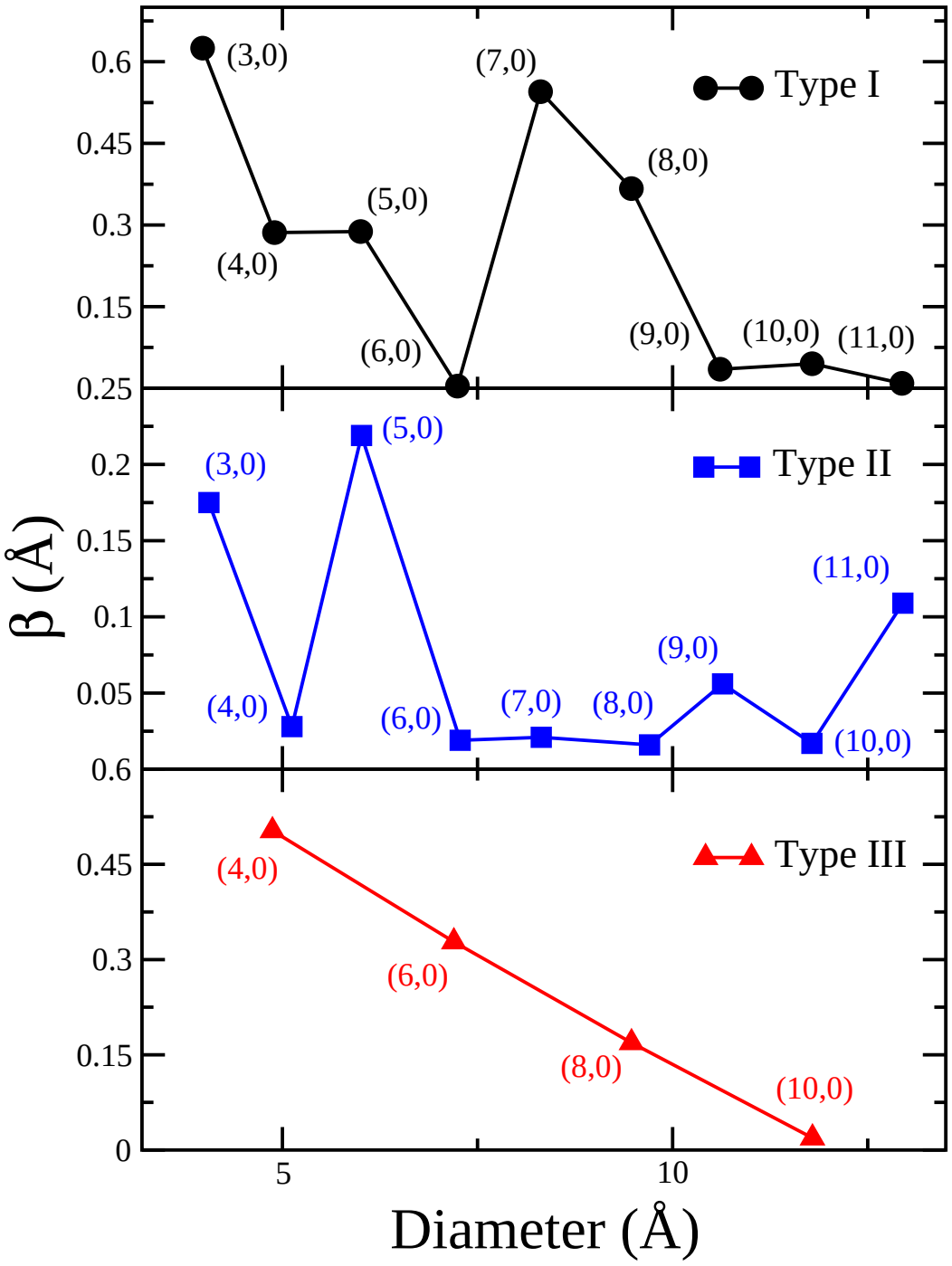

Figure 5.7 Tube buckling versus diameter for SiGe zigzag nanotubes.

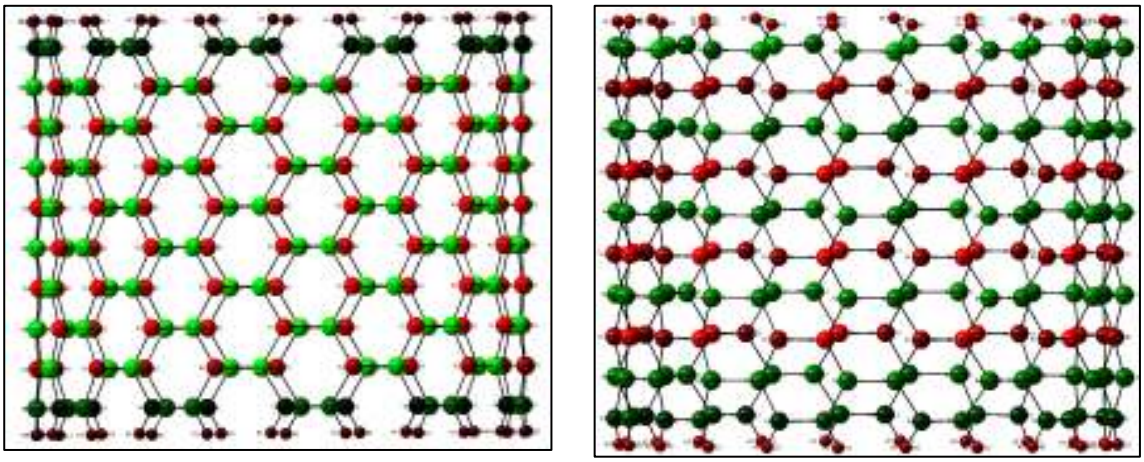

(a) (b)

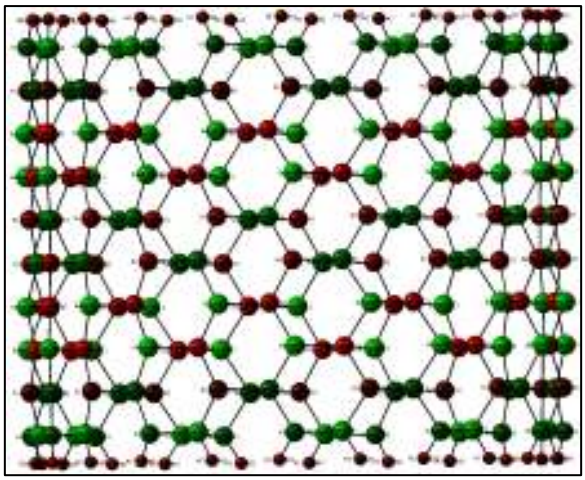

(c)

Figure 5.8 Mulliken charge distributions for armchair (11, 11) nanotubes. (a) type I (b) type II and (c) type III. Silicon atoms gained and germanium atoms, lost charge.

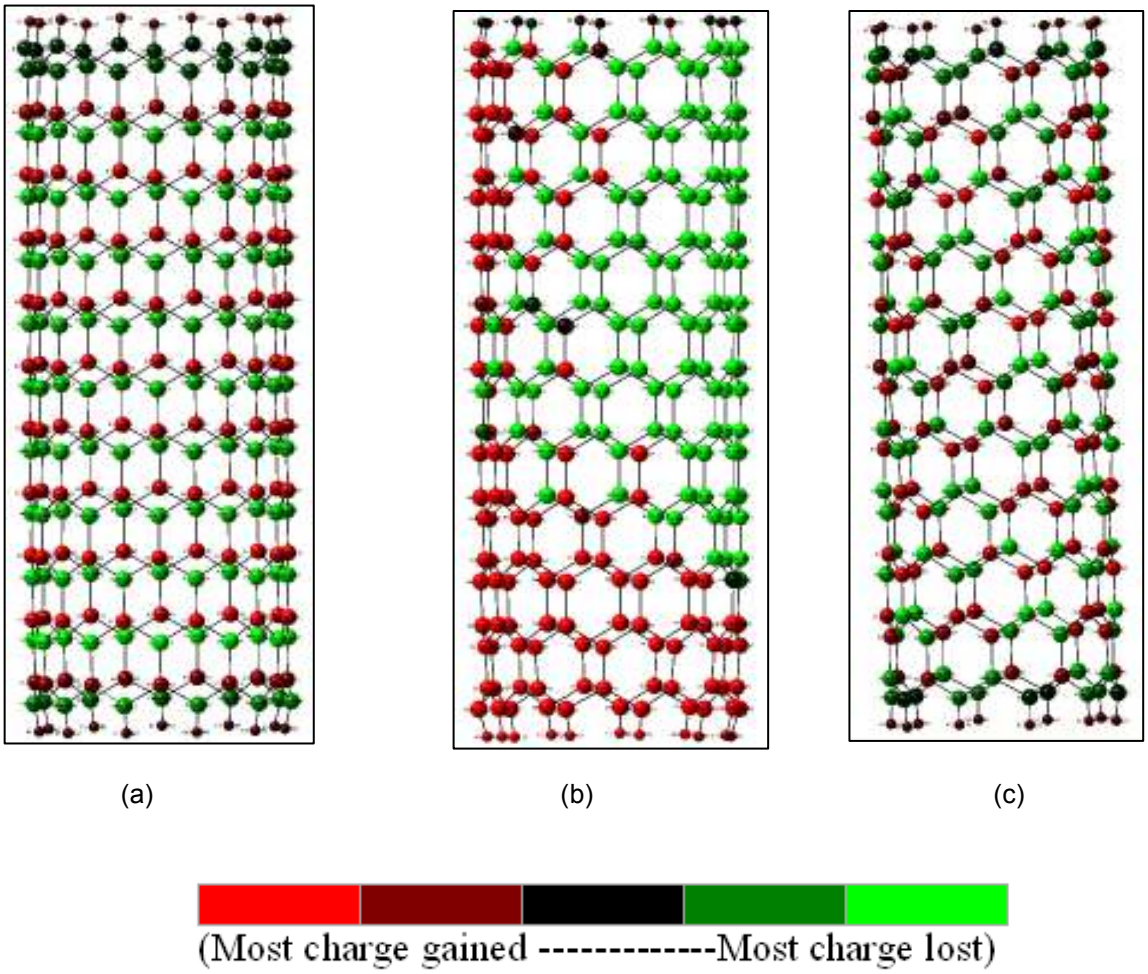

Figure 5.9 Mulliken charge distributions for zigzag (11, 0) nanotubes. (a) type I, (b) type II and (c) type III.

Thus, to an extent, we can say that the mechanism of charge transfer between atoms influences the stability of the nanotubes.

The energy difference between the highest-occupied-molecular-orbital (HOMO) and lowest-unoccupied-molecular-orbital (LUMO) level is regarded as band gap energy. To investigate the possible metallic or semi-conducting behavior of the nanotubes, we have calculated these HOMO-LUMO gaps of all the nanotubes. Tables 5.1 through 5.6 and figures 5.10 and 5.11 illustrate the calculated gaps as a function of the diameters of the corresponding nanotubes. It is evident that all SiGe nanotubes are semi-conducting in nature, with a wide spectrum of band gaps. Armchair SiGe nanotubes have the largest gaps in all types than corresponding zigzag nanotubes. The gap is decreasing with increasing diameter and approaching saturation. These saturation values are approximately 1eV, 0.94eV and 0.90eV for types I, II, and III, respectively. On the other hand in zigzag SiGe nanotubes for all types, gap and tube diameter have an alternating relationship. However unlike in the other two types, gap and tube diameter relationship in type III zigzag nanotubes can be characterized by a predominant decreasing trend. It is interesting to notice that relative position of Si and Ge atoms in armchair SiGe nanotubes is affecting the electronic properties but it does not have any significant influence in zigzag configurations. The average band gap values for types I, II, and III armchair nanotubes are 1.21eV, 1.09 eV and 1.08eV, respectively. The corresponding values for zigzag nanotubes are 0.44eV, 0.48eV and 0.38eV. Relatively stronger ionic nature of type I armchair nanotubes may be responsible for the localizing electronic states which results in wider band gap values. In general electrons are more localized in armchair tubes than corresponding zigzag structures, a greater value of band gaps is expected. The pronounced irregularities in gap values for the zigzag tubes can possibly be a manifestation of smaller diameters which ultimately gives rise to atomic interactions well beyond the nearest neighbors. Band gaps for all the nanotubes with increase in diameter are expected to approach the limiting values of the corresponding graphene like sheets.

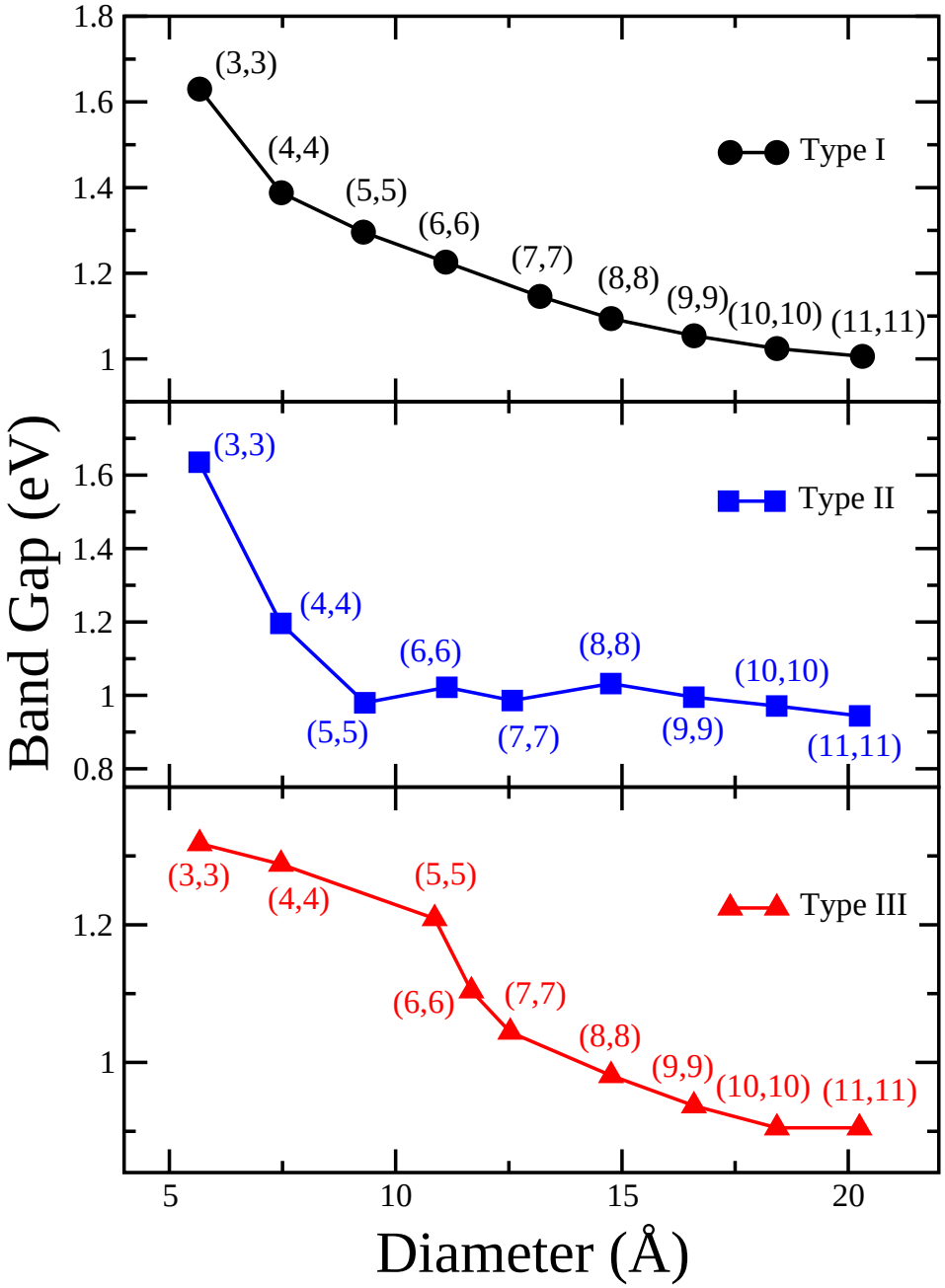

Figure 5.10 HOMO-LUMO gaps versus diameter for SiGe armchair nanotubes.

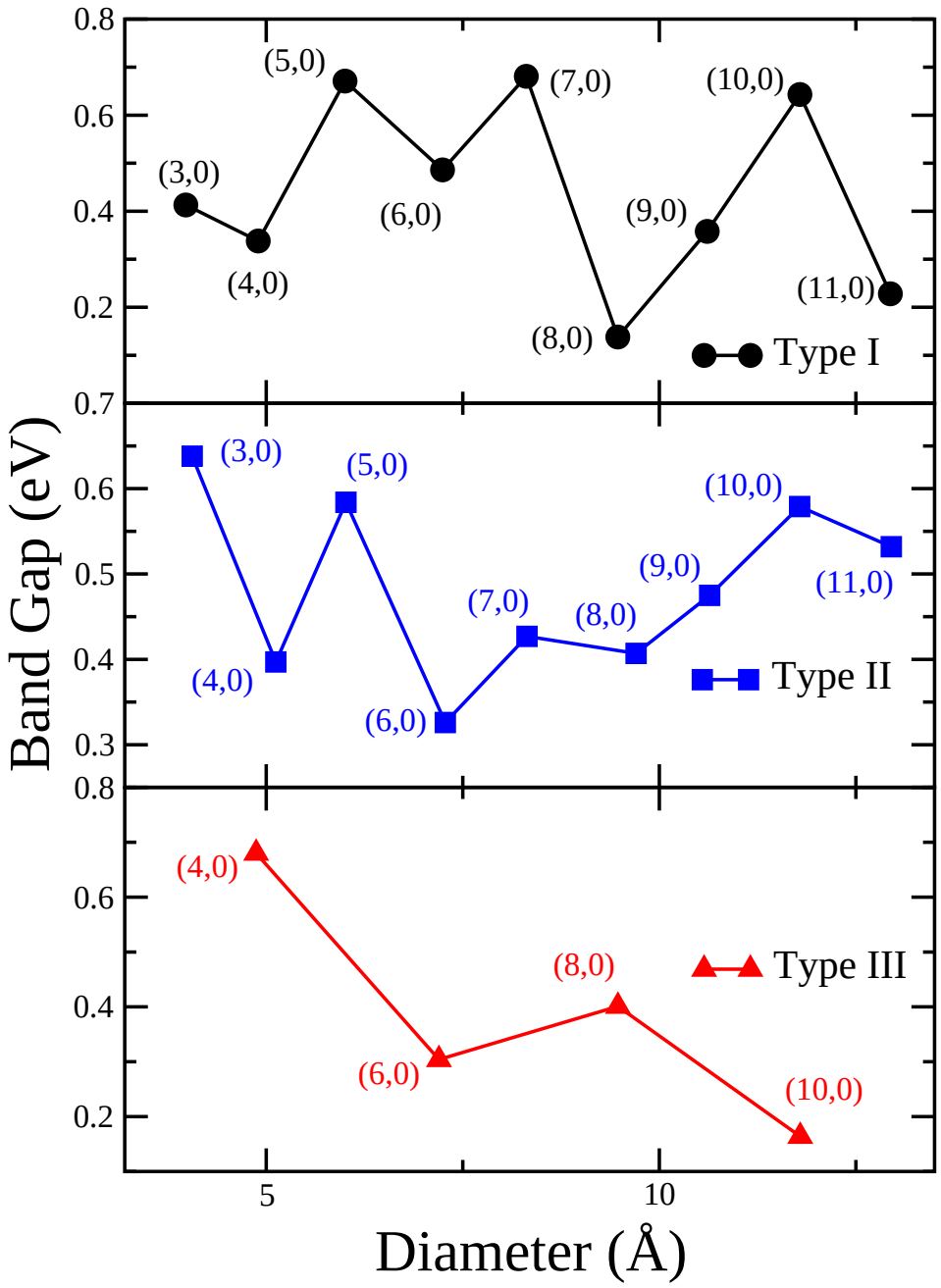

Figure 5.11 HOMO-LUMO gaps versus diameter for SiGe zigzag nanotubes.

The highest occupied molecular orbitals (HOMO) and lowest unoccupied molecular orbitals (LUMO) of all the different types of nanotubes are shown in figures 5.12 to 5.17. It is evident from the figures that HOMO is localized to Si atoms in armchair nanotubes consistent with the higher charge transfer from Ge to Si atoms. All the HOMO orbitals are mainly composed of p orbitals of the respective atoms. The slight delocalized nature of the electrons in types II and III is observed, which is a manifestation of mixed ionic and covalent behavior of the nanotubes. In general orbitals are of localized character in armchair tubes. For zigzag SiGe tubes delocalized nature of the orbitals is clearly visible in the plots. Interestingly, this diffused behavior of orbitals is not distributed along the tube length. This fact exposes some of the possible regions where the electron delocalization is unfavorable. As mentioned earlier in comparison to armchair tubes, SiGe nanotubes in zigzag form have lower values of band gaps, which can also be possibly linked with the delocalized nature of the electrons which is known for reducing the band gap values. HOMO and LUMO energy level plots also expose many possible favorable sites on the surface of SiGe nanotubes where external functionalized groups can be comfortably adsorbed, and that can significantly tune the electronic properties. As proposed earlier, a technique to saturate the less stable nanotubes is hydrogen passivation, but while doing so one can significantly alter the electronic properties, specifically band gaps of the nanotubes open up as hydrogen atoms will trap the extra electrons from the tubes.

Figures 5.18 and 5.18 show the energy density of states (DOS) for (7, 7) armchair and (4, 0) zigzag nanotubes, respectively. The DOS is convoluted with a Gaussian of width 0.05 eV and HOMO is adjusted to zero. The large gaps of armchair tubes compared to the gaps in the zigzag tubes are clearly visible. Finally, further into the future, we expect the SiGe nanotubes to open up many unique avenues in the field of nanoelectronics. Such areas include the developments of novel nano solar cells and photovoltaics, nanojuntions and interconnects, and nano device components.

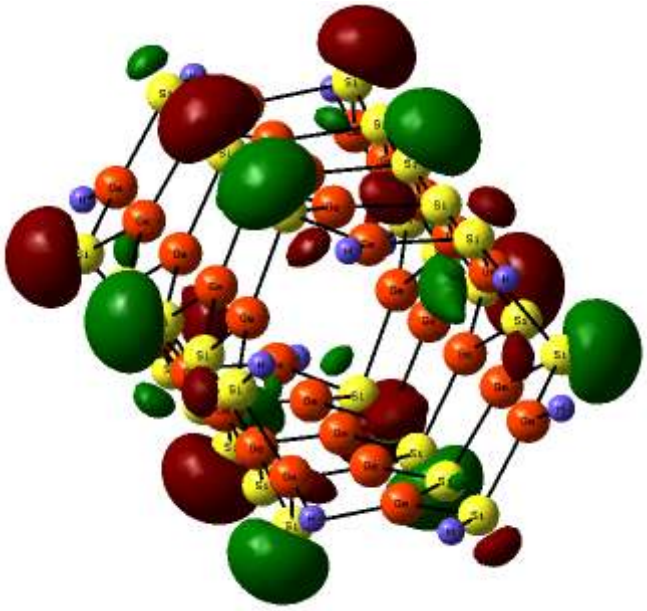

(a)

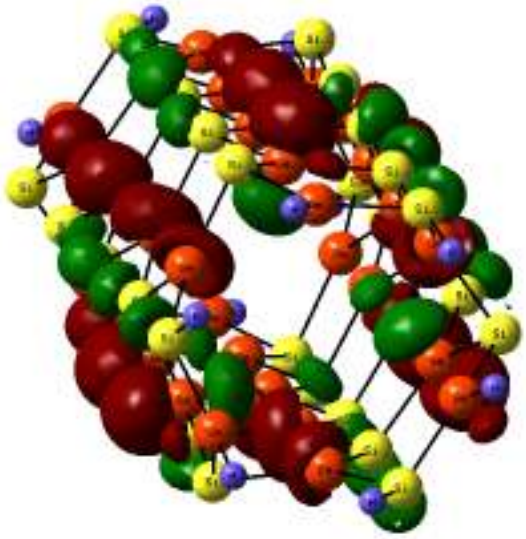

(b)

Figure 5.12 Type I (3, 3) HOMO (top) and LUMO (bottom).

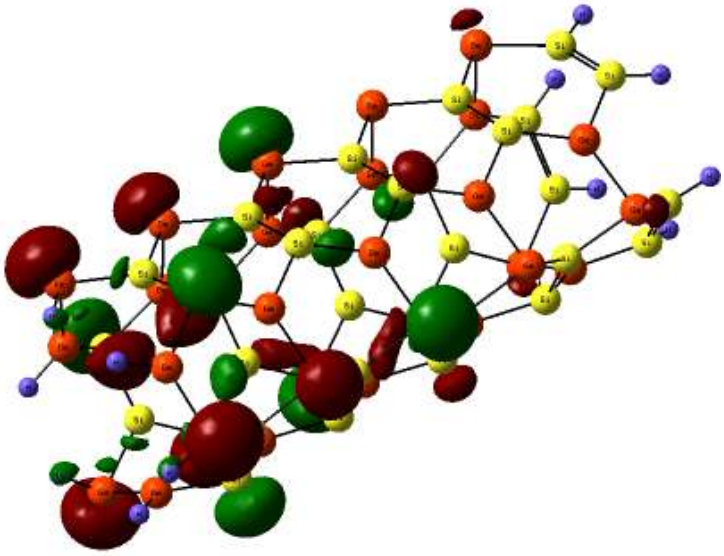

(a)

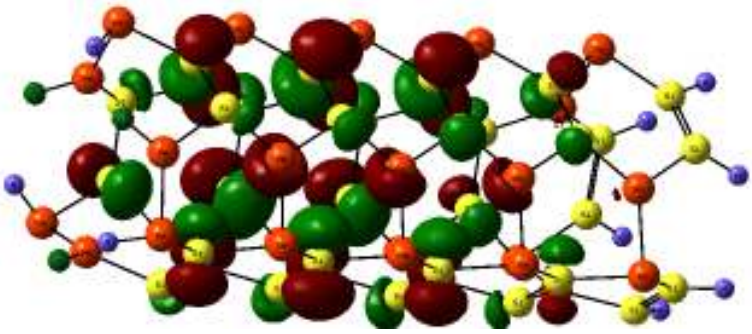

(b)

Figure 5.13 Type II (3, 3) HOMO (top) and LUMO (bottom).

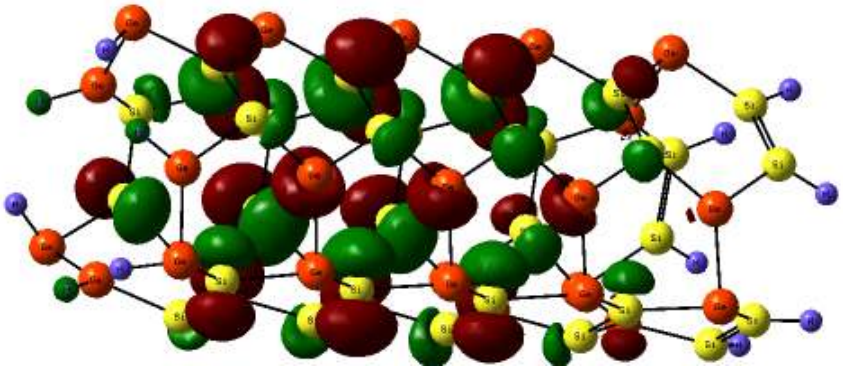

(a)

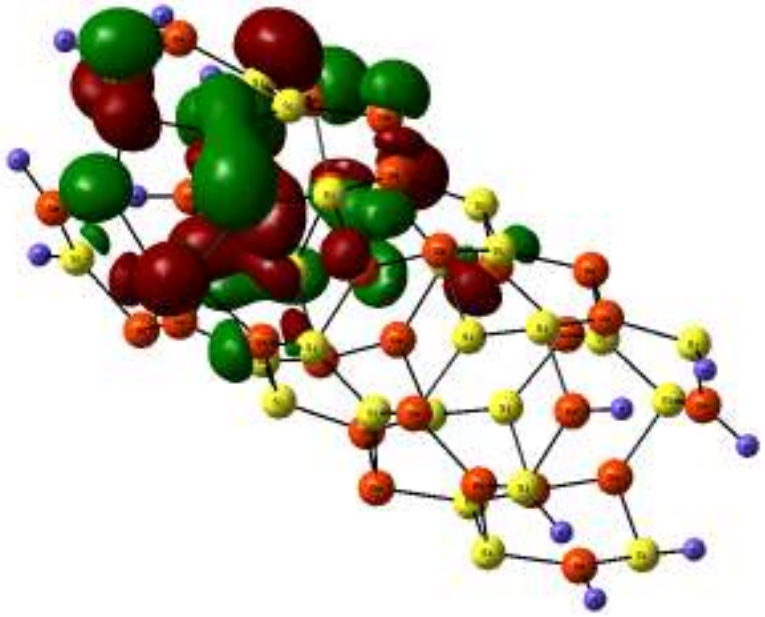

(b)

Figure 5.14 Type III (3, 3) HOMO (top) and LUMO (bottom).

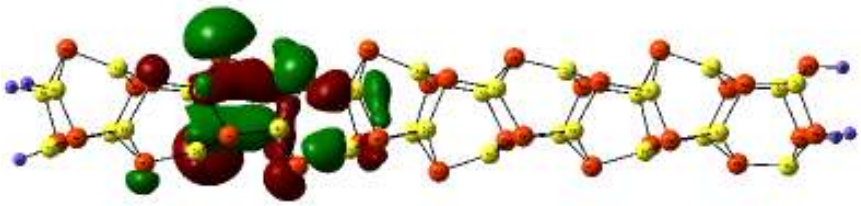

(a)

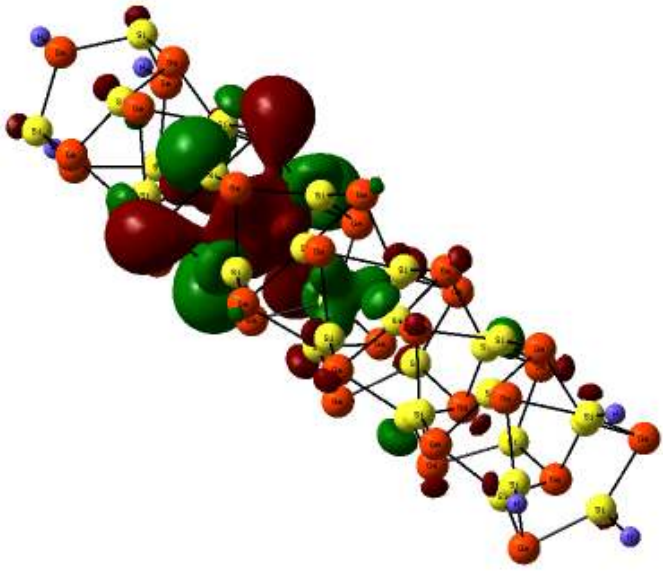

(b)

Figure 5.15 Type I (3, 0) HOMO (top) and LUMO (bottom).

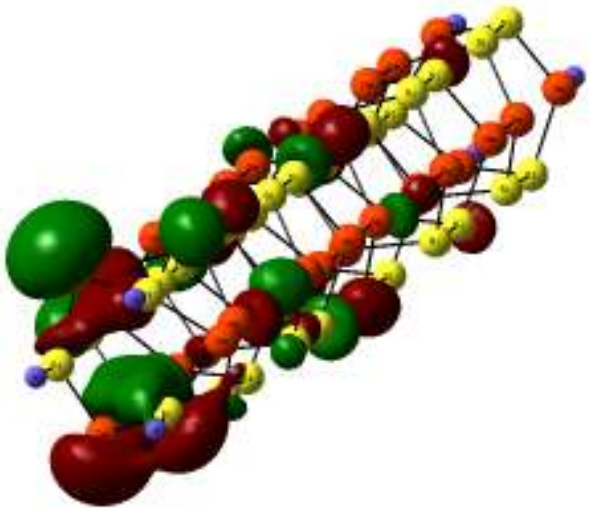

(a)

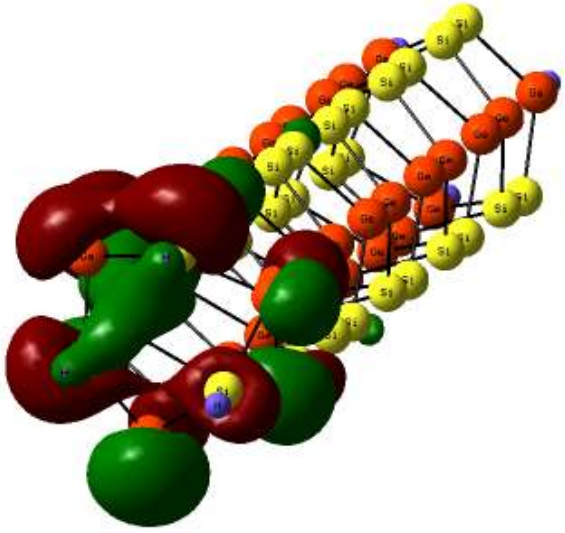

(b)

Figure 5.16 Type II (3, 0) HOMO (top) and LUMO (bottom).

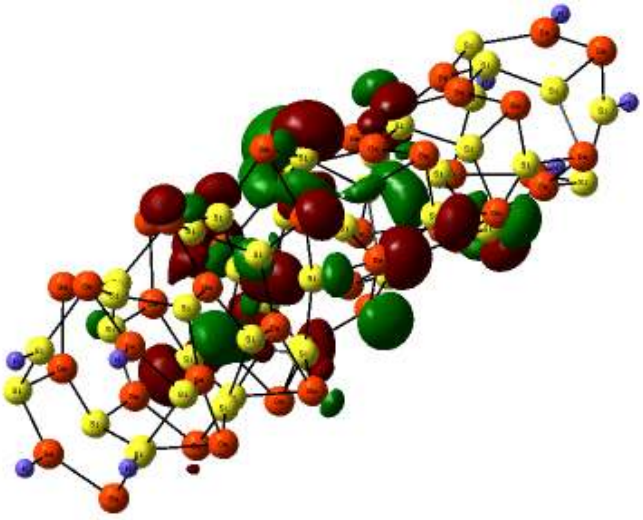

(a)

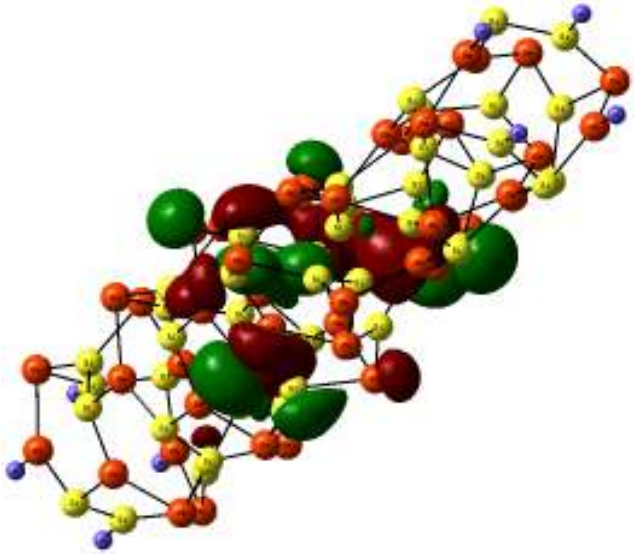

(b)

Figure 5.17 Type III (4, 0) HOMO (top) and LUMO (bottom).

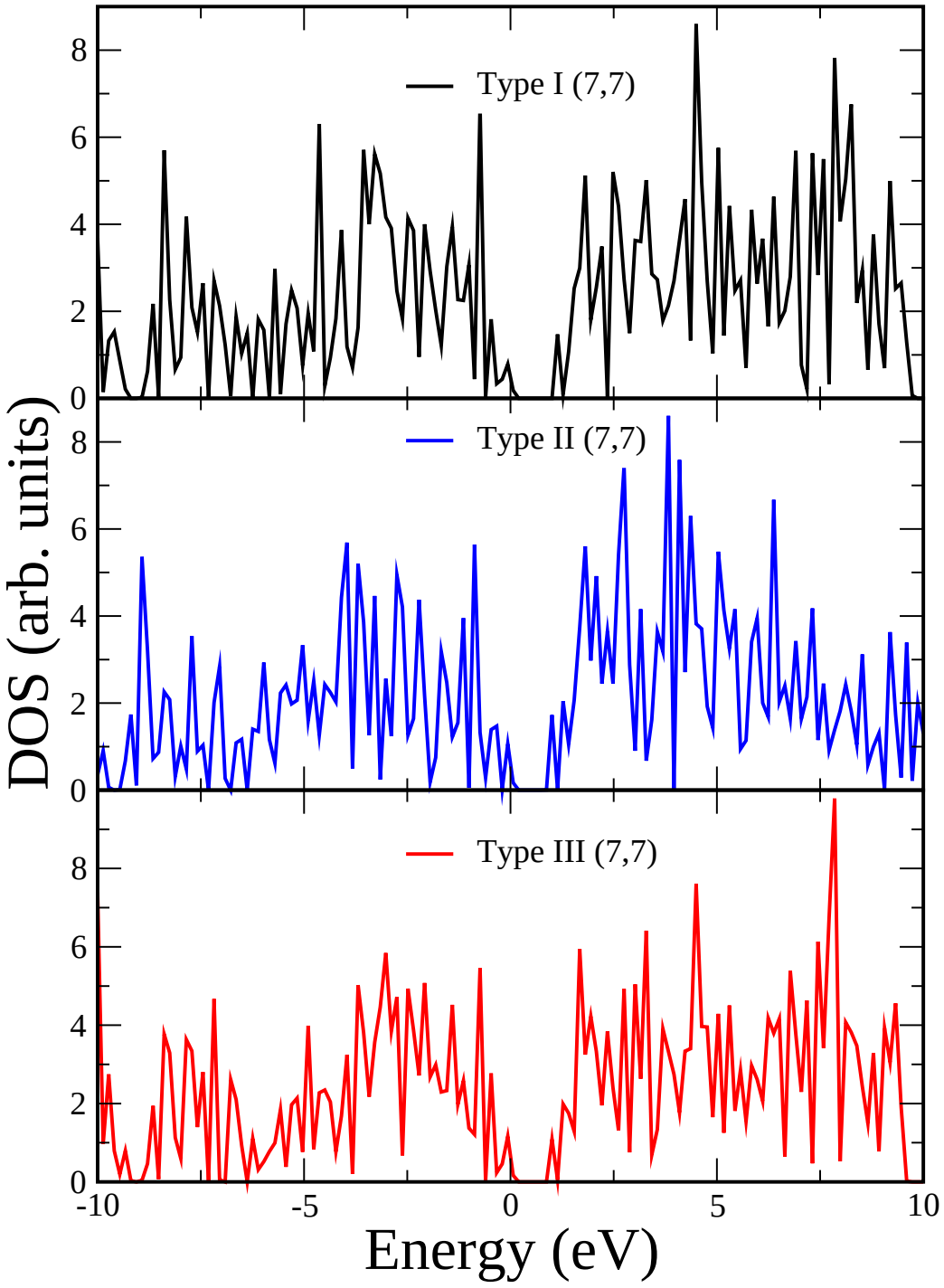

Figure 5.18 Gaussian broadened (width = 0.05 eV) density of states (DOS) plots for armchair nanotubes. HOMO energy is set to zero.

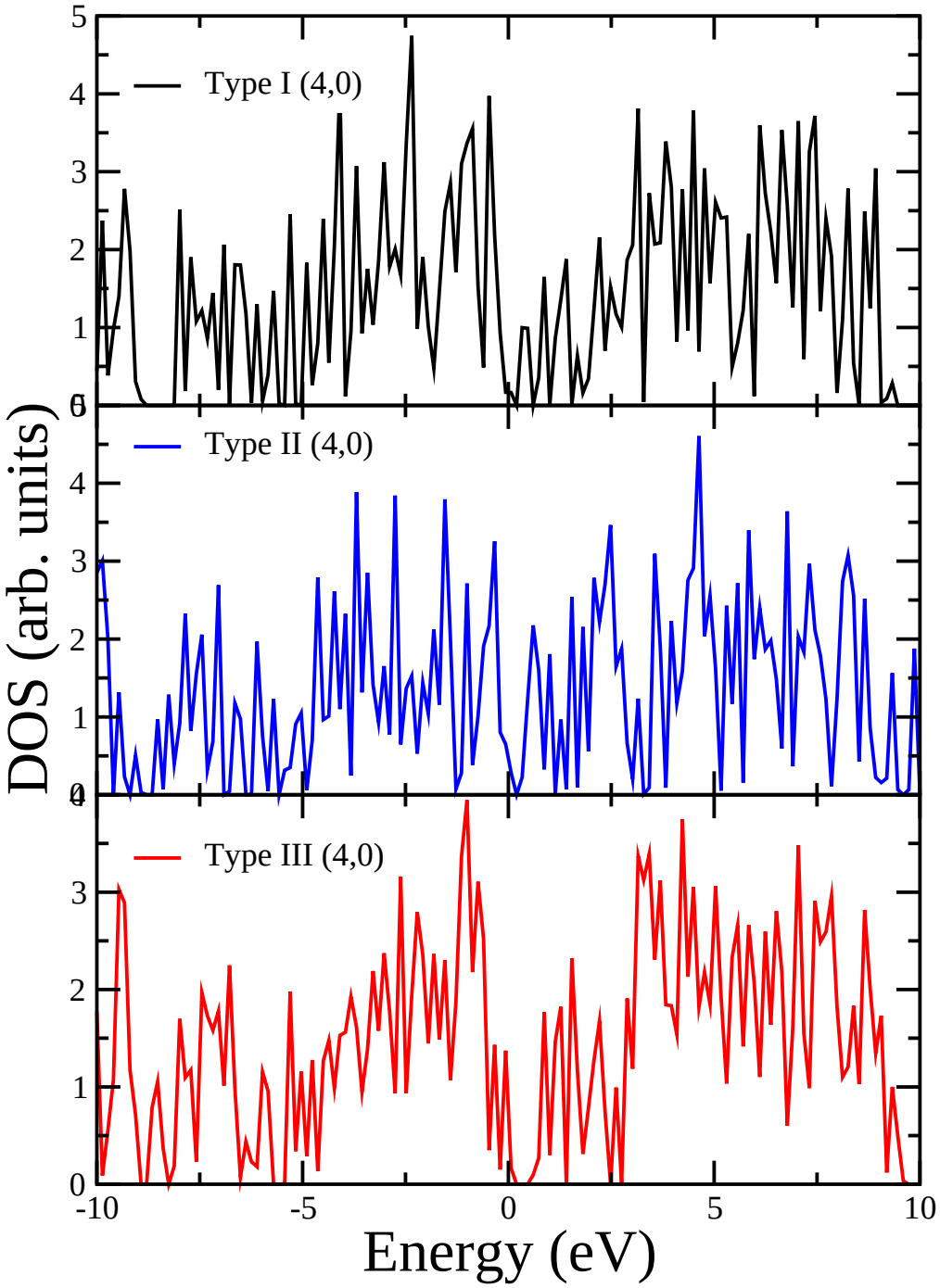

Figure 5.19 Gaussian broadened (width = 0.05 eV) density of states (DOS) plots for zigzag nanotubes. HOMO energy is set to zero.

CHAPTER 6

CONCLUSIONS

In summary, *ab initio* calculations using hybrid density functional theory and finite cluster approach have been performed for pure Si nanotubes. We have reviewed briefly the past work on Si nanotubes and presented a systematic analysis of armchair, zigzag, and chiral nanotubes. Our result showed that Si-Si bond length alternation is more pronounced in SiNTs than that in CNTs which shows a strong tendency for bond delocalization. Also as the number of Si atoms and tube diameter increases, the binding energy per atom for all zigzag and chiral nanotubes approaches saturation value. This is consistent with our previous research for armchair Si. The band gaps of all the different nanotubes that we have studied vary from 0.22 eV for zigzag (8, 0) to 1.15 eV for chiral (6, 3) which follows an oscillatory fashion between semi-metallic and small gap semiconductors. These results may have potential applications in nanodevices of the future. The Mulliken charge analysis shows that the zigzag structures have predominantly ionic bonding while the armchair and some of the chiral structures are covalently bonded. At this point we predict that the stability and electronic properties of SiNTs can be further increased by providing a suitable sp^3 bonding environment either by doping with other elements or by proper hydrogenation.

Using the same functional and basis set, we have studied three different types of armchair and zigzag GeC and pure Ge nanotubes. Detailed analysis and comparison for stability and geometry have been performed along with the evolution of electronic properties with the tube diameters. The three different types of nanotubes type I, type II, and type III have different atomic arrangement with the constraint of Ge to C ratio as 1:1 is maintained in all different GeC structures. The spatial positions of the Ge and C atoms, ionicity, and curvature

are the primary governing factors in the determinations of the stabilities and the electronic behaviors of the nanotubes. In both the cases armchair and zigzag GeC, type I tubes are found to be the most stable nanotubes among the three different types. As the nanotube diameter increases the cohesive energy of nanotubes increases and tends to approach saturation level with exception of type III zigzag GeC nanotubes. The results also suggest that all the nanotubes studied are semi-conducting in nature, with type I GeC tubes having widest band gap values. In types II and III for armchair and zigzag GeC tubes, the Ge atoms shift outwards and C atoms tend to move towards the axis of the nanotubes resulting in significant radial buckling. A reverse trend with negligible buckling values is obtained for type I tubes. In the case of pure Ge nanotubes the cohesive energy values tend to saturate as the diameter is increased. Also pure Ge tubes are semi-conducting with mixed ionic and covalent bonding nature. Rippled surfaces of relaxed zigzag Ge tubes are also observed after the relaxation.

Within the same theoretical framework we have extended our work to type I, II and III armchair, and zigzag SiGe nanotubes. Detailed analysis and comparison for stability and geometry have been performed along with the evolution of electronic properties with the tube diameters. The constraint of Si to Ge ratio as 1:1 is also maintained in all different SiGe structures. Once again the relative positions of the Si and Ge atoms, ionicity, and curvature are the primary governing factors in the determinations of the stabilities and the electronic behaviors of the nanotubes. Despite of surface reconstructions and structural distortions, tubes retained their cylindrical structures, which justify the stable single walled tubular forms of SiGe. The results also suggest that all the nanotubes studied are semi-conducting in nature, with a wide spectrum of band gaps. Also structure relaxation leads to a change in the radial geometry of the cylindrical structures making types II and III tubes Ge coated, and type I tubes to be Si coated with some exceptions.

Finally, further into the future it is envisioned that Ge based tubes will have potential applications in wide band gap nano-optoelectronic devices and selective bandgap circuitry of

future. Particularly type I GeC nanotubes have wide band gaps and can potentially be used in the low voltage based nanoelectronics circuits as insulators where the excitation energy is not enough to overcome the gap barrier. Furthermore, band gaps and other properties of GeC nanotubes can be modified by attaching external functionalized groups. Doping with proper impurities (p type or n type) can also lead to desired change in electronic properties. Nano interconnect junctions in the circuitry can also be designed using some of these tubes. Specifically, smaller diameter tubes can be neatly anchored over the vacancy in the wall of larger diameter tubes to form different nano-junctions. GeC nanotubes can also be successfully envisioned as futuristic hydrogen storage devices owing to surface charge distributions. Some of the SiGe nanotubes due to their unique charge distribution pattern can be exploited in the developing the nano p-n junction type devices where different sections have different charge concentrations. It is also envisioned that SiGe tubes should have potential applications in novel nano solar cells and photovoltaics, nanojuntions and interconnects, and nano device components.

.

APPENDIX A

CODE TO GENERATE THE COORDINATES AND SAMPLE COORDINATES

```
C CODE TO GENERATE COORDINATES
C RAYMOND ATTA-FYNN AND SOMILKUMAR RATHI
      IMPLICIT NONE
      INTEGER NMAX, II, JJ, KK, LL, NCOUNT, ICOUNT, NUNIT
      INTEGER NAT, NC, N1, N2, N0, N, TP1, TP2, TP3, R
      INTEGER ALPHA, BETA, EULER, WW2
      REAL*8  PI, A, A0, FAC1, FAC2, NNDIST, D, PHI0, Z0
      REAL*8  SN, THETA, Q, ZZ0, PHI, DSIH
      REAL*8  INP1, INP2, INP3, WW1, WW, RR, X0, Y0
      PARAMETER(NMAX=10000)
      REAL*8  XX(NMAX), YY(NMAX), ZZ(NMAX)
      INTEGER NNMAP(NMAX,10), ILIST(NMAX)
      CHARACTER*2 PP(NMAX)
      PI = 2.0*ASIN(1.0)
      FAC1 = SQRT(3.0)
      NNDIST = 2.352
      DSIH   = 1.547
      A0 = NNDIST*FAC1
      WRITE(*,*)'ENTER FIRST DIMENSION'
      READ(*,*)N1
      WRITE(*,*)
      WRITE(*,*)'ENTER SECOND DIMENSION'
      READ(*,*)N2
      WRITE(*,*)
      WRITE(*,*)'ENTER THE NUMBER OF UNIT CELLS'
      READ(*,*)NUNIT
```

```
      N = N1*N1 + N1*N2 + N2*N2
      SN = SQRT(FLOAT(N))
      D = SN*A0/PI
      IF(N1.EQ.0)N0=N2
      IF(N2.EQ.0)N0=N1
      IF((N2.NE.0) .AND. (N1.NE.0))THEN
         CALL GCD(N1, N2, N0)
      END IF
      WRITE(*,'(A,X,I3,X,A,X,I3,X,A,X,I3)')
     >     'GCD OF' , N1, 'AND', N2, 'IS', N0
      WRITE(*,*)
        N = N1*N1 + N1*N2 + N2*N2
      SN = SQRT(FLOAT(N))
      D = SN*A0/PI
           TP1 = N1 - N2
      TP2 = 3*N0
      TP3 = MOD(TP1,TP2)
      IF(TP3.EQ.0)THEN
        R = 3
      ELSE
        R = 1
      END IF
      NC = 4*N/(N0*R)
      NAT = NUNIT*NC
      THETA = ACOS((N1 + 0.5*N2)/SN)
      A = A0*SQRT(FLOAT(3*N))/(FLOAT(N0*R))
```

```
WRITE(*,*)'PARAMETERS FOR SILICON CHIRAL NANOTUBE ARE:'
WRITE(*,*)
WRITE(*,'(A,A,I3,A,I3,A)')'DIMENSIONS:', '(',N1,',',N2,')'
WRITE(*,*)
WRITE(*,'(A,F12.6)')'DIAMETER (IN ANGSTROM):',D
WRITE(*,*)
WRITE(*,'(A,F12.6)')'CHIRAL ANGLE (IN DEGREES):',THETA*180./PI
WRITE(*,*)
WRITE(*,'(A,I3)')'NUMBER OF ATOMS PER UNIT CELL:', NC
WRITE(*,*)
WRITE(*,'(A,I3)')'NUMBER OF UNIT CELLS REQUESTED:', NUNIT
WRITE(*,*)
WRITE(*,'(A,I3)')'TOTAL NUMBER OF ATOMS TO BE GENERATED:', NAT
WRITE(*,*)
Q = 0.5*FLOAT(NC)
EULER = 0
TP3 = N1/N0
IF(TP3.EQ.1)EULER=1
IF(TP3.EQ.2)EULER=1
IF(TP3.EQ.3)EULER=2
IF(TP3.EQ.4)EULER=2
IF(TP3.GT.4)THEN
  DO II = 1, TP3-1
    CALL GCD(II, TP3, TP2)
    IF(TP2.EQ.1)EULER = EULER + 1
  END DO
```

```
END IF
 WRITE(*,'(A,I3,A,X,I3)')'EULER FUNCTION OF',TP3, 'is', EULER
WRITE(*,*)
INP1 = FLOAT(N1-N2)/FLOAT(N1)
INP1 = 3.0 - 2.0*INP1
INP1 = INP1*FLOAT(N0)/(Q*FLOAT(R))
INP2 = FLOAT(N1-N2)/FLOAT(N0)
INP2 = INP2**(EULER-1.)
INP2 = INP2*FLOAT(N0)/FLOAT(N1)
  WRITE(*,*)'Symmetry Parameter =', WW1
WRITE(*,*)'Integral part =', WW2
WRITE(*,*)'Fractional part =', WW
WW = WW*Q
WW = WW/FLOAT(N0)
Z0 = (FLOAT(N1-N2)*A0*0.5)/SQRT(FLOAT(3*N))
PHI0 =  (PI*FLOAT(N1+N2))/FLOAT(N)
NCOUNT = 0
ALPHA = 0
BETA  = 0
ICOUNT = 0
II = 0
DO WHILE(NCOUNT.LT.NAT)
DO JJ = 0, N0-1
  DO KK = 0, 1
    IF(KK.EQ.0)THEN
      INP1 = (WW*FLOAT(II))/Q
```

```
        INP2 = FLOAT(JJ)/FLOAT(N0)
        INP3 = (A*FLOAT(II*N0))/Q
        PHI = PHI0 + 2.*PI*(INP1 + INP2)
        ZZ0 = Z0 + INP3
        NCOUNT = NCOUNT + 1
        XX(NCOUNT) = 0.5*D*COS(PHI)
        YY(NCOUNT) = 0.5*D*SIN(PHI)
        ZZ(NCOUNT) = ZZ0
        PP(NCOUNT) = 'Si'
       ELSE
        INP1 = (WW*FLOAT(II))/Q
        INP2 = FLOAT(JJ)/FLOAT(N0)
        INP3 = (A*FLOAT(II*N0))/Q
        PHI = -PHI0 + 2.*PI*(INP1 + INP2)
        ZZ0 = -Z0 + INP3
        NCOUNT = NCOUNT + 1
        XX(NCOUNT) = 0.5*D*COS(PHI)
        YY(NCOUNT) = 0.5*D*SIN(PHI)
        ZZ(NCOUNT) = ZZ0
        PP(NCOUNT) = 'Si'
       END IF
   END DO
END DO
II=II+1
END DO
```

```
WRITE(*,*)NCOUNT, NAT
DO II=1,NAT
  CALL MAP(XX,YY,ZZ,NAT,NNDIST,II,NNMAP,ILIST)
END DO
DO II=1,NAT
  IF((ILIST(II).EQ.1) .OR.(ILIST(II).EQ.2))THEN
          PP(II)='H'
  END IF
END DO
DO II=1,NAT
  IF(PP(II)=='H')THEN
     DO JJ=1,ILIST(II)
       LL = NNMAP(II,JJ)
       IF(PP(LL)=='Si')THEN
         X0 = XX(LL)-XX(II)
         Y0 = YY(LL)-YY(II)
         Z0 = ZZ(LL)-ZZ(II)
         RR=X0*X0+Y0*Y0+Z0*Z0
         RR = SQRT(RR)
         X0= X0/RR
         Y0= Y0/RR
         Z0= Z0/RR
         XX(II) = XX(LL)-DSIH*X0
         YY(II) = YY(LL)-DSIH*Y0
         ZZ(II) = ZZ(LL)-DSIH*Z0
       END IF
```

```
          END DO
        END IF
      END DO
      WRITE(*,*)'PRINTING COORDINATES'
      OPEN(12,FILE='CHIRAL.xyz',STATUS='UNKNOWN')
      WRITE(12,*)NCOUNT
      WRITE(12,*)
      DO II = 1, NCOUNT
        WRITE(12,44)PP(II), XX(II), YY(II), ZZ(II)
      END DO
      CLOSE(12)

44    FORMAT(A,3F14.7)
      STOP
      END
*     Find greatest common divisor using the Euclidean algorithm
      SUBROUTINE GCD(NA, NB, NGCD)
      IMPLICIT NONE
      INTEGER IA, IB, NA, NB, ITEMP, NGCD
       IA = NA
       IB = NB
1     IF (IB.NE.0) THEN
        ITEMP = IA
        IA = IB
        IB = MOD(ITEMP, IB)
        GOTO 1
```

```
  END IF
  NGCD = IA
  RETURN
END
SUBROUTINE MAP(XX,YY,ZZ,NAT,RCUT,II,NNMAP,ILIST)
IMPLICIT NONE
INTEGER II,JJ,NNMAP(10000,10),ILIST(10000),NAT
REAL*8  X1,Y1,Z1,XX(10000),YY(10000),ZZ(10000),RCUT,RR,EPS
EPS=0.00001
ILIST(II)=0
    DO JJ=1,10
      NNMAP(II,JJ)=0
    END DO
    DO JJ=1,NAT
      IF(II.NE.JJ)THEN
        X1=XX(II)-XX(JJ)
        Y1=YY(II)-YY(JJ)
        Z1=ZZ(II)-ZZ(JJ)
        RR=SQRT(X1*X1+Y1*Y1+Z1*Z1)
        IF(RR<(RCUT+EPS))THEN
          ILIST(II)=ILIST(II)+1
          NNMAP(II,ILIST(II))=JJ
        END IF
      END IF
    END DO
    RETURN
```

END

Sample coordinates generated using this code are shown in following page.

Pure Silicon nanotube (3, 3).

ATOM	X	Y	Z
H	2.78054	1.81958	0.69545
H	-2.96607	1.49823	0.69545
H	0.18553	-3.31781	0.69545
H	2.78054	-1.81958	0.69545
H	0.18553	3.31781	0.69545
H	-2.96607	-1.49823	0.69545
Si	-0.58502	3.31781	2.03689
Si	-2.5808	-2.16555	2.03689
Si	3.16582	-1.15226	2.03689
Si	3.16582	1.15226	2.03689
Si	-2.5808	2.16555	2.03689
Si	-0.58502	-3.31781	2.03689
Si	-3.16582	1.15226	4.07378
Si	0.58502	-3.31781	4.07378
Si	2.5808	2.16555	4.07378
Si	0.58502	3.31781	4.07378
Si	-3.16582	-1.15226	4.07378
Si	2.5808	-2.16555	4.07378
Si	-2.5808	-2.16555	6.11068
Si	3.16582	-1.15226	6.11068

Si	-0.58502	3.31781	6.11068
Si	-2.5808	2.16555	6.11068
Si	-0.58502	-3.31781	6.11068
Si	3.16582	1.15226	6.11068
Si	0.58502	-3.31781	8.14757
Si	2.5808	2.16555	8.14757
Si	-3.16582	1.15226	8.14757
Si	-3.16582	-1.15226	8.14757
Si	2.5808	-2.16555	8.14757
Si	0.58502	3.31781	8.14757
Si	3.16582	-1.15226	10.18446
Si	-0.58502	3.31781	10.18446
Si	-2.5808	-2.16555	10.18446
Si	-0.58502	-3.31781	10.18446
Si	3.16582	1.15226	10.18446
Si	-2.5808	2.16555	10.18446
Si	2.5808	2.16555	12.22135
Si	-3.16582	1.15226	12.22135
Si	0.58502	-3.31781	12.22135
Si	2.5808	-2.16555	12.22135
Si	0.58502	3.31781	12.22135
Si	-3.16582	-1.15226	12.22135
Si	-0.58502	3.31781	14.25824
Si	-2.5808	-2.16555	14.25824
Si	3.16582	-1.15226	14.25824
Si	3.16582	1.15226	14.25824

Si	-2.5808	2.16555	14.25824
Si	-0.58502	-3.31781	14.25824
Si	-3.16582	1.15226	16.29513
Si	0.58502	-3.31781	16.29513
Si	2.5808	2.16555	16.29513
Si	0.58502	3.31781	16.29513
Si	-3.16582	-1.15226	16.29513
Si	2.5808	-2.16555	16.29513
Si	-2.5808	-2.16555	18.33203
Si	3.16582	-1.15226	18.33203
Si	-0.58502	3.31781	18.33203
Si	-2.5808	2.16555	18.33203
Si	-0.58502	-3.31781	18.33203
Si	3.16582	1.15226	18.33203
Si	0.58502	-3.31781	20.36892
Si	2.5808	2.16555	20.36892
Si	-3.16582	1.15226	20.36892
Si	-3.16582	-1.15226	20.36892
Si	2.5808	-2.16555	20.36892
Si	0.58502	3.31781	20.36892
H	2.96607	-1.49823	21.71036
H	-0.18554	3.31781	21.71036
H	-2.78054	-1.81958	21.71036
H	-0.18553	-3.31781	21.71036
H	2.96607	1.49823	21.71036
H	-2.78054	1.81958	21.71036

APPENDIX B

CODE TO GENERATE DOS PLOT

```
C       Simple f77 code to compute EDOS using data from Gaussian log file
C       R. Atta-Fynn S J Rathi.
C       Alpha/beta eigienvalues (mixed or single).
C       reads HOMO and LUMO and sets HOMO to zero
C       Further modification by R. Atta-Fynn on Sep. 30, 3007
      implicit none
      real*8 energy(20000),edos(20000),ehomo,elumo
      real*8 emin, emax,  de, xx, yy, sigma, norm, pi
      integer NEIGEN,ii, jj, np, ncount,iset
      character*25 ppc, ppc2, fname1, fname2
      call rwfiles
      pi = 2.*asin(1.)
      ncount = 0
      open(14,file='dos_parameters.dat',status='unknown')
      read(14,*)ppc,np
      if(np .le. 1)then
        write(*,*)'Energy points must be greater than 1'
        stop
      end if
      read(14,*)ppc,emin
      read(14,*)ppc,emax
      read(14,*)ppc,sigma
      read(14,*)fname1
      read(14,*)ppc,ehomo
      read(14,*)ppc2,elumo
      close(14)
```

```
      open(12,file=fname1,status='unknown')
      read(12,*)NEIGEN
      do ii=1,NEIGEN
         read(12,*)energy(ii)
      end do
      close(12)
      de = (emax - emin)/float(np-1)
      do ii = 1,np
        edos(ii)=0.
      end do
      do ii = 1, np
        xx = emin + float(ii-1)*de
         do jj = 1,NEIGEN
            yy = xx - energy(jj)
            edos(ii) = edos(ii) + exp( -yy*yy/(sigma*sigma))
         end do
      end do
c      norm = sqrt(pi) * sigma * float(np)
      norm = 1.
       open(15,file='EDOS.dat',status='unknown')
       do ii = 1,np
         yy = edos(ii)/norm
         xx = emin + float(ii-1)*de
         write(15,*)xx-ehomo, yy
      end do
      close(15)
```

```
      write(*,*)
      write(*,*)
      write(*,*)
      write(*,*)
      write(*,*)'E_HOMO has been shifted to zero energy in DOS'
      write(*,*)
      write(*,*)'Gaussian broadening factor in eV =', sigma
      write(*,*)
      write(*,*)'DOS data is in the file EDOS.dat'
      write(*,*)
      write(*,*)'Good Luck'
      write(*,*)
      write(*,*)
      stop
      end
C     This subroutine rearranges EIGENVALUS from
C     Gaussian'03 log file
C     Raymond Atta-Fynn, Dept. of Physics
C     The University of Texas at Arlington
C     Date: 09-30-2007
C     Use at your own risk
      subroutine rwfiles
      implicit none
      real xx(1,1500),EMIN,EMAX,sigma
      real yy(1,4500),alpha_gap,beta_gap,gap
      real fac,xx2(1,1500),yy2(1,4500),ehomo, elumo
```

```
integer occupied, unoccupied,ii,np,jj,iset
integer occupied2, unoccupied2
character*20 fname1, fname2, contcheck
write(*,*)
write(*,*)
write(*,*)
write(*,*)'*******************************************'
write(*,*)'*                                         *'
write(*,*)'*  Program Gaussian_dos                   *'
write(*,*)'*  Computes DOS from Gaussian log file     *'
write(*,*)'*                                         *'
write(*,*)'*  Written by RAY ATTA-FYNN AND SOMIL RATHI *'
write(*,*)'*  PHYSICS DEPT.                          *'
write(*,*)'*  THE UNIVERSITY OF TEXAS AT ARLINGTON    *'
write(*,*)'*  Copyright Sep. 2007                    *'
write(*,*)'*                                         *'
write(*,*)'*  See SOMIL RATHI FOR INPUT FILE FORMAT   *'
write(*,*)'*                                         *'
write(*,*)'*  USE AT YOUR OWN RISK                   *'
write(*,*)'*                                         *'
write(*,*)'*******************************************'
write(*,*)
write(*,*)
write(*,*)
write(*,*)'DO YOU WANT TO CONTINUE?'
write(*,*)
```

```
      write(*,*)'ENTER yes or no'
      read(*,*)contcheck
      write(*,*)
      write(*,*)
      if(contcheck=='yes')goto 156
      if(contcheck=='no')then
        write(*,*)'ABORTING .........'
        write(*,*)'GOODBYE           '
        write(*,*)
        write(*,*)
      if(contcheck=='yes')goto 156
        stop
      end if
156    continue
      write(*,*)'Enter 0 for only ALPHA or 1 for ALPHA-BETA'
      read(*,*)iset
      fac=2.*13.605698
      if(iset.eq.0)then
      open(11,file='ALPHA_EIG.DAT',status='unknown')
      read(11,*)occupied
      read(11,*)(xx(1,jj),jj=1,occupied)
      read(11,*)unoccupied
      read(11,*)(yy(1,jj),jj=1,unoccupied)
      close(11)
      elumo = yy(1,1)*fac
      ehomo = xx(1,occupied)*fac
```

```
alpha_gap = yy(1,1) - xx(1,occupied)
alpha_gap = alpha_gap*fac
gap = alpha_gap
ii=occupied+unoccupied
open(14,file='alpha_data.out',status='unknown')
fname1 = 'alpha_data.out'
write(14,*)ii
do jj=1,occupied
  write(14,'(f13.6)')xx(1,jj)*fac
end do
do jj=1,unoccupied
  write(14,'(f13.6)')yy(1,jj)*fac
end do
close(14)
open(15,file='dos_parameters.dat',status='unknown')
write(15,*)'np 150'
write(15,*)'EMIN',  ehomo - 10.
write(15,*)'EMAX',  ehomo + 10.
write(15,*)'sigma 0.05'
write(15,*)fname1
write(15,*)'HOMO',xx(1,occupied)*fac
write(15,*)'LUMO',yy(1,1)*fac
close(15)
goto 125
end if
open(11,file='ALPHA_EIG.DAT',status='unknown')
```

```
open(12,file='BETA_EIG.DAT',status='unknown')
read(11,*)occupied
read(11,*)(xx(1,jj),jj=1,occupied)
read(11,*)unoccupied
read(11,*)(yy(1,jj),jj=1,unoccupied)
read(12,*)occupied2
read(12,*)(xx2(1,jj),jj=1,occupied2)
read(12,*)unoccupied2
read(12,*)(yy2(1,jj),jj=1,unoccupied2)
close(11)
close(12)
alpha_gap = yy(1,1) - xx(1,occupied)
alpha_gap = alpha_gap*fac
beta_gap = yy2(1,1) - xx2(1,occupied2)
beta_gap = beta_gap*fac
gap = min(alpha_gap,beta_gap)
ii=occupied+unoccupied+occupied2+unoccupied2
open(14,file='alpha_data.out',status='unknown')
fname1 = 'alpha_data.out'
write(14,*)ii
do jj=1,occupied
  write(14,'(f13.6)')xx(1,jj)*fac
end do
do jj=1,unoccupied
  write(14,'(f13.6)')yy(1,jj)*fac
end do
```

```
do jj=1,occupied2
  write(14,'(f13.6)')xx2(1,jj)*fac
end do
do jj=1,unoccupied2
  write(14,'(f13.6)')yy2(1,jj)*fac
end do
close(14)
open(15,file='dos_parameters.dat',status='unknown')
write(15,*)'np 150'
write(15,*)'EMIN',  ehomo - 10.
write(15,*)'EMAX',  ehomo + 10.
write(15,*)'sigma 0.05'
write(15,*)fname1
IF(gap.eq.alpha_gap)THEN
  elumo = yy(1,1)*fac
  ehomo = xx(1,occupied)*fac
  write(15,*)'HOMO',xx(1,occupied)*fac
  write(15,*)'LUMO',yy(1,1)*fac
END IF
IF(gap.eq.beta_gap)THEN
  elumo = yy2(1,1)*fac
  ehomo = xx2(1,occupied2)*fac
  write(15,*)'HOMO',xx2(1,occupied2)*fac
  write(15,*)'LUMO',yy2(1,1)*fac
END IF
close(15)
```

```
125       continue
          write(*,*)
          write(*,*)
          write(*,*)' E_LUMO=', elumo
          write(*,*)
          write(*,*)' E_HOMO=', ehomo
          write(*,*)
          write(*,*)' Band gap in eV =', gap
          write(*,*)
          return
          end
```

REFERENCES

[1] S. Iijima, *Nature* 354, 56 **(1991)**; S.Iijima and T. Ichihashi, *Nature* 363, 603 **(1993).**

[2] J. W. Mintmire, B. I. Dunlap, and C. T. White, *Phys. Rev. Lett.* 68, 631 **(1992)**.

[3] W. Liang, M. Bockrath, D. Bozovic, J. H. Hafner, M. Tinkham, and H. Park, *Nature* 411, 665 **(2001).**

[4] S. P. Franh, P. Poncharal, Z. L. Wang, and W.A. de Heer, *Science* 280, 1744 **(1998).**

[5] M. J. Bieruck, M. C. Llaguno, M. Radosavljevic, J. K, Hyun, A. T. Johnson, and J.E. Fisher, *Appl. Phys. Lett.* 80, 2767 **(2002).**

[6] Y. Chen, D. T. Shaw, X. D. Bai, E. G. Wang, C. Lund, W. M. Lu, and D. D. L. Chung, *Appl. Phys. Lett.* 78, 2128 **(2002).**

[7] A. C. Dillion and M. J. Heben, *Appl. Phys. A* 72, 133 **(2001).**

[8] N. S. Lee, D. S. Chung, I. T. Han, J. H. Kang, Y. S. Choi, H. Y. Kim, S H. Park, Y. W. Jin, W. K. Yi, M. J. Yun, J. E. Jung, C. J. Lee, J. H. You, S. H. Jo, C. G. Lee, and J. M. Kim, *Diam. Mater.* 10, 265 **(2001).**

[9] H. Sugie, M. Tanemura, V. Fillip, K. Iwata, K. Takahashi, and F. Okuyama, *Appl. Phys. Lett.* 78, 2578 **(2001)**.

[10] C. L. Cheung, J. H. Hafner, T. W. Odom, K. Kim, and C. M. Lieber, *Appl. Phys. Lett.* 76, 3136 **(2000)**

[11] P. G. Collin, K. Bradley, M. Ishigami, and A. Zett, *Science* 287, 1801 **(2000)**.

[12] R. Satio, G. Dresselhaus, and M. S. Dresselhaus, *Physical Properties of Carbon Nanotubes* , Imperical College Press, London, (**2003**).

[13] N. Hamada, S. I. Sawada and A. Oshimiya, *Phys. Rev. Lett.* 68, 1579 **(1992).**

[14] J. W. G. Wildoer, L. C. Venema, A. G. Rinzler, and R. E. Smalley, *Nature* 391, 59 **(1998).**

[15] R. Saito, M. Fujiata, G. Dresselhaus, and M. S. Dresselhaus, *Appl. Phys. Lett.* 60, 2204 **(1992).**

[16] T. W. Odom, J. L. Huang, P. Kim, and C. M. Lieber, *Nature* 391, 62 **(1998).**

[17] R. A. Jishi, J. Bragin, and L. Lou, *Phys. Rev. B* 59, 9852 **(1999).**

[18] O. Gulseren, T. Yildirim, and S. Ciraci, *Phys. Rev. Lett.* 65, 3405 **(2002).**

[19] R. S. Lee, H. J. Kim, J. E. Fischer, A. Thess, and R. E. Smalley, *Nature* 388, 255 **(1997).**

[20] X. Yang and J. Ni, *Phys. Rev. B* 71, 165438 **(2005).**

[21] Y. Q. Feng, R. Q. Zhang , K. S. Chan, H. F. Cheung, and S. T. Lee, *Phys. Rev. B* 66, 45404 **(2002).**

[22] F. Leonard and J. Tersoff, *Phys. Rev. Lett.* 88, 258302 **(2002).**

[23] J. A. Misewich, R. Martel, Ph. Avouris, J. C. Tsang, S. Heinze, J. Tersoff, *Science* 300, 5620 **(2003)**.

[24] J. Suehiro, G. Zhou, and M. Hara, *Sensor and Actuators B: Chemical*, 105, 164 **(2005)**.

[25] M. Penza, G. Cassano, P. Aversa, A. Cusano, A. Cutolo, M. Giordano, and L. Nicolais, *Nanotech.*, 16, 2536 **(2005).**

[26] S. Koller, L. Mayrhofer, and M. Grifoni, *New J. Phys.* 9, 348 **(2007).**

[27] C. Schonenberger, *Semiconductor Sci. Tech*. 2, 102 **(2006).**

[28] M. Bockrath, D. H. Cobden, P. L. McEuen, N. G. Chopra, A. Zettl, A. Thess, R. E. Smalley, *Science* 275,1922 **(1997).**

[29] R. Martel, T. Schmidt, H. R. Shea, T. Hertel, and P. Avouris *Appl. Phys. Lett.* 73, 2447 **(1998).**

[30] N. A. Bruque, R. R. Pandey, and R. K. Lake, *Phys. Rev. B* 76, 205322 **(2007).**

[31] J. Kong, N. Franklin, C. Zhou, S. Peng, J.J. Cho, and H. Dai, *Science* 287, 622 **(2000).**

[32] N. G. Chopra, R. J. Luyken, K. Cherrey, V. H. Crespi, M. L. Cohen, S. G. Louie, and A. Zettl, *Science* 269, 966 **(1995).**

[33] A. Loiseau, F. Willaime, N. Demoncy, G.Hug and H. Pascard, *Phys. Rev. Lett*. 76, 4737 **(1996).**

[34] M. Terrones, W. K. Hsu, H.Terrones, J. P. Zhang, S. Ramos , J.P. Hare, R. Castillo, K. Prasides, A. K. Cheetham, H. W. Froto, and D. R. M. Walton, *Chem. Phys. Lett.* 259, 568 **(1996).**

[35] M. Terrones, A. M. Benito, C. Manteca-Diego, W. K. Hsu, O.I. Osman, J. P. Hare, D. G. Reid, H. Terrones, A. K. Cheetham, K. Prasides, H. W. Kroto, and D. R. M. Walton, *Chem. Phys. Lett.* 257, 576 **(1996).**

[36] K. Suenaga, C. Colliex, N. Demoncy, A. Loiseau, H. Pascard, and F. Willaime, *Science* 278, 653 **(1997).**

[37] Y. R. Hacohen, E. Grunbaum, R. Tenne, J. Sloand and J. L. Hutchinson, *Nature* 395, 336 **(1998).**

[38] Y. R. Hacohen, R. Popovitz-Biro, E. Grunbaum, Y. Prior, and R. Tenne, *Adv. Mater.* 14, 1075 **(2002)**.

[39] Q. Chen, W. Zhou, G. Du, and L-M. Peng, *Adv. Mater.* 14, 1208 **(2002).**

[40] M. Cote, M. L. Cohen, and D. J. Chadi, *Phys. Rev. B* 58, 4277 **(1998)**.

[41] G. Seifert and E. Hernandez , *Chem. Phys. Lett.* 318, 355 **(2000).**

[42] J. W. Kang , J. J. Seo, H. J. Hwang, *J. Phys. Cond. Matter* 14, 8997 **(2002)**.

[43] C. Su, H.T. Liu , and J. M. Li, *Nanotech*. 13, 746 **(2002).**

[44] N. Wang, Y. H. Tang, Y. F. Zhang, C. S. Lee, and S.T. Lee, *Phys. Rev. B* 58, R16024 **(1998).**

[45] J. Hu, M. Ouyang, P. Yang, and C.M. Lieber, *Nature* 399, 48 **(1999).**

[46] M. Menon and E. Richter, *Phys. Rev. Lett.* 83, 792 **(1999).**

[47] B. Marsen and K. Sattler, *Phys. Rev. B* 60, 11593 **(1999).**

[48] U. Landman, R.N. Barnett, A. G. Scherbakov, and P. Avouris, *Phys. Rev. B* 61, 9994 **(2000).**

[49] R. Q. Zhang, S.T. Lee, C. K. Law, W. K. Li, and B. K Teo, *Chem. Phys. Lett.* 364, 251 **(2002).**

[50] S. B. Fagan, R. J. Baierle, R. Mota, A. J. R. da Silva, and A. Fazzio. *Phys. Rev. B* 61 9994 **(2000).**

[51] S. B. Fagan, R. Mota, R. J. Baierle, G. Paiva, A. J. R. da Silva, and A. Fazzio, *J. Mol. Struct. (Theochem)*, 539, 101 **(2001).**

[52] G. Seifert, Th. Kohler, H. M. Urbassek, E. Hernandez, Th. Frauenheim, *Phys. Rev. B* 63, 193409 **(2001).**

[53] R. Q. Zhang, S. T. Lee, C.-K. Law, W.-K. Li and B. K. Teo, *Chem. Phys. Lett.* 364251 **(2002).**

[54] A. S. Barnard, S. P. Russo, *J. Phys. Chem. B* 107, 7577 **(2003)**.

[55] M. Zhang, Y. H. Kan, Q. J. Zang, Z. M. Su , R. S. Wang, *Chem. Phys. Lett.* 379, 81 **(2003).**

[56] R. Q. Zhang , Ho-Lam Lee, W-K Li , B. K. Teo, *J. Phys. Chem. B* 109, 8605 **(2005).**

[57] X. Yang and J. Ni, *Phys. Rev. B* 72, 195426 **(2005).**

[58] M. Zhao, R. Q. Zhang, Y. Xia, C. Song, and S.-T. Lee, *J. Phys. Chem. C* 111, 1234 **(2007).**

[59] O. Ponomarenko, M. W. Radny, and P. V. Smith, *Surface Science* 562, 257 **(2004).**

[60] J. W. Kang, J. J. Seo, and H. J. Hwang, J. Nanosci. *Nanotech.* 2, 687 **(2002)**

[61] Y.-R. Jeng, P.-C. Tsai, and T.-H. Fang, *Phys. Rev. B* 71, 085411 **(2005)**.

[62] J. Bai, X. C. Zeng , H. Tanaka, and J. Y. Zeng, *Proc, Natl. Acad. Sci.* U S A. 101 , 2664 **(2004).**

[63] J. W. Kang and H. J. Hwang, *Nanotech.* 14, 402 **(2003).**

[64] A. K. Singh, T. M. Briere, V. Kumar, and Y.Kawazoe, *Phys. Rev. Lett.* 91, 146802 **(2003).**

[65] Y.-R. Jang, C. Jo, and J. I. Lee, *IEEE Transactions on Magnetics* 41, 10 **(2005)**.

[66] A. K. Singh, V. Kumar, and Y.Kawazoe, *J. Mater. Chem.* 14, 555 **(2004)**.

[67] P. Castrucci, M. Scarselli, M. De Crescenzi, M. Diociaiuti, P. S. Chaudhari, C. Balasubramanian, T. M. Bhave and S. V. Bhoraskar, *Thin Solid Films* 508, 226 **(2006)**.

[68] M. De Crescenzi, P. Castrucci, M. Scarselli, M. Diociaiuti, P. S. Chaudhari, C. Balasubramanian, T. M. Bhave and S. V. Bhoraskar, *Appl. Phys. Lett.* 86, 231901 **(2005)**.

[69] S. Yamada, and H. Fujiki, *Japanese Jour. Appl.* Phys. 45, L837 **(2006).**

[70] Y. H. Tang, L. Z. Pei, Y. W. Chen, and C. Guo, *Phys. Rev. Lett.* 95, 116102 **(2005).**

[71] J. Sha, J. Niu, X. Ma, J. Xu, X. Zhang, Q. Yang, and D. Yang, *Adv. Mater.* 14,1219 **(2002).**

[72] S. Jeong, J. Kim, H. Yang, B. Yoon, S. Choi, H. Kang, C. Yang, and Y. Lee, *Adv. Mater.* 15, 1172 **(2004).**

[73] O. G. Schmidt and K. Eberl, *Nature* 410, 168 **(2001)**.

[74] J. Zang, M. Huang, and F. Liu, *Phys.Rev.Lett*. 98, 146102 **(2007)**.

[75] G. Seifert, Th. Kohler, Z. Hajnal, Th. Frauenheim, *Sol. State Comm*. 119, 653 **(2001).**

[76] A. K. Singh, V. Kumar, and Y. Kawazoe, *Eur. Phys. J. D* 34, 295 **(2005).**

[77] O. F. Sankey, A. A. Demkov, W. T. Petuskey, and P. F. McMillan, Model. Simul. Mater. Sci. Eng. 1, 741 **(1993).**

[78] A. Mahmood and L. E. Sansores, *J. Mater. Res.* 20, 5 **(2005)**

[79] P. Kazimierski, *J. Non-Cryst. Sol*. 325, 206 **(2003).**

[80] G. A. Domrachev, A. M. Ob'edkov, B. S. Kaverin, A. A. Zaitsev, S. N. Titova, A. I. Kirillov, A. S. Strahkov, S. Y. Ketkov, E. G. Domracheva, K. B. Zhogova, M. V. Kruglova, D.

O. Filatov, S. S. Bukalov, L. A. Mikhalitsyn, and L. A. Leites, *Chem. Vap. Depo*. 12, 357 **(2006).**

[81] D. B. Migas, and V. E. Borisenko, *Phys. Rev. B* 76, 035440 **(2007).**

[82] O. G. Schmidt, and K. Eberl, *Nature* 410, 168 **(2001).**

[83] J. Zang, M. Huang, and F. Liu, *Phys. Rev. Lett*. 98, 146102 **(2007).**

[84] L. H. Thomas, *Proc. Cambridge Plilos. Soc.* 23, 542 **(1927).**

[85] E. Fermi, *Z. Phys*. 48, 73 **(1928).**

[86] P. A. M. Dirac, *Proc. Cambridge Plilos. Soc*. 26, 376 **(1930).**

[87] P. Hohenberg and W. Kohn, *Phys. Rev.* 136, B864 **(1964).**

[88] R. G. Parr and W. Yang, *Density Functional Theory of Atoms and Molecules* (Oxford University Press, New York, 1989).

[89] W. Kohn and L. J. Sham, *Phys Rev.* 140**,** A1133 **(1965).**

[90] D. M. Ceperley and B. J. Adler, *Phys. Rev. Lett.* 45, 566 **(1980).**

[91] W. Kohn, A.D. Becke and R. G. Parr, *J. Phys. Chem*. 100, 12974 **(1996).**

[92] R. O. Jones and O. Gunnarsson, *Rev. Mod. Phys*. 61, 689 **(1989).**

[93] G. Sentore and N. H. march, *Rev. Mod. Phys.* 66, 445 **(1996).**

[94] J. F. Dobson, G. Vignale, and M. P. Das (Eds.), *Electronic Density Functional Theory: Recent Progress and New Directions, (Plenum Press, New York and London, 1998).*

[95] D. R. Hartree, *Proc. Cambridge PHilos. Soc.* 24, 89 **(1928).**

[96] V. Fock, *Z. Phys.* 61, 126 **(1930).**

[97] J. C. Slater, *Phys. Rev.* 35, 210 **(1930).**

[98] C. Coulson, *Rev. Mod. Phys.* 32, 170 **(1960).**

[99] U. von Barth and L. Hedin, *J. Phys. C: Solid State Phys*. 5, 1629 **(1972)**.

[100] O. Gunnarsson and B. I. Lundqvist, *Phys. Rev.* 13, 4274 **(1976).**

[101] S. H. Vosko, L. Wilk, and M. Nusair, *Can. J. Phys.* 58, 1200 **(1980).**

[102] M. Rasolt and D. J.W. Geldart, *Phys. Rev. B* 34, 1325 **(1986).**

[103] J. P. Perdew, *Phys. Rev. B* 33, 8822 **(1986)**; 34, 7406 **(1984)**.

[104] A. D. Becke, *J. Chem. Phys*. 98, 1372 **(1993)**; 98, 5648 **(1993).**

[105] C. Lee, W. Yang, and R. G. Parr, *Phys. Rev. B* 37, 785 **(1988).**

[106] J. P. Perdew, J. A. Chevary, S. H. Vosko, K. A. Jackson, M. R. Pederson, D. J. Singh, and C. Fiolhais, *Phys. Rev. B* 48, 4978 **(1993)**; K. Burke, J. P. Perdew, and Y. Wang, in *Electronic Density Functional Theory: Recent Progress and New Directions,* Ed. J. F. Dobson, G. Vignale, and M. P. Das (Plenum, New York, 1998).

[107] J. P. Perdew, K. Burke, and M. Ernzerhof, *Phys .Rev. Lett.* 77, 3865 **(1996)**; 78, 1396 **(1997).**

[108] J. P. Perdew, *Electronic Structure of Solids'91*, edited by P. Ziesche and H. Eschig (Akademie Verlag, Berlin, 1991); J. P. Perdew and Y. wang, *Phys. Rev. B* 46, 12947 **(1992)**; *Phys. Rev. B* 46, 6671 **(1992).**

[109] P. J. Hay and W. R. Wadt, *J. Chem. Phys.* 82, 270 **(1995)**; T. H. Dunning and P. J. Hay 1976, *Modern Theoretical Chemistry* (New York: Plenum).

[110] *Gaussian 03*, M. J. Frisch, *et al.* Gaussian Inc. Pittsburgh*, Pa*, **(2003)**; W. J. Hehre, L. Radom, P. v. R. Schleyer, J. A. Pople, *Ab intio molecular orbital theory*, Wiley Publications **(1986).**

[111] *CRC Handbook of Chemistry and Physics*, 76th Ed., CRC Press **(1995).**

[112] M. S. Dresselhaus, G. Dresselhaus, and R. Saito, *Phys. Rev. B* 45, 6234 **(1992)**.

[113] K. M. Alam and A. K. Ray, *Phys. Rev. B* 77, 035436 **(2008)**; Nanotech. 18, 495706 **(2007)**; *J. Nano Part.* (to be published), *J. Comp. Theo. Nanosci*. (to be published).

[114] P. Pradhan and A. K. Ray, *J. Comp. Theo. Nanosci*. 3, 128 **(2006)**; S. J. Rathi and A. K. Ray, *J. Comp. Theo. Nanosci.* 5, 464 **(2008)**; Nanotech. (in press); S. J. Rathi and A. K. Ray (to be published).

[115] I. Cabria, J. W. Mintmire, and C. T. White, *Inter. J. Quant. Chem*. 91, 51 **(2003)**.

BIOGRAPHICAL INFORMATION

The author completed his undergraduate degree in Electrical Engineering from Gujarat University, India. His undergraduate project was on design of AC motor protection scheme. He was among the top five students in his undergraduate class of 130 students.

His current research interests are directed at developing and understanding of the electronic and optical properties of novel nano materials, techniques of preparation and characterization of lower dimensional nanostructures with specific applications in field photovoltaics and solar cell related technology. He has authored few papers in scientific journals and presented papers at national conferences under the mentorship of Dr. A. K. Ray. Recently he has received an opportunity to work as a PhD student at Colorado School of Mines in collaboration with the National Renewable Energy Laboratory (NREL). He intends to continue his research activities in academia or industry after completion of his PhD.